CHAPTER I

GENERAL INTRODUCTION

As I was contemplating how to start the GENERAL INTRODUCTION section of my thesis, the following idea came into my mind: since essentially all the scientific parts of the introduction will be included in each chapter that follows, here I would like to focus on how I have come across with these seemingly not-so-connected, various projects about forebrain, choroid plexus, cerebellum development and cerebellar tumorigenesis. I wish that by describing how my naïve scientific endeavors proceeded I can document my constant debating thoughts and perhaps learn more a bit about how things evolve in a logical way.

The functional role of cholesterol modification of Shh was once a controversial topic, with different conclusions suggesting that the cholesterol is either facilitating (Callejo et al., 2006; Dawber et al., 2005; Gallet et al., 2006) or restraining (Gallet et al., 2006) (Lewis et al., 2001) the long-range trafficking of Shh. When I first came to the Chiang lab, we had a good set of tools, the *ShhN* mutant mice, to answer that important question since the ShhN protein cannot be modified by cholesterol. While Yina and Huimin, former graduate students in the Chiang lab, were looking at the limb bud phenotype of *ShhN* mutants, Chin asked me to look into the developing spinal cord. Naturally, by analyzing a panel of marker gene expressions I was able to map out the dorsal-ventral patterning difference, which is minimal since all the neuronal types are present, among the spinal cords of control, *ShhN/+* and *ShhN/-* mutants. However, the

1

phenotype is not dramatic and I spent quite some time pondering how to proceed with the data to formulate a good, publishable story. It was not until one day when Yina pointed out that both the *ShhN/+* and *ShhN/-* mutants had very "funny heads", or scientifically what we call enlarged brain ventricles, that I realized that I could perhaps do something about the brain and compare the development between the brain and the spinal cord in the mutants. Indeed, the *ShhN/-* mutant forebrain does not develop the most ventral neuronal structures while the *ShhN/+* mutant forebrain develops too many ventral derivatives at the expense of dorsal structures, all owing to the ectopic long-range trafficking of ShhN protein that cannot be modified by cholesterol. Therefore, I continued to perform a series of experiments in an attempt to explain the underlying reason as to why *ShhN/-* mutants are able to develop all the ventral neurons in the spinal cord but not in the forebrain (Huang et al., 2007b). In addition, I noticed that the *ShhN/+* mutants display a single forebrain ventricle and many other developmental anomalies that are seen in human patients with holoprosencephaly (HPE), the most common forebrain congenital disease. Chin wisely pointed out that there was a paper reporting that a point mutation in a human patient might actually make his genotype *SHHN/+*. With a couple of months work, we were able to fully characterize the *ShhN/+* forebrain phenotype and publish its implication for human HPE (Huang et al., 2007a). Through these early works, I have learned that one of the most essential part of doing science is to always keep a sharp eye for interesting observations: Yina pointed out the "funny heads", and Chin located the human patient that may be *SHHN/+*.

During my studies of forebrain development, I extensively used the *Ptch1$^{LacZ/+}$* mice in which ß-galactosidase activity indicates Shh pathway activation. I have occasionally

sectioned the $Ptch1^{LacZ/+}$ embryo throughout the forebrain, midbrain and hindbrain, and one day discovered that the cerebellar ventricular zone also displayed active Shh signaling. It was quite surprising as my literature reading (Dahmane and Ruiz-i-Altaba, 1999; Wallace, 1999a; Wechsler-Reya and Scott, 1999b) indicated to me that there is no source for Shh, hence Shh signaling, within the embryonic cerebellar tissue. I got immensely interested in this observation and performed a series of experiments to determine the source and the functional role of this Shh signaling. Now with several lines of evidence we suggest that it is the hindbrain choroid plexus (hChP) that secretes Shh protein to promote proliferation of the embryonic cerebellar ventricular zone progenitors. We have also determined that the hChP epithelium-derived Shh regulates the progenitor proliferation in the hChP epithelium itself (Huang et al., 2009). From these experiences, I have learned that extensive scientific literature reading of the things you are or not doing, is always good, otherwise I would have not paid attention to the unexpected Shh signaling in the cerebellar ventricular zone.

Finally, during my study of hChP development, I generated the gain-of-function mutant of Shh signaling by using the *Gdf7-cre* driver reportedly only expressed in the hChP epithelium. However, the mutant mice not only displayed abnormal hChP, but also developed tumors in their cerebella. I later determined that *Gdf7* is also expressed in the progenitors that give rise to cerebellar external granule neuron precursors, discovering a new tissue derivative of Gdf7-expressing progenitors as well as a novel cellular origin for cerebellar tumors. From this, I realized that it is sometimes rewarding to look outside of the box.

When I ask myself: what are the most valuable results that I have gained throughout my Ph.D study? I would not think of my publications, conference talks or awards, but a few things that I shall always keep in mind such as observe, read, think, doubt and act.

CHAPTER II

REGION-SPECIFIC REQUIREMENT OF CHOLESTEROL MODIFICATION OF SONIC

HEDGEHOG IN PATTERNING THE TELENCEPHALON AND SPINAL CORD

Introduction

The appearance of distinct neuronal cell types at defined positions in the ventral

neural tube is dependent on inductive signaling mediated by Shh (Agarwala et al., 2001;

Dale et al., 1997; Fuccillo et al., 2006; Jessell, 2000; Sur and Rubenstein, 2005). In mice

lacking Shh, most ventral neuronal cell types were lost along the rostral-caudal axis of

the neural tube while dorsal structures were expanded ventrally (Chiang et al., 1996;

Rallu et al., 2002). It is thought that neurons generated in progressively more ventral

regions in the spinal cord require correspondingly higher level of Shh for their induction

(Briscoe and Ericson, 2001; Jessell, 2000). In the basal ganglion of the telencephalon, the

medial ganglionic eminence (MGE) and lateral ganglionic eminence (LGE), which give

rise to the globus pallidus and striatum, respectively, are generated sequentially in

response to Hedgehog (Hh) signaling (Ericson et al., 1995; Kohtz et al., 1998;

Shimamura and Rubenstein, 1997a).

Although Shh can elicit diverse cell fates in the neural tube, much less is known

about the factors that regulate Shh range and activity gradient. The active Shh is dually

lipid-modified (ShhNp), with palmitic acid at its N-terminus and cholesterol at its C-

terminus (Mann and Beachy, 2004). The hydrophobic nature of lipids indicates that there

might be a dedicated release mechanism for Shh. mDisp1, a multi-pass transmembrane

protein, appears to fulfill this mechanistic requirement (Caspary et al., 2002; Kawakami et al., 2002; Ma et al., 2002), as its function is necessary only for lipidated Shh secretion (Li et al., 2006; Tian et al., 2005). Lipid-modified Shh has also been shown to form a large multimeric complex *in vitro* (Chen et al., 2004a; Zeng et al., 2001). It has been suggested that the lipid moieties are embedded in the core of these complexes, analogous to micelles, thus facilitating Shh interaction with and its spreading across the extracellular matrix (Zeng et al., 2001). The biological function of lipid moieties in regulating Shh function has been investigated recently. Misexpression studies in rats indicated that palmitoylation is required for Shh to induce ectopic ventral cell fates in the dorsal telencephalon (Kohtz et al., 2001), suggesting that palmitoylation is required for Hh activity. Indeed, mice either deficient in an enzyme that catalyzes palmitoylation or carrying a variant of Shh that is incapable of being palmitoylated showed developmental defects similar to that of loss of Shh function (Chen et al., 2004a).

In contrast to palmitoylation, Shh lacking cholesterol modification (ShhN) does not appear to significantly affect its intrinsic potency. It has been shown that ShhN isolated from tissue culture cells can induce ectopic ventral cell types in neural explants with comparable or higher efficiency than ShhNp at similar concentration (Feng et al., 2004). Instead, the cholesterol moiety appears to affect the range of Hh spreading in the target field. Recent mosaic studies with *Drosophila* wing imaginal discs showed that Hh lacking cholesterol (Hh-N) has extended range of spreading and signaling capacity for inducing ectopic low threshold Hh target genes, although the expressions of high threshold target genes near the source were reduced (Callejo et al., 2006; Dawber et al., 2005; Gallet et al., 2006). However, another report indicated that wing disc clones that

6

expressed Hh-N were unable to elicit low threshold Hh target genes at a distance (Gallet et al., 2006). Therefore, the precise role of cholesterol moiety in regulating *Drosophila* Hh signaling remains controversial.

Previous efforts to understand the role of cholesterol modification in mice concluded that the cholesterol moiety is required for long-range spreading and signaling in the mouse limb buds (Lewis et al., 2001). Accordingly, it has been proposed that cholesterol modification of Shh is required for the formation of multimers involved in long-range signaling and proper vertebrate forebrain patterning (Feng et al., 2004). However, a more recent study suggested that ShhN retained some paracrine activity as it was capable of inducing several ventral neuronal cell types in the spinal cord (Tian et al., 2005). Given this controversy, the role of cholesterol moiety in Shh function has been re-assessed recently in the limb bud (Li et al., 2006). The study found that cholesterol modification is required to restrict the spread of Shh across the anteroposterior axis of the limb bud similar to Hh-N function in *Drosophila*. The extended range of ShhN movement across the A/P axis of the limb bud also resulted in appreciable reduction of local ShhN levels, suggesting that the cholesterol moiety not only regulates the range but also the shape of the Shh morphogen gradient.

In this study, we utilized mice exclusively expressing ShhN to address the function of the cholesterol moiety in patterning the spinal cord and telencephalon. We revealed that dorsoventral patterning of the telencephalon in embryos lacking cholesterol modification of Shh was severely compromised as indicated by the lack of MGE progenitors and appearance of widespread ectopic LGE progenitors in the dorsal telencephalon. In contrast, patterning of the ventral spinal cord was largely unaffected

7

and no ectopic expressions of ventral cell fates at dorsal sites were observed in *ShhN/-* embryos. These findings suggest that patterning of the telencephalon is highly sensitive to alteration in Shh spreading behavior.

Experimental procedures

Mice

To generate conditional *Shh^{flox/+}* mice, loxp sequences were inserted flanking the Shh processing domain, which is situated in exon 3 (Li et al., 2006). The resulting mice containing *Shh^{flox}* (unrecombined) allele were maintained as heterozygotes, because homozygotes die soon after birth (Li et al., 2006). The *Shh^{flox}* allele has reduced capacity to generate lipid-modified Shh (ShhNp) due to interference of the loxp site with the Shh autocatalytic processing reaction (Li et al., 2006), thus it should be considered hypomorphic. Embryos uniquely expressing Shh without cholesterol modification (ShhN) were generated by mating *Shh^{flox/+}* animals with *Shh^{+/-};Sox2-Cre* deleter strain as previously described (Li et al., 2006). *ShhN/+;mDisp1^{-/-}* embryos were obtained from crosses between *Shh^{flox/+};mDisp1^{+/-}* and *Sox2-Cre;mDisp1^{+/-}*. *mDisp1^{+/-}* mice have been described (Ma et al., 2002). *Sox2-Cre* mice (Hayashi et al., 2002) and *Ptch1-lacZ* mice (Goodrich et al., 1997) were obtained from the Jackson Laboratory. All control embryos were either *Shh^{+/+}* or *Shh^{+/-}*; we have not observed any apparent difference during development or Shh staining patterns amongst these embryos.

Immunohistochemistry and Western analysis

All immunohistochemistry analyses were performed on tissue sections collected from OCT- or paraffin-embedded embryos as previously described (Li et al., 2006). The primary antibodies used were rabbit anti-Foxa2 (1:100), mouse anti-Nkx2.2 (DSHB, 1:2), mouse anti-Isl1/2 (DSHB, 1:10), sheep anti-Chx10 (Exalpha Biologicals, 1:50), mouse anti-En1 (DSHB, 1:5), mouse anti-Pax7 (DSHB, 1:2), mouse anti-Pax6, (DSHB, 1:1), mouse anti-Nkx2.1, (Neomarkers, 1:100), rabbit anti-Nkx6.1 (gift of Christer Betsholz, 1:3000), rabbit anti-Oligo2 (gift of Hirohide Takebayashi), mouse anti-Mash1 (gift of Jane Johnson, 1:100), rabbit anti-Gsh2 (gift of Kenneth Campbell, 1:500), mouse anti-Tuj1 (Sigma, MO, 1:400), goat anti-Shh (Santa cruz Biotechnology, H-160, 1:1000). For Western analysis, protein lysate samples, 200ug each, collected from E15.5 whole brains, were resolved on 6% SDS-polyacrylamide gels. Gli3-190 and Gli3R species were detected by using a Gli3 N-terminal specific antibody as described (Litingtung et al., 2002).

Analysis of cell proliferation and apoptosis

5-BromodeoxyUridine (BrdU) *in vivo* labeling and TUNEL analysis were performed as previously described (Litingtung et al., 1998). Proliferative and apoptotic cell countings were carried out with at least 5 sections from three different embryos for each genotype. To quantify BrdU- or TUNEL-positive cells, coronal sections of the telencephalic neuroepithelium were subdivided into three regions; ventral (v), dorsal (d) and dorsal midline (dm). v is defined as the region of neuroepithelial cells ventral to the dorsal edge of the morphologically distinct LGE (see arrowhead in Fig. 2). The dm region consists of 200 neuroepithelial cells situated at the center of the dorsal midline and

its immediate neighbors. The d region is located between regions v and dm. The percentage of BrdU-positive cells was determined by counting these positive cells in segments of 200 cells within the designated region of the telencephalon and dividing by the total number of cells in the segment. All sections were counterstained with the nuclear dye DAPI to highlight the total number of cells. At least five segments in each region were counted to generate a statistical comparison.

X-gal staining and transcript detection

X-gal staining was performed according to standard protocols (Hogan et al., 1994). Whole-mount and section *in situ* hybridizations were performed as described (Li et al., 2004). The following cDNAs were used as templates for synthesizing digoxygenin-labeled riboprobes: *Shh* (Li et al., 2006), *Ptch1* (Goodrich et al., 1996) and *Nkx2.1* (Lazzaro et al., 1991).

Statistics

To assess differences among groups, statistical analyses were performed using a one-way analysis of variance (ANOVA) with Microsoft Excel (Microsoft Corporation) and significance accepted at $p<0.05$. Results are presented as mean +/- SEM.

<div align="center">

Results

</div>

Absence of morphologically distinct medial (MGE) and lateral (LGE) ganglionic eminences in *ShhN/-* telencephalon

<div align="center">

10

</div>

To investigate the effect of ShhN on forebrain development, sections of control and *ShhN/-* mutant embryos in the telencephalic region were H&E stained and analyzed for morphological differences. At E9.5, we did not detect apparent external morphological abnormalities between the brains of *ShhN/-* and control embryos (Fig. 1). At E10.5, however, *ShhN/-* mutant forebrain exhibited several distinct malformations including enlarged brain ventricles and narrowed frontal nasal processes (Fig. 1C, D compared to control in Fig. 1A, B). At E10.5, the MGE is evident as a neuroepithelial eminence protruding into the lateral ventricles of control embryo telencephalon; the MGE is also a proliferative zone that later gives rise to the globus pallidus (Fig. 1B, H). Strikingly, the *ShhN/-* telencephalon failed to form MGE, but instead developed a flattened neuroepithelium (Fig. 1D, J). The LGE, a second morphologically distinct ventral structure, develops between E11.5 and E12.5 in control embryos and is situated between the cortex and MGE (Fig. 1H). No LGE bulge could be observed in E12.5 *ShhN/-* telencephalon (Fig. 1J). The loss of morphologically distinct ganglionic eminences is indicative of impaired ventral patterning in *ShhN/-* telencephalon. Notably, the *Shh*^{-/-} telencephalon also did not display any ventral structures (Fig. 1E, F, K, L). In addition to ventral defects, dorsal telencephalic midline structures such as the hippocampus (HC) primodium and choroid plexus (ChP) were also malformed in *ShhN/-* mutant (compare Fig. 1B, H with Fig. 1D, J). Interestingly, the widely separated telencephalic ventricles in *ShhN/-* clearly differed from that of *Shh*^{-/-} embryo, in which the telencephalic ventricles were fused (compare Fig. 1C with Fig. 1E), suggestive of an altered Shh signaling gradient in *ShhN/-* forebrain rather than a loss of signaling activity. Analysis of E18.5 *ShhN/-* embryos revealed several characteristics of the holoprosencephaly (HPE)-like

Figure 1. *ShhN/-* mutant forebrain displays HPE-like phenotypes

(A-F) Frontal view of control (A, B), *ShhN/-* (C, D), *Shh-/-* (E, F) forebrains at E10.5. B, D, and F represent hematoxylin and eosin-stained (H&E) coronal sections. *ShhN/-* telencephalon shows enlarged forebrain ventricles (white arrowheads in A and C) and lacks MGE bulge (black arrowheads). Additionally, frontal nasal process (fnp) is closely positioned in *ShhN/-* mutant (compare white arrows in A and C) and displays a single nasal pit (npt, black arrows in B, D). Note that ventricles of *ShhN/-* telencephalon are distinct from those of *Shh$^{-/-}$*, which are collapsed into a small ventricle (asterisk in F and K). (G-L) Sagittal view of control (G, H), *ShhN/-* (I, J), *Shh$^{-/-}$* (K, L) embryos at E12.5. H, J and L showing hematoxylin and eosin-stained sections. Enlarged forebrain (fb), midbrain (mb) and hindbrain (hb) ventricles in *ShhN/-* are clearly evident (G, I). In addition to MGE, other morphologically distinct structures such as LGE and choroids plexus (cp) are absent or defective in *ShhN/-* telecephalon (arrows and arrowheads in H, J). (M-R) E18.5 control and *ShhN/-* embryos showing frontal (M, P), coronal (N, Q) and dorsal (O, R) views. Note hypoplasia of the lower jaw (P, arrow), single nostril (P, arrowheads), absence of olfactory bulb (R, arrow) and enlarged cerebral cortex (ctx) and midbrain (R) in *ShhN/-* mutants.
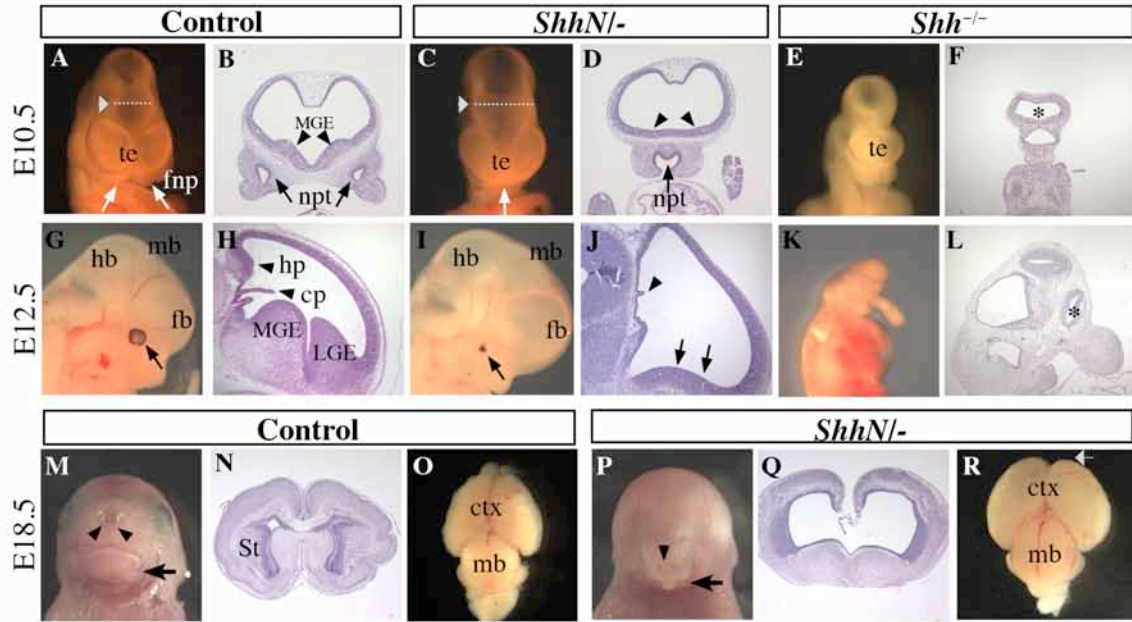
phenotype including defective eye formation, hypoplastic mid-facial structures, a single centrally located nostril and the absence of olfactory bulb in the forebrain (Fig. 1M-R).

Increased apoptosis, proliferation and reduced differentiation in *ShhN/-* telencephalon

To determine whether altered cell apoptosis and/or proliferation might contribute to the defective development of ganglionic eminences in *ShhN/-* mutants, we performed the TUNEL cell death and BrdU proliferation assays. Analysis of E11.5 embryos indicated that cell death in the Mash1+ LGE domain and the cortex of the neuroepithelial layer and its surrounding mesenchyme was increased in *ShhN/-* telencephalon compared with control (Fig. 2A, B, D, E). Intriguingly, the percentages of BrdU-positive cells in the proliferative zones of the LGE (Fig. 2H, K; 42 ± 3.7 vs 58 ± 1.8, p<0.001) and the cortex (Fig. 2I, L; 50 ± 1.8 vs 66 ± 4.7, p<0.001) were moderately increased in *ShhN/-* telencephalon, raising the possibility that this increase in cell proliferation may be attributed to exposure of neural progenitors to low level long-range Shh signaling.

We next determined whether the capacity for neural progenitor cells to proceed with differentiation is altered in *ShhN/-* mutant telencephalon. We stained *ShhN/-* and control sections with an antibody against neuronal Class III-Tubulin (Tuj1) that marks all differentiated neurons. At E11.5, Tuj1-positive cells normally consisted of a thick layer of differentiated neurons within the subventricular zone and mantle zone of MGE and LGE (Fig. 2O). However, in *ShhN/-* mutants, we observed significant reduction in the population of differentiating neurons within the presumptive LGE domain (Fig. 2T). There was no obvious difference in differentiation in the cortex and dorsal midline region

14

between control and *ShhN/-* embryos at this stage (Fig. 2P,Q, U, V). Similarly, Isl1, a ventral specific differentiation marker, also showed significant reduction in differentiation capacity of *ShhN/-* ventral neural epithelium (Fig. 2R,S, W, X). Collectively, these observations suggest that increased apoptosis and reduced neuronal differentiation contribute to the defective development of LGE in *ShhN/-* mutants.
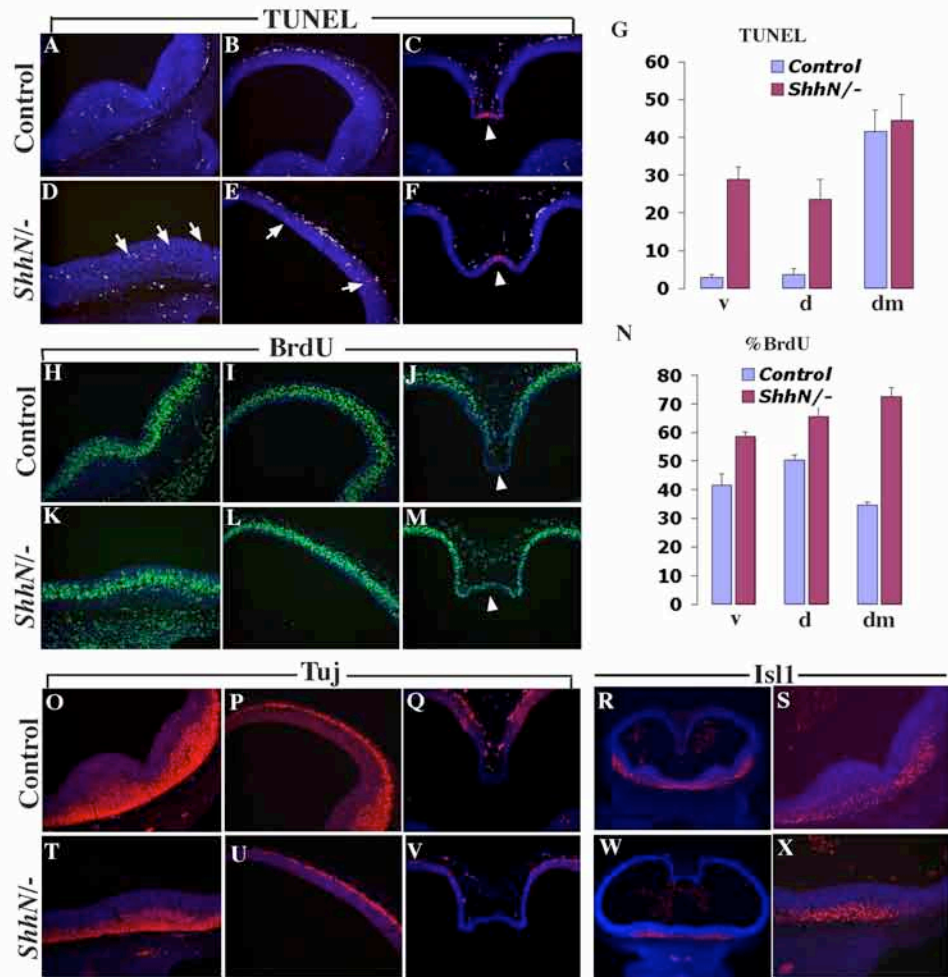
In addition to basal ganglions, dorsal midline derivatives such as the secretory epithelial cells of the choroid plexus and hippocampus primodium were also affected in *ShhN/-* (Fig. 1H, J). The rapid invagination and remodeling of the dorsal midline neuroepithelium is normally accompanied by reduced proliferation and increased cell death (Furuta et al., 1997; Nagai et al., 2000). Although cell death in the dorsal roof still occurred in *ShhN/-* (Fig. 2C, F; 41 ± 5.7 vs 44 ± 6.9, p= 0.48), we observed near 100% increase in cell proliferation in the roof and medial wall of the dorsal midline (Fig. 2J, M, arrowheads; 34.4 ± 1 vs 72 ± 3, p<0.001), suggesting that ShhN may have long-range effects on dorsal midline development. Taken together, the results indicate that the cholesterol moiety of Shh is required for normal development of both dorsal and ventral telencephalic structures.

Absence of MGE progenitors in *ShhN/-* telencephalon

To gain further insight into the effect of ShhN on telencephalic patterning, we performed molecular characterization by examining markers that are regulated by Shh signaling. *Nkx2.1* is a homeobox gene that is first detectable in the basal telencephalic neuroepithelium at three somite stage in the mouse, and subsequently Nkx2.1 expression localizes to a morphologically distinct region, the MGE (Shimamura et al., 1995). At

Figure 2. Cell proliferation, apoptosis and differentiation in *ShhN/-* telencephalon

(A-F) TUNEL analysis of sections from E11.5 wild type (A-C) and *ShhN/-* (D-F) embryos at the level of ventral (A, D), dorsal (B, E) and dorsal midline (C, F). Note that there are more apoptotic cells in ventral and dorsal regions of *ShhN/-* telencephalon (G, arrows in D and E). The number of apoptotic cells is comparable in the dorsal midline between *ShhN/-* and control (arrowheads in C and F). (H-M) Coronal sections of E11.5 control (H-J) and *ShhN/-* (K-M) telencephalon labeled with BrdU antibody. There is statistically significant increase in the percentage of BrdU-positive cells in ventral (v), dorsal (d) and dorsal midline (dm) of *ShhN/-* telencephaic neuroepithelium compared with controls (N). (O-V) Immunofluorescence of E11.5 control (O-S) and *ShhN/-* (T-X) telencephalic sections labeled with Tuj (O-Q, T-V) and Isl1 (R, S, W, X) antibodies to highlight neuronal differentiation. Note that differentiation in the ventral region is visibly reduced in *ShhN/-* neuroepithelium (compare O, R, S to T, W, X). v, Mash1+ ventral region; d, Pax6+ dorsal region; dm, dorsal midline.

TUNEL

Control

A   B   C

ShhN/-

D   E   F

G   TUNEL

BrdU

Control

H   I   J

ShhN/-

K   L   M

N   %BrdU

Tuj

Control

O   P   Q

ShhN/-

T   U   V

Isl1

Control

R   S

ShhN/-

W   X

E12.5, Nkx2.1 was uniformly expressed in the MGE of control embryo, while no Nkx2.1 protein expression could be detected in *ShhN/-* mutant telencephalon, indicating severe loss of MGE identity (Fig. 3A, B). *Mash1*, which encodes a neural basic helix-loop-helix transcription factor, is expressed in the pan-ventral telencephalic region, including the MGE and LGE (Casarosa et al., 1999; Horton et al., 1999; Lo et al., 1991). Mash1 expression in these regions is regulated by Hh signaling and marks a transient population of committed neural precursors before differentiation (Fuccillo et al., 2004). While Mash1 expression was present in both MGE and LGE of control embryos, we found that Mash1-positive cells encompassed a relatively large ventral portion of *ShhN/-* mutant telencephalon (Fig. 3E, F), indicating that LGE progenitor cells were present despite lack of development of a morphologically distinct LGE structure. Pax6 expression is normally confined to the dorsal cortical region abutting the LGE boundary (Fig. 3I). We observed prominent expansion of Pax6 expression in the ventral neuroepithelium, with reduced level in the presumptive LGE domain (Fig. 3J, arrowheads). Expanded Pax6 expression domain was observed in *Shh$^{-/-}$* mutant telencephalon, which often collapsed at this stage with no expression of ventral markers such as Mash1 and Nkx2.1 (Fig. 3D, H, L). Although these results point to a requirement of the cholesterol moiety of Shh in patterning the ventral telencephalon, the possibility remains that the expression level of *ShhN* allele is not as high as the wildtype allele, when it is expressed alone in *ShhN/-* embryos and thus generating haploinsufficiency. Because it is not possible to generate *ShhN* homozygous mutants (see Methods), we compared the patterning capacity of *Shh^{flox}* allele in which *ShhN* allele is generated upon Cre-mediated deletion of the sequence encoding the C-terminal autoprocessing domain. The protein products generated from

18

these two alleles are same with the exception of the cholesterol moiety. However, the Shh^{flox} allele is hypomorphic in that it generated a lower level of bioactive lipid-modified ShhNp protein due to interference of loxp sequence with autoprocessing of the Shh precursor (Li et al., 2006). Thus, $Shh^{flox/-}$ embryos died soon after birth with multiple defects including cleft secondary palate and distorted eye formation (data not shown), characteristics of impaired Shh signaling (Rice et al., 2004; Zhang and Yang, 2001). However, dorsal-ventral patterning of telencephalon was maintained in hypomorphic $Shh^{flox/-}$ mutants, although a reduction of the LGE domain was evident (Fig. 3C, G, K). Therefore, the severe patterning defect in $ShhN/-$ is primarily attributed to failure of cholesterol modification rather than haploinsufficiency, which is also consistent with ectopic activation of Shh pathway activity observed in the dorsal telencephalon (see below).

Widespread activation of ventral LGE marker expression in *ShhN/-* telencephalic neuroepithelium

As noted above, we observed increased cell proliferation in *ShhN/-* telencephalon at E11.5, suggestive of long-range spreading of ShhN. Indeed, we detected ectopic expression of Shh-responsive genes that mark LGE neurons in the dorsal *ShhN/-* telencephalon beginning at E13.5. Specifically, we found that Gsh2, a homeobox protein, was ectopically expressed in the dorsal midline region at E13.5 in *ShhN/-* telencephalon (Fig. 4C, Ca) compared to its normally restricted expression in the ventricular zone of control MGE and LGE (Fig. 4A, Aa). Similarly, Mash1 is also ectopically expressed at the dorsal midline (Fig, 4B, D). By E15.5, Gsh2 and Mash1 expressions were detected in

Figure 3. Absence of MGE progenitors in *ShhN/-* telencephalon

(A, B, C, D) Nkx2.1 expression in control (A), *ShhN/-* (B), *Shh$^{flox/-}$* (C), and *Shh-/-* (D) telencephalons. Nkx2.1 is an MGE marker (arrows in A points to the boundary of Nkx2.1 expression domain) and its expression maintained in *Shh$^{flox/-}$*, but lost in *ShhN/-* and *Shh-/-* telencephalons. (E, F, G, H) Mash1 expression in control (E), *ShhN/-* (F), *Shh$^{flox/-}$* (G) and *Shh$^{-/-}$* (H) telencephalons. Mash1 expression delineates the ventral region of the control telencephalon, encompassing the MGE and LGE. Mash1 expression was reduced in the LGE domain of *Shh$^{flox/-}$* when compared to control. Mash1 expression was maintained in the ventral *ShhN/-* telencephalon (arrows in D and E points to the boundary of Mash1 expression domain). No Mash1-positive cells were found in *Shh$^{-/-}$* telencephalon at this stage. (I, J, K, L) Pax6 expression in the telencephalon of control (I), *ShhN/-* (J) *Shh$^{flox/-}$* (K) and *Shh$^{-/-}$* (L). Pax6 normally marks the dorsal telencephalon with the exception of distal dorsal midline. Note that weak Pax6 expression extends to the ventral region in *ShhN/-* telencephalon (arrows in I and J points to the presumptive boundary between neocortex (ncx) and LGE). *Shh$^{flox/-}$* showed comparable Pax6 expression to that of control, while *Shh$^{-/-}$* telencephalon was completely dorsalized at this stage.
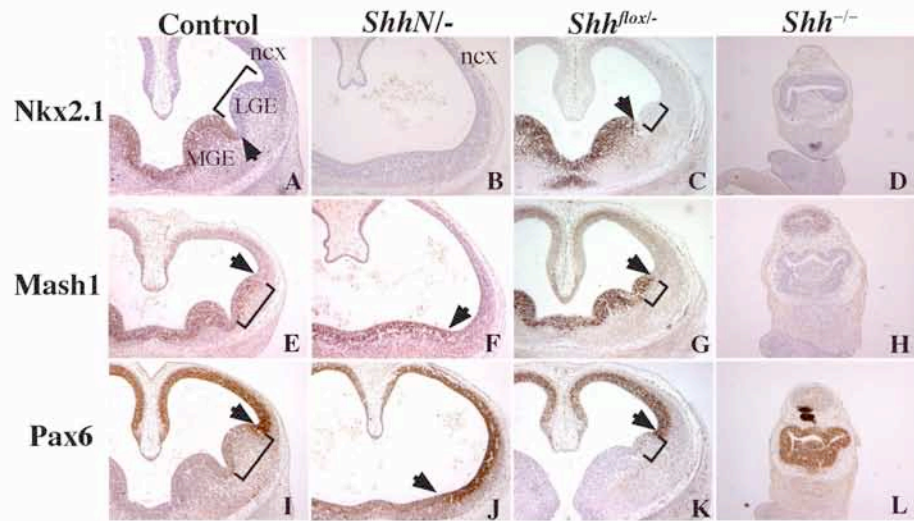
the ventricular zone of the striatum, a derivative of LGE, but not in the cortical region (Fig. 4E, Ea, F). However, in *ShhN/-*, their expressions were prominent along the dorsoventral axis of the telencephalic neuroepithelium (Fig. 4G, Ga-Gc, H, Ha-Hc). We found that the expression of *Gli3*, which encodes a zinc finger transcriptional repressor in the absence of Shh signaling, was selectively excluded from the dorsal midline in *ShhN/-* as well as control telencephalon (Figure 4 I, Ia, J, Ja). This observation is consistent with the finding that dorsal midline cells were more sensitive to the long-range patterning effect of ShhN than the lateral cortex where *Gli3* is expressed.

The emergence of ectopic LGE marker expression and defective midline dorsal structures at late gestation in *ShhN/-* are consistent with the notion that dorsal telencephalon may be exposed to low level of ectopic ShhN signal. Indeed, we detected low but consistent Shh pathway activation in the dorsal telencephalon of *ShhN/-* mutants as indicated by sensitive *Ptch1-lacZ* reporter expression (Fig. 5B), while no dorsal Shh signaling could be found in a comparable region of the control embryo (Fig. 5A). Because Shh pathway activation leads to accumulation of full length Gli3 (Gli3-190) through the inhibition of Gli3 repressor (Gli3R) formation (Litingtung et al., 2002; Wang et al., 2000), we determined the relative amount of Gli3R to Gli3-190 as another readout of Shh signaling. Consistent with widespread Ptch1 reporter expression, we observed as much as 50% reduction in Gli3R/Gli3-190 ratio in E15.5 whole brain extracts of *ShhN/-* mutants compared with controls (Fig. 5C, D). Ectopic Shh signaling is not the result of aberrant ectopic Shh expression as we did not observe Shh-expressing cells or their descendents in the dorsal telencephalon using a *Shh-Cre* transgenic line that we

22

Figure 4. Global appearance of LGE fate in *ShhN/-* telencephalic neuroepithelium at later developmental stages.

(A-D) E13.5 control (A, Aa, B) and *ShhN/-* (C, Ca, D) coronal sections immunostained with LGE marker, Gsh2 or Mash1 as indicated. Aa and Ca are higher magnification views of A and C (labeled box), respectively. (E-Hc) E15.5 control (E, Ea, F) and *ShhN/-* (G, Ga-Gc, H, Ha-c) coronal sections stained with Gsh2 or Mash1 antibody as indicated. Ea-c and Ha-c are higher magnification views of E and H (labeled box), respectively. At E13.5, ectopic Gsh2 or Mash1 expression in *ShhN/-* is restricted to the dorsal midline (Ca, D). By E15.5, ectopic LGE marker expressions were also detected in the neocortex region (Gb, Hb, arrows). (I, Ia, J, Ja) *Gli3* expression in E13.5 control and *ShhN/-* telencephalon. (I, Ia) Strong *Gli3* expression was detected in control telencephalic cortex and LGE, weak expression was present in MGE, whereas no *Gli3* expression in cortical hem and developing choroid plexus was detected. (J, Ja) *Gli3* expression was prominent along the dorsal-ventral axis of *ShhN/-* telencephalon, but selectively absent in the dorsal midline.
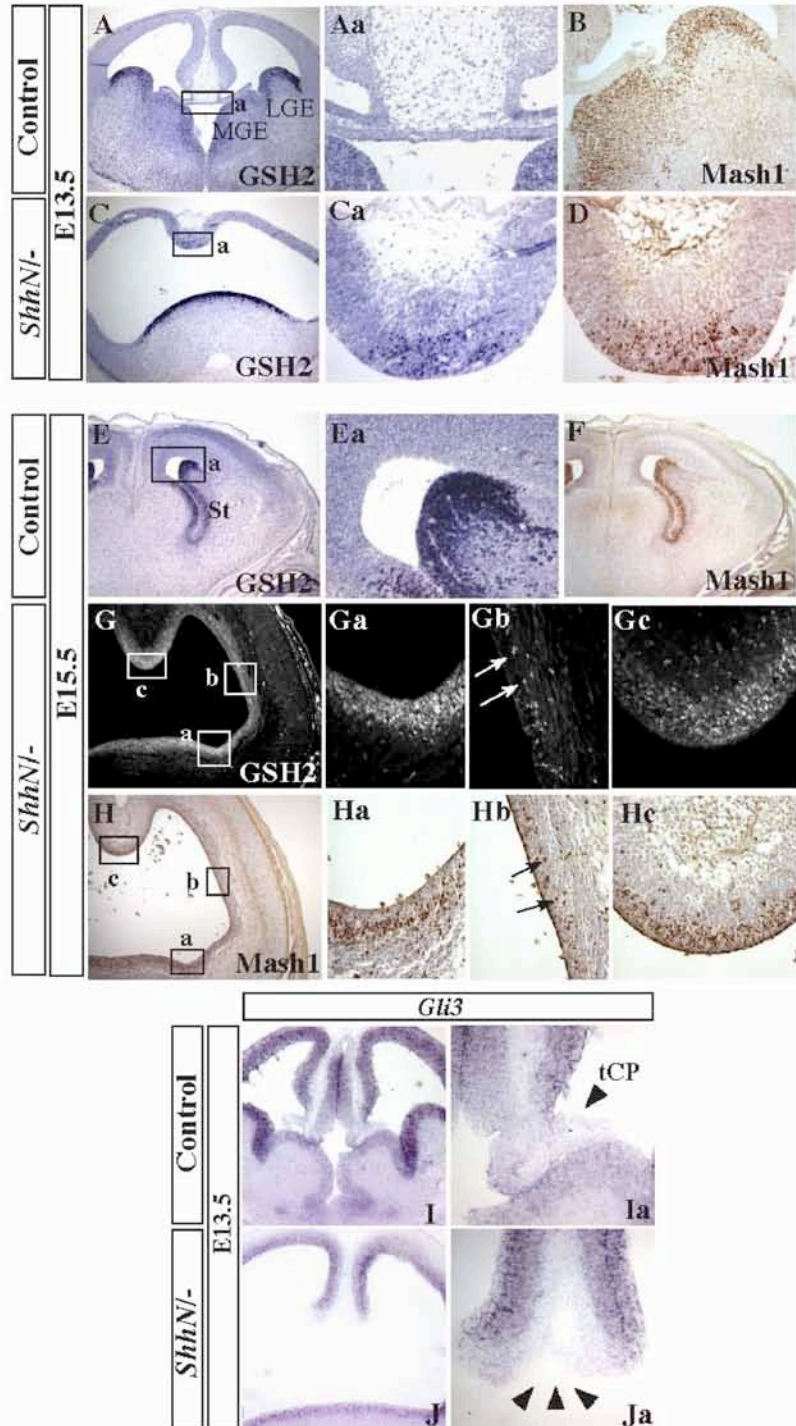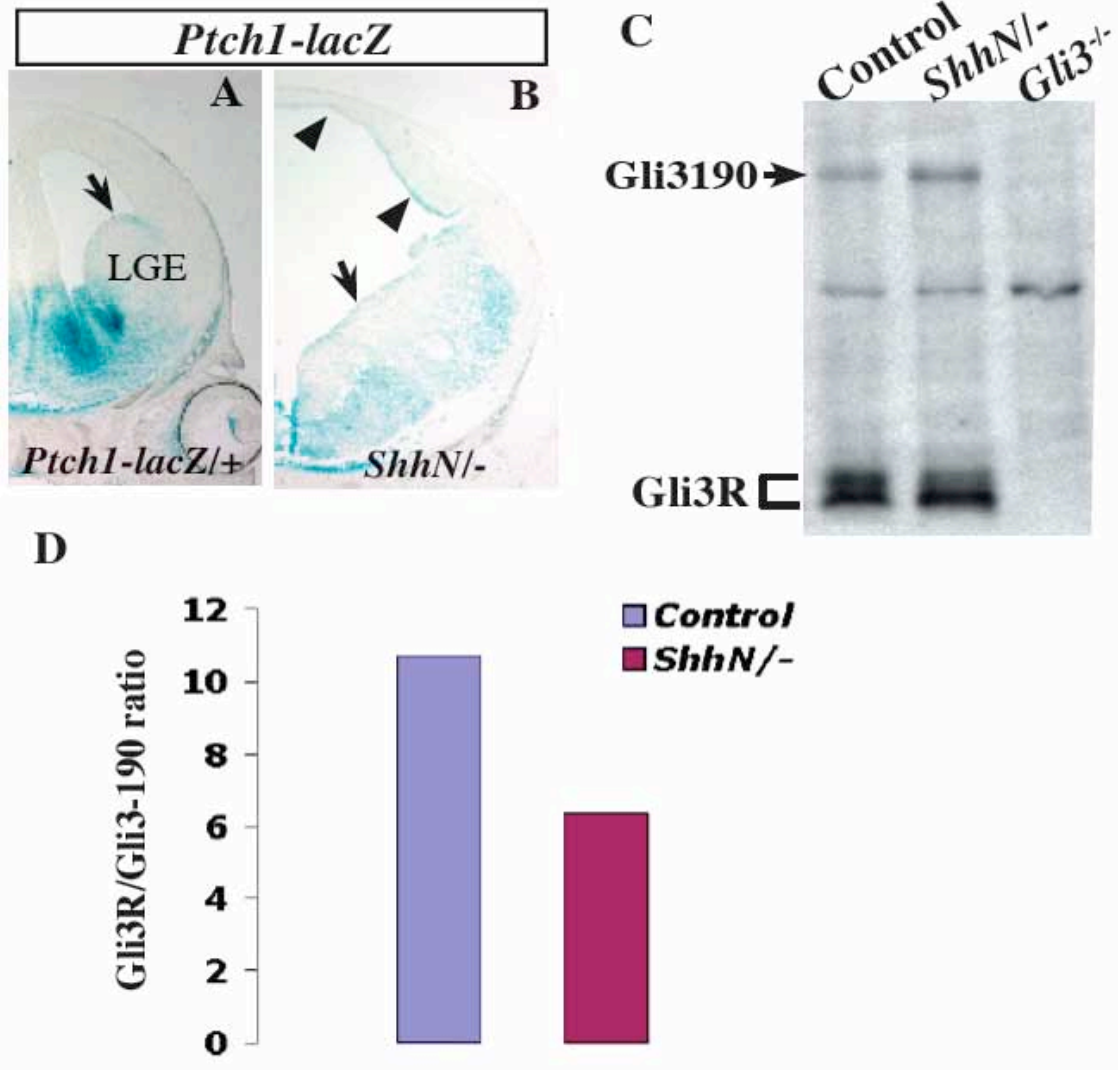
Figure 5. Ectopic activation of Shh signaling in the dorsal region of *ShhN/-* telencephalon.

(A, B) E14.5 *Ptch1-lacZ* (A) and *ShhN/-;Ptch1-lacZ* coronal sections stained with X-gal to highlight sites of Shh signaling in the telencephalon. In control embryos, lacZ expresssion is restricted to the basal ganglions, with weaker lacZ expression in the LGE domain (A, arrow). In *ShhN/-* embryos, weak lacZ expression is additionally detected at many sites in the dorsal telencephalon (B, arrowheads), consistent with ectopic LGE marker expressions. (B, C) Gli3R/Gli3190 ratio is reduced in E15.5 *ShhN/-* brain. (B) Immunoblotting of whole brain protein extracts followed by incubation with a Gli3-specific antibody recognizing full-length (Gli3-190) and repressor forms (Gli3R) of Gli3. (C) Histogram showing relative Gli3R/Gli3-190 ratio.

Ptch1-lacZ

A Ptch1-lacZ/+

LGE

B ShhN/-

C

Control   ShhN/-   Gli3⁻/⁻

Gli3190→

Gli3R

D

Gli3R/Gli3-190 ratio

12
10
8
6
4
2
0

☐ *Control*
☐ *ShhN/-*

previously reported (Li et al., 2006). Thus, it appears that the cumulative effect of long-range ectopic ShhN signaling resulted in induction of ventral marker expression in the dorsal neural progenitor population.

The cholesterol moiety is required for progenitor cell expansion but not subtype specification in the spinal cord

In order to determine whether specification of ventral cell types was similarly compromised in *ShhN/-* mutant spinal cord, as in the telencephalon, we analyzed the expression patterns of several homeodomain transcription factors that identify different cell types including neuronal progenitors in the spinal cord (Briscoe and Ericson, 2001; Jessell, 2000). Pax7 is a class I factor that is repressed by Shh and is expressed in all dorsal progenitor domains, while Nkx6.1 is a class II factor that is induced by Shh and expressed in the broad ventral progenitor domains of V2 (p2), V3 (p3) interneurons and motor neuron (pMN). Similarly, Olig2 and Nkx2.2 are class II factors that are selectively expressed in the pMN and p3 progenitors, respectively. In *ShhN/-* mutants, all ventral cell types were generated at defined locations (Fig. 6), in agreement with previously reported ShhN function in the spinal cord (Tian et al., 2005). The number of floor plate cells labeled by Foxa2 is comparable between control and *ShhN/-* embryos (Fig. 6C, D, N). However, there was an overall reduction in the total number of ventral neuronal progenitor domains and corresponding Chx10+ (V2, p=0.001), En1+ (V1, p=0.001) and Isl1+ (MN, p=0.007) neuronal subtypes which correlated with the reduced neural tube size in *ShhN/-* embryos (Fig. 6N, O). Taking into account the difference in neural tube

size at E10.5 (control spinal cord was about 44% larger than *ShhN/*), the Nkx6.1+ (p3,
pMN and p2) progenitor domains in *ShhN/-* were slightly reduced when compared to
control (M, 35 $\pm$ 3% vs 31 $\pm$ 3%, p=0.05). Notably, there is an apparent expansion of
Pax7+ progenitor domain (M, 49 $\pm$ 2% vs 63 $\pm$ 2%, p< 0.001) and concomitant reduction
of p0+p1 (V0 and V1 progenitors) progenitor domains (M, 16 $\pm$ 2% vs 6.2 $\pm$ 1%, p<
0.001). The expansion of Pax7+ domain is not a consequence of maintaining dorsal tissue
mass as a result of reduced neural tube size, as ventral expansion of dorsal progenitors
was still observed at E9.5 when *ShhN/-* spinal cord exhibited a size comparable to
control. The result indicates that although neuronal subtypes are specified and patterned
in *ShhN/-* spinal cord, the cholesterol moiety of Shh is, nevertheless, required for normal
expansion of ventral progenitors, particularly p0+p1 progenitor populations.

ShhN protein does not accumulate at its site of synthesis

We next examined *ShhN* protein distribution in the telencephalon and spinal cord at
stages when ventral neural progenitors were being specified. In the developing forebrain,
Shh expression is first detected in the dorsal foregut endoderm (also referred to as the
prechordal plate, see Shimamura et al., 1997) underlying the future telencephalic
neuroepithelium, and the ventral neuroepithelial expression of *Shh* does not occur until
the 8-somite stage (Echelard et al., 1993; Shimamura and Rubenstein, 1997a) (Fig. 7A,
C). In *ShhN/-* embryos, *Shh* RNA expression in the dorsal foregut was maintained (Fig.
7E, arrow), but its protein level was significantly reduced (Fig. 7G, arrow). Accordingly,
Shh RNA expression in the overlying neuroepithelium was nearly undetectable
(arrowheads in Fig. 7E, G). By E9.5, *Shh* expression was completely abolished, although

Figure 6. Dorsal-ventral patterning is largely unperturbed in *ShhN/-* spinal cord.

(A-L) Cross sections of E10.5 control (A, C, E, G, I, K) and *ShhN/-* (B, D, F, H, J, L) spinal cord stained with indicated markers of neural progenitors and differentiated neurons at the branchial level. Nkx6.1 is expressed in the broad ventral domains encompassing p3, pMN and p2 progenitor domains. Oligo2 is selectively expressed in the pMN progenitor domain. Pax7 is expressed in all dorsal progenitor domains. The domain that is negative for Pax7 and Nkx6.1 represents p0 and p1 progenitor domains (brackets in A, B). (M), Quantifications of Pax7, Nkx6.1 and p0+p1 progenitor domain size as a percentage of total D-V dorsal-ventral length of the neural tube. (N, L) Quantifications of total number of cells in the FP (Foxa2+), pMN (Olig2+), p3 (Nkx2.2), MN (Isl1+), V2 (Chx10 +) and V1 (En1+) domains.
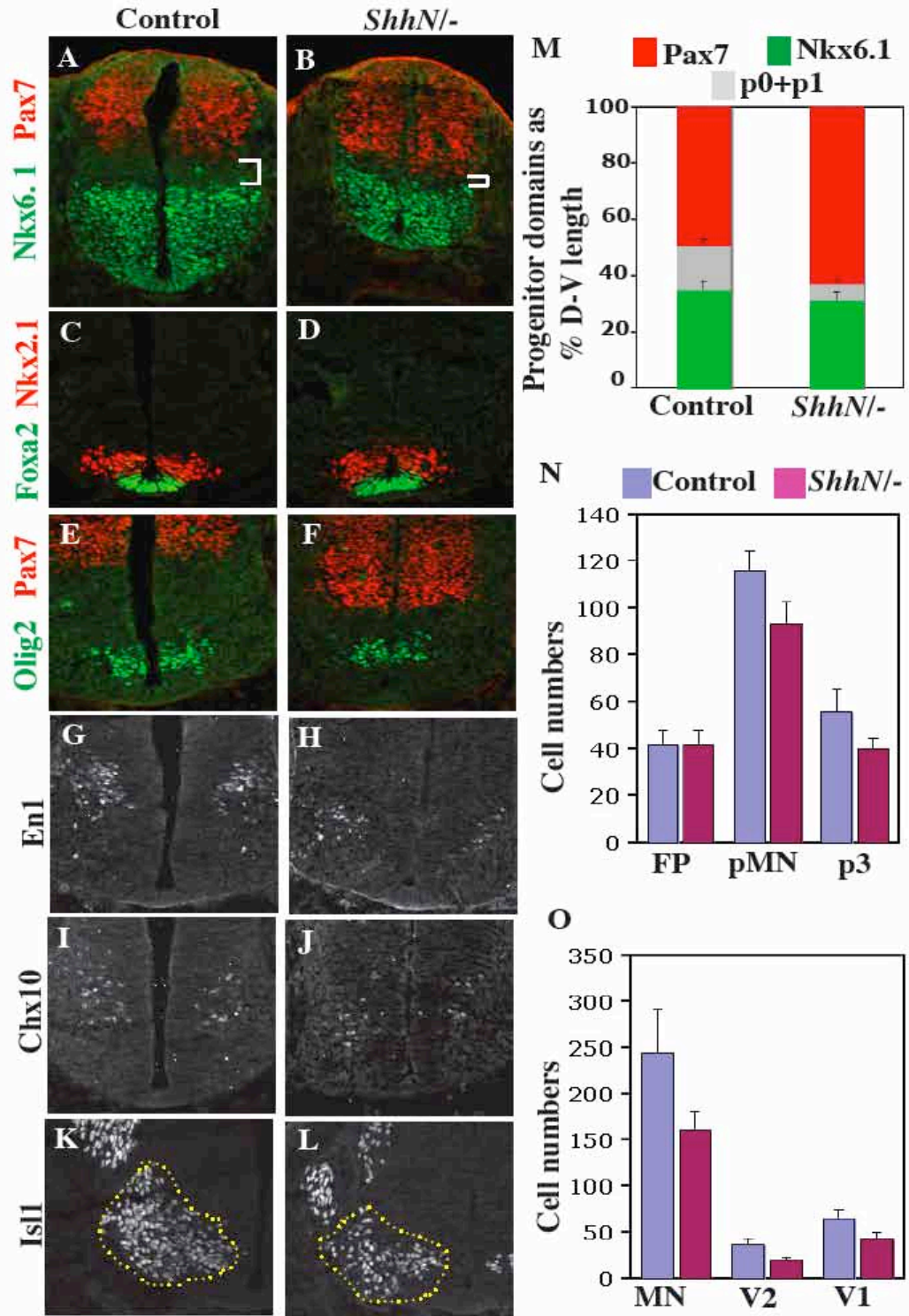
its expression in other regions of the brain was maintained (Fig. 7B, F). Similarly, we failed to detect ShhN protein signal in *ShhN/-* ventral telencephalon while Shh protein signal was always observed in the midline of control embryos (Fig. 7D, H). As expected, Nkx2.1 expression which overlapped with Shh expression in the ventral telencephalon was not observed (Fig. 7I, M). The expression of *Ptch1*, a downstream target of Shh signaling (Goodrich et al., 1996), was also severely compromised in this region (Fig. 7J, N). In contrast to the telencephalon, *Shh* transcript and ShhN protein expression in the floor plate and notochord at E10.5 were clearly detectable, but ShhN protein level was significantly reduced (Fig. 7K, L, O, P). Interestingly, ShhN protein predominantly localized to the apical membrane of floor plate cells (arrowheads in Fig. 7P), whereas ShhNp protein localized to both apical and basolateral membranes. This observation is in agreement with a recent study in *Drosophila* where Hh-N accumulated only at the apical membrane (Callejo et al., 2006). Intriguingly, we found that ShhNp protein was distributed along the cell membrane of ependymal cells (Fig. 7L, arrows), which line the central canal of the spinal cord. By contrast, we never observed ependymal localization of ShhN in the mutant spinal cord. It is possible that this ependymal cell layer represents an active site where ShhNp is normally concentrated and perceived for proper expansion of ventral progenitor populations. Thus, the results suggest that ShhN has propensity to spread away from its site of synthesis at the expense of its local concentration similar to that observed in the limb bud (Li et al., 2006). As Shh expression in the ventral telencephalon is induced by the underlying prechordal plate (Ericson et al., 1995; Shimamura and Rubenstein, 1997a), the ventral patterning defects observed in *ShhN/-* telencephalon are likely attributed to the inability of telencephalic neuroepithelium to

31

establish *Shh* expression in response to altered Shh spreading behavior in the prechordal plate.

ShhN rescues spinal cord, but not telencephalon, patterning in *mDispA-/-;ShhN/+* embryos

To confirm that the differential effects of ShhN on the development of the telencephalon and spinal cord were primarily mediated by paracrine signaling, we examined the patterning effects of ShhN in m*Disp1*$^{-/-}$ background, in which all Shh paracrine activities are elicited by ShhN since ShhNp is retained in Shh-producing cells. *mDispA*$^{-/-}$ single mutants normally die at or prior to E9.5 with phenotype resembling *Smo*$^{-/-}$ embryos (Caspary et al., 2002; Kawakami et al., 2002; Ma et al., 2002). However, the gross morphology of *mDisp1*$^{-/-}$*;ShhN/+* embryos largely resembled that of *ShhN/-* embryos with enlarged brain ventricles, closely positioned frontal nasal process and defective eye formation (Fig. 8B). As expected, we observed unperturbed dorsoventral neuronal patterning in E10.5 *mDispA*$^{-/-}$*;ShhN/+* spinal cord, as demonstrated by well-defined dorsal Pax7 and ventral Nkx6.1 marker expressions (Fig. 8G). Notably, we found an expanded pool of floor plate cells in *mDisp1*$^{-/-}$*;ShhN/+* spinal cord that often co-expressed V3 interneuron marker, Nkx2.2, and floor plate marker, Foxa2 (Fig. 8H-J). This is consistent with the notion that ShhN protein is capable of inducing floor plate formation and ShhNp cannot travel beyond the floor plate in the absence of mDisp1 function, resulting in elevated local concentration of Shh in the floor plate region (Fig. 8F, note the robust floor plate Shh staining and the absence of ependymal Shh staining which differ from that of control and *ShhN/-* embryos)

32

Figure 7. Expression of Shh RNA, protein and target genes in *ShhN/-* neural tube.

(A-H) Comparison of Shh RNA and protein expressions in control and *ShhN/-* forebrains. At 9-somite stage, *Shh* expression can be detected in the forebrain neuroepitehium (arrowheads in A, E) and the underlying dorsal foregut endoderm (arrows). Note that *Shh* RNA expression is selectively lost in *ShhN/-* telencephalon (arrowheads in E, F). Similarly, Shh protein is also undetectable in the ventral *ShhN/-* telencephalon (H, arrowhead in G), while protein expression in the dorsal foregut is significantly reduced at 8-somite stage (G, arrow). (D, E, K, L) *Nkx2.1* and *Ptch1* expressions in control and *ShhN/-* forebrain at E9.5. (K, L, O, P) Comparison of Shh RNA and protein expressions in control and *ShhN/-* spinal cord at E10.5. Shh protein is detected in both the basal and apical surfaces of the floor plate as well as ependymal cells that line the central canal of the neural tube (L, arrows). However, in *ShhN/-*, Shh protein resides exclusively at the apical compartment of floor plate cells (arrowheads in P) and does not accumulate at the ependymal cell surface.

34
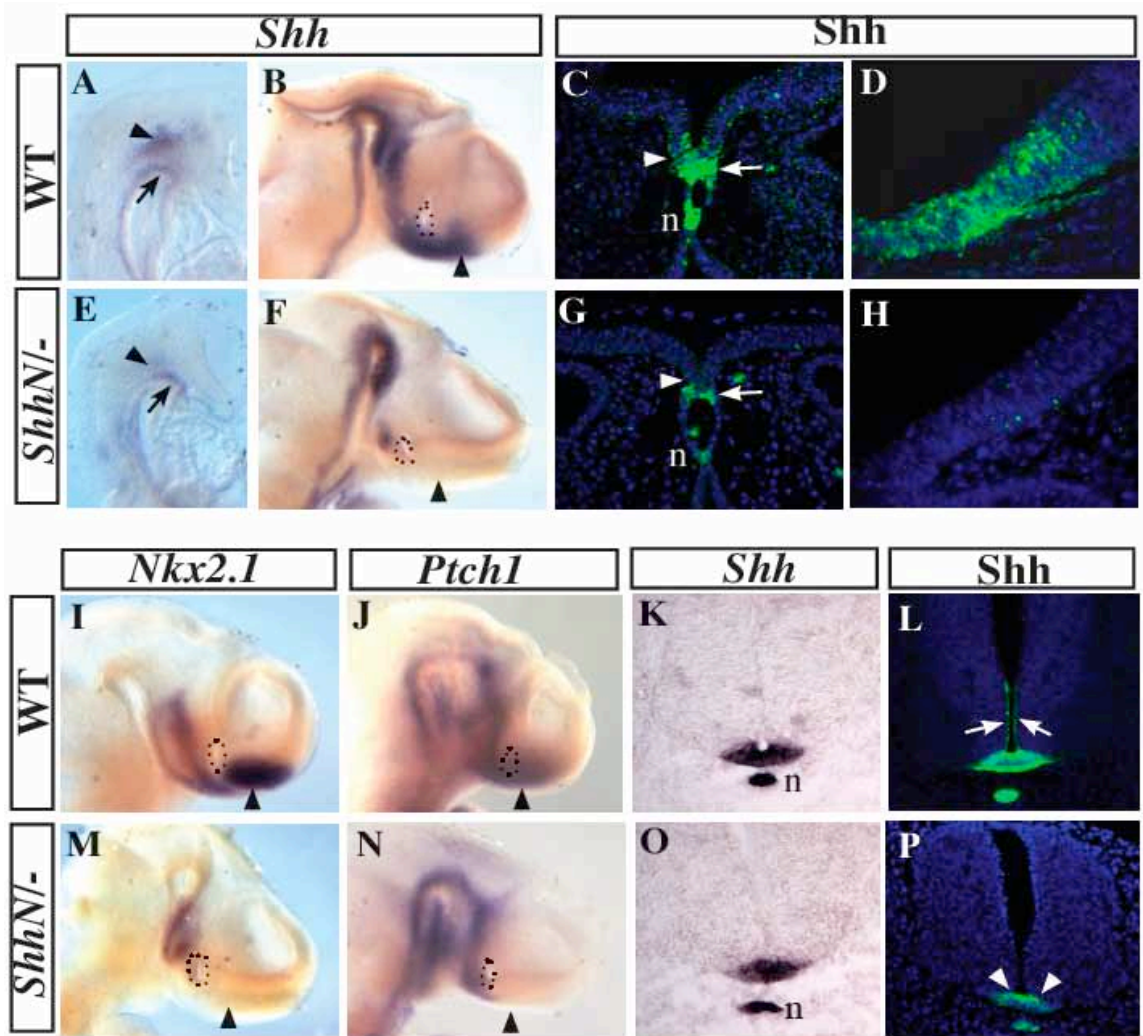
By contrast, *mDisp1⁻ᐟ⁻;ShhN/+* telencephalon showed patterning defects similar to that of *ShhN/-* embryos at E12.5, with the absence of MGE neurons and ventral expansion of dorsal marker Pax6 (Fig. 8C-E), commensurate with the absence of Shh protein in the telencephalon (Fig. 8A). The above results support the notion that there is a more stringent requirement for cholesterol-modified Shh in patterning the ventral telencephalon.
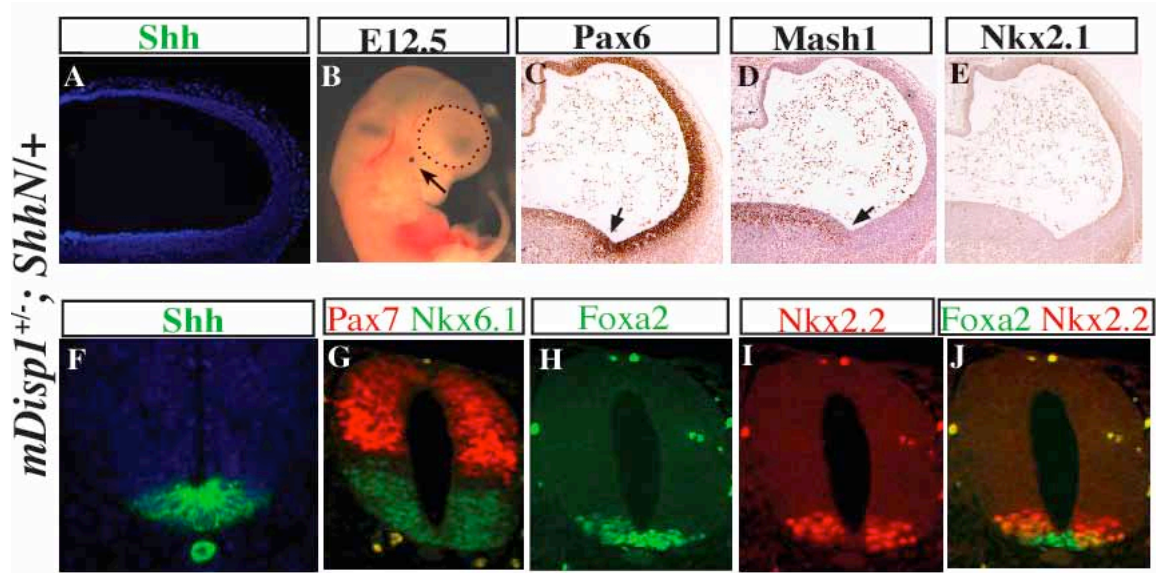
Discussion

To our knowledge, Shh is the only metazoan protein that has been shown to be covalently modified by a cholesterol moiety. To fully appreciate the biological function of this post-translational event, it is important to understand not only the role of cholesterol in regulating Shh protein trafficking, but also the tissue-specific requirement of this cholesterol adduct. This study indicates that cholesterol modification of Shh is required for patterning the telencephalon. In *ShhN/-* telencephalon, induction of ventral and dorsal anatomical structures and their corresponding cellular and molecular identities were significantly impaired. By contrast, Shh activity is not required for the generation of different ventral neuronal cell types in the spinal cord, although it is required for the full expansion of ventral progenitor domains. Thus, alteration of Shh local concentration and spreading behavior resulted in more profound effects on the development of the telencephalon than the spinal cord.

Enlarged brain ventricles in *ShhN/-* mutant

Figure 8. ShhN rescues patterning defects in the spinal cord but not in the telencephalon of *mDispA-/-* embryos.

(A-E) The *mDispA⁻ᐟ⁻;ShhN/+* mutant telencephalon shows characteristics similar to those of the *ShhN/-* telencephalon, including absence of Shh (A) and Nkx2.1 (E) expressions, enlarged forebrain ventricles (B, dotted circle), reduced eye (B, arrow), ventrally extended Pax6 expression (C), presence of Mash 1 expression (D). Arrows in C and D mark the presumptive boundary between LGE and cortex. (F) Robust Shh protein signal is visualized in notochord and floor plate; note the absence of ependymal cell Shh protein staining. (G-J) Dorsal-ventral patterning is established in *mDispA⁻ᐟ⁻;ShhN/+* mutant spinal cord, as demonstrated by defined expression domains of Pax7 and Nkx6.1 (G). Note the presence of V3 interneuron by Nkx2.2 staining (I) and the expanded pool of floor plate cells (H).

Shh	**E12.5**	**Pax6**	**Mash1**	**Nkx2.1**
A	B	C	D	E

mDisp1⁺ᐟ⁻; ShhN/+

Shh	**Pax7 Nkx6.1**	**Foxa2**	**Nkx2.2**	**Foxa2 Nkx2.2**
F	G	H	I	J

One of the characteristic features in early development of the vertebrate brain is the appearance of brain ventricles. Generating a uniform and coordinated outgrowth of neuroepithelium from the neural tube involves balanced cell proliferation, apoptosis and differentiation. Previous studies provided evidence that Shh is an essential player to initiate and maintain ventricle expansion (Britto et al., 2002). Ablating Shh signaling by removing notochord resulted in elevated apoptosis and significantly reduced cell proliferation throughout the neuroepithelium of the developing avian midbrain and forebrain (Britto et al., 2002). This growth retardation resulted in a collapse of the telencephalon and metencephalon ventricles. Furthermore, gradual blockade of Shh signaling with increasing amount of cyclopamine led to progressive brain collapse associated with defective cell proliferation and massive apoptosis (Cooper et al., 1998). $Shh^{-/-}$ forebrain development was also severely affected and developed into one fused ventricle (Chiang et al., 1996). In contrast to reduced or collapsed brain ventricles associated with a reduction or absence of Shh signaling, *ShhN/-* embryos showed enlarged forebrain ventricles which were more evident at later stages of development, where ectopic activation of Shh signaling was detectable. This observation suggested that the cholesterol moiety of Shh plays a key role in maintaining forebrain ventricle expansion by regulating the range of Shh spreading.

Temporal dependence of ectopic signaling mediated by ShhN

The ability of ShhN to enhance dorsal midline cell proliferation and elicit ectopic Shh-responsive gene expressions in the dorsal telencephalon is consistent with the capacity of ShhN to spread long range. However, the induction of these genes can only

be detected beginning at E13.5, suggesting that either dorsal telencephalon is incompetent to receive ShhN signal or long-range ShhN concentration is below the threshold for target gene expressions at earlier stages. We favor the latter possibility, as previous neural explant studies showed that the competence to receive Shh signal in the dorsal telencephalon was diminished by E11.5 (Kohtz et al., 1998). Interpretation of a morphogen signal by responding cells is achieved by the signaling intensity, which is conveyed by the concentration of ligand, and duration of exposure. (Gurdon and Bourillot, 2001). Long-lasting residence of ligand-receptor signaling complex has been shown to lead to prolonged signaling event in activin-dependent TGF-β signaling (Jullien and Gurdon, 2005). Interestingly, the activated form of Smoothened, a seven-pass transmembrane receptor that activates downstream effectors of the Shh pathway, is internalized in a Shh-dependent manner (Chen et al., 2004b). Recent time-course analysis suggested that spinal cord progenitor cells could integrate the level of signaling over time, providing evidence that in addition to signaling strength, the signaling duration is another important parameter to control dorsal-ventral patterning of the spinal cord (Stamataki et al., 2005). Therefore, we speculate that prolonged exposure of telencephalic neuroepithelium to ShhN has a cumulative effect on mediating gradual deposition of activated Smoothened intracellularly, which may in turn lead to widespread expression of Shh-responsive genes such as *Gsh2* and *Mash1* in *ShhN/-* telencephalic neuroepithelium at later stages.

Regulation of long-range spreading of Shh by its cholesterol moiety in the neural tube

39

While the mechanism of Shh spreading is not well understood, lipid-dependent Hh multimers have been proposed to regulate Hh spreading by interacting with extracellular matrix molecules such as heparan sulfate proteoglycans (HSPG) (Callejo et al., 2006). Furthermore, Hedgehog-interacting protein (Hip), a membrane glycoprotein, can bind to Shh thereby inhibiting its spread (Chuang et al., 2003; Chuang and McMahon, 1999). A recent mathematical model for Shh signaling dynamics predicted that the restrictive effect of these Shh interacting molecules lowers the diffusion constant and concentrate the ligand near its secreting source (Saha and Schaffer, 2006). It is therefore possible that ShhN protein can escape the synergistic regulatory mechanisms exerted by Shh interacting molecules, generating a high diffusion rate as predicted by the recent model (Saha and Schaffer, 2006). Given that ShhN transcript is undetectable in the ventral telencephalon and that ShhN would have to traverse across the neural epithelium, a relatively long distance, to activate Shh-responsive gene expressions extending to the dorsal midline, we favor the idea that ShhN could spread into the subjacent cerebrospinal fluid (CSF) from its site of synthesis in the neural tube. This proposition is analogous to the situation where Hh-N is expressed from peripodial cells of the wing imaginal disc, in which Hh-N was proposed to be secreted into the lumen and activate low threshold target genes as it accumulates near the apical surface (Gallet et al., 2006).

Diffusive molecules and proteins of the CSF can play critical roles in regulating neuroepithelial cell behavior and it has been shown that CSF promotes neuroepithelial cell survival, proliferation and neurogenesis in mesencephalic explants (Gato et al., 2005; Parada et al., 2005). Recent studies have suggested that the Slit family of chemorepulsive proteins may be secreted in the CSF to generate a cilia-dependent concentration gradient

40

necessary for vectorial migration of neuroblasts in the brain (Sawamoto et al., 2006). In this context, it is interesting to note that Shh-expressing Cos cells implanted within the lumen of the midbrain can rescue normal midbrain expansion defects generated by extirpation of the notochord, suggesting that the precise source of Shh signaling activity is not critical for normal morphogenesis of early brain ventricles (Britto et al., 2002). Furthermore, we found that ventral spinal cord ependymal cells may be an important site at which ShhNp protein concentrates and/or through which it travels. Intriguingly, by immunostaining, we found that ShhNp protein can be visualized along the apical side of the innermost ventricular zone neuroepithelial cells as early as E9.5. Although the significance of apical surface neuroepithelial expression is not clear, the fact that this pattern is absent in ShhN mutant suggests that it may be required for expansion of ventral progenitor domains. Recent studies in the chick spinal cord have also reported similar apical surface neuroepithelial expression at the onset of oligodendrogenesis suggesting a role of ShhNp in the expansion of oligodendrocyte precursors (Danesin et al., 2006). We envision two possible explanations for how Shh is localized to this region; one is that a significant amount of Shh protein can travel in a planar direction through the innermost neuroepithelial cell layer, and subsequently spread laterally into the ventricular zone to establish different neuronal progenitor identities. Alternatively, it is possible that ShhNp protein from the floor plate is secreted into the CSF, and ShhNp receptors that reside on the apical membrane of neuroepihelial cells function to concentrate and endocytose ShhNp from the CSF. These two tentative explanations are not mutually exclusive. Megalin, or LRP2, is a member of the low density lipoprotein (LDL) receptor-related protein family. Megalin function is essential for forebrain formation and its abundant

expression at the apical surface of the CNS neuroepithelium at midgestation is very similar to ShhNp expression, notably at the apical surface of neuroepithelial cells (Assemat et al., 2005; Willnow et al., 1996). A mechanism has been proposed in which Megalin is required to supply sufficient cholesterol to the rapidly dividing neuroepithelium before neural tube closure, possibly through the endocytosis of cholesterol-containing lipoprotein (Herz et al., 1997). Since it has been shown in tissue culture studies that Megalin could function as an endocytic Shh receptor (McCarthy et al., 2002), it is possible that Megalin has a direct role in propagating Shh signaling. Another endocytic receptor, Cubulin, an EGF-CUB protein, has a nearly identical apical surface neuroepithelial expression pattern as Megalin (Assemat et al., 2005). Interestingly, a Cubulin-related protein encoded by Zebrafish *Scube 2* gene has been shown to mediate Shh signaling in embryos (Hollway et al., 2006; Woods and Talbot, 2005). Therefore, it is possible that these two proteins act synergistically in promoting Shh signaling during mammalian development. It would be interesting to investigate the functional relationship of Shh, Megalin and Cubulin in ependymal cells and the existence of secreted Shh protein in the CSF.

Region-specific effects of ShhN in patterning the neural epithelium

Our study suggests that alteration of Shh spreading behavior has differential effects in patterning the telencephalon versus spinal cord. This is most likely attributed to regional differences in the generation and maintenance of *Shh* expression in the neuroepithelium. In the spinal cord, the development of ventral progenitor cells is mediated by Shh secreted from the notochord and floor plate (Jessell, 2000). *Shh*

expression in the floor plate is induced and maintained by the notochord which is in close contact with the overlying spinal cord for an extended period of time. In the telencephalon, the development of basal ganglia appears to be mediated initially by Shh secreted from the prechordal plate (the dorsal foregut) and then by the ventral neuroepithelium (Ericson et al., 1995; Shimamura and Rubenstein, 1997a). In contrast to the floor plate, *Shh* expression in the ventral telencephalic neuroepithelium becomes quickly independent of the influence of the underlying prechordal plate. Thus, reduction of local Shh concentration in the prechordal plate and notochord, as shown in *ShhN/-* embryos, would have more profound effects on *Shh* expression and maintenance in the telencephalon than in the spinal cord.

An unexpected finding is that ShhN exerted no effect on dorsal progenitors since there was no evidence of expansion or ectopic ventral progenitor cell fates in the dorsal region of the spinal cord. This observation is in contrast to findings in the telencephalon and limb buds (Li et al., 2006), where ectopic Shh pathway activation was detected far from the source of ShhN synthesis. There are at least two possible explanations for this difference that are not mutually exclusive. First, temporal responsiveness to ectopic ShhN may be different between dorsal telencephalon and dorsal spinal cord. Neural explant studies in rats indicated that E11.5 dorsal telencephalon (~ E10.5 in mouse) remained competent to receive exogenous Shh stimulation (Kohtz et al., 1998), whereas E11 (~E10 in mouse) spinal cord did not demonstrate such competence (Charron et al., 2003). Likewise, the spinal cord may have lost competence to respond to ectopic ShhN by the time the signal reaches a threshold concentration necessary for cell fate specification.

Alternatively, the concentration threshold required for ShhN to elicit ectopic patterning effects in the dorsal spinal cord is higher than the dorsal telencephalon.

CHAPTER III

ECTOPIC SONIC HEDGEHOG SIGNALING IMPAIRS MOUSE TELENCEPHALIC

DORSAL MIDLINE DEVELOPMENT: IMPLICATION FOR HUMAN

HOLOPROSENCEPHALY

Introduction

The telencephalon, the most anterior portion of the developing neural tube, can be

generalized into two subdivisions, the pallium and subpallium. Secreted molecules

generated by patterning centers extending from the embryonic telencephalic midline

induce and maintain the molecular identities of each subdivision (Campbell, 2003; Grove

and Fukuchi-Shimogori, 2003; Sur and Rubenstein, 2005). Within the subpallium,

development of the medial ganglionic eminence (MGE) and lateral ganglionic eminence

(LGE), which largely make up the anlage of the basal ganglia, requires Shh secreted

initially from the prechordal plate and subsequently from the ventral telencephalic

midline (Chiang et al., 1996; Rallu et al., 2002; Shimamura and Rubenstein, 1997b). Loss

of Shh signaling in these ventral patterning centers leads to impaired ganglionic eminence

development at the expense of dorsal cell types (Rallu et al., 2002), whereas ectopic Shh

signaling in the cortex can induce ventral telencephalic marker gene expressions (Gaiano

et al., 1999; Kohtz et al., 2001). The roof plate is a dorsal patterning center that organizes

the development of the dorsal and medium pallium, including the hippocampus and

choroid plexus (Monuki and Walsh, 2001). The BMP subfamily of the TGFβ superfamily

45

plays a critical role in patterning the dorsal neural tube (Lee and Jessell, 1999). Multiple *Bmp* genes are expressed in the roof plate of the telencephalon (Furuta et al., 1997) and mice deficient in type I Bmp receptor BmprIa or with ablation of Gdf7 (Bmp12)-expressing cells display abnormal choroid plexus development (Currle et al., 2005; Hebert et al., 2002), consistent with a primary role of Bmps in dorsal telencephalic patterning. The Wnt-rich cortical hem lying dorsal to the choroid plexus and ventral to the hippocampus has been proposed to provide patterning cues to both the developing hippocampus and choroid plexus (Shimogori et al., 2004). Targeted inactivation of *Wnt3a*, or the downstream Wnt signaling co-factor *Lef-1*, severely impairs hippocampal development (Galceran et al., 2000; Lee et al., 2000b), whereas early inactivation of β-catenin, a key mediator of canonical Wnt signaling in the telencephalon, leads to disrupted growth of the hippocampus and choroid plexus (Backman et al., 2005). The current model suggests that Fgf8 expressed in the anterior margin of the telencephalon functions to coordinate the cross-regulation between dorsal and ventral patterning centers. Specifically, ventrally-derived Shh promotes and maintains the proper dose of Fgf8 signaling, which in turn maintains a balance of dorsally-derived Bmp and Wnt signalings to modulate telencephalic outgrowth and patterning (Storm et al., 2006; Sur and Rubenstein, 2005).

Holoprosencephaly (HPE) is the most common developmental anomaly of the human forebrain, and in its severe form, the cerebral hemispheres fail to separate into two distinct halves (Cohen, 2006; Hayhurst and McConnell, 2003; Kinsman et al., 2000). It is thought that disturbance of ventral forebrain induction underlies the disruption of hemispheric bifurcation. Consistent with this model, human patient studies have

identified a battery of mutations involved in the SHH and NODAL signaling pathways, both of which are required for proper ventral forebrain patterning (Cohen, 2006; Muenke and Beachy, 2000). However, these studies do not explain the observation that some HPE patients suffer from failure of hemispheric division yet have relatively normal ventral brain structures, notably those with a condition known as Middle Interhemispheric Holoprosencephaly (MIH), a recognizable variant of HPE with differing clinical prognosis (Barkovich and Quint, 1993; Lewis et al., 2002; Pulitzer et al., 2004; Simon et al., 2002). Since mutation in human ZIC2, a zinc finger protein homologous to *Drosophila* odd-paired, has been identified in one MIH patient and knockdown of mouse *Zic2* expression leads to deregulation of roof plate cell proliferation and apoptosis (Brown et al., 2001; Nagai et al., 2000), ZIC2 mutations have been generally associated with the MIH syndrome (Simon et al., 2002). However, predominantly, ZIC2 mutations are associated with classical HPE (Brown et al., 2001), and given the heterogeneity of MIH and the lack of Zic2 mutations in many MIH patients, it is unlikely that ZIC2 mutations underlie the etiology of MIH in many patients.

We have previously generated mice expressing non-cholesterol-modified Shh (ShhN) and demonstrated that ShhN can spread far from its site of synthesis to elicit ectopic Shh pathway activation in the limb bud (Li et al., 2006). In this study, we show that persistent ectopic ShhN signaling in the dorsal telencephalon severely alters Bmp and Wnt signalings from dorsal patterning centers that are crucial for proper dorsal midline development, resulting in altered behavior of roof plate cells and impaired roof plate invagination. Hence, the cortical hem does not form and development of the choroid plexus and hippocampus is severely disrupted. Strikingly, we found that *ShhN/+* mice

exhibited a spectrum of phenotypic features such as partial division of cerebral hemispheres, hydrocephalus and cleft palate while their external craniofacial features were largely unaffected. All of these characteristics were observed in a human patient with milder HPE and predicted to produce SHHN protein due to a truncation mutation in one SHH allele. Thus, our results suggest a novel mechanism by which ectopic Shh signaling impairs dorsal forebrain development, resulting in non-cleavage of midline structures. Additionally, our study may shed light on the molecular pathogenesis of MIH, a variant of HPE that preferentially shows disruption of telencephalic dorsal midline structures.

Experimental procedures

Mice

Generation of embryos expressing ShhN was carried out by mating $Shh^{flox/+}$ animals with *Sox2-Cre* deleter strain as previously described (Li et al., 2006). *Sox2-Cre* (Hayashi et al., 2002), TOPGAL (DasGupta and Fuchs, 1999) and $Ptch1^{lacZ}$ mice (Goodrich et al., 1997) were obtained from the Jackson Laboratory. $Bmp4^{lacZ}$ mice were kindly provided by Brigid Hogan. The perinatal death of $Shh^{flox/flox}$, *ShhN/+* and *ShhN/-* mice precludes analysis of *ShhN/N* phenotype. Three to six embryos from wildtype and *ShhN/+* were used for each morphological/molecular analysis shown in each figure.

Immunohistochemistry and Western analysis

All immunohistochemistry analyses were performed on tissue sections collected from OCT- or paraffin-embedded embryos as previously described (Li et al., 2006). The primary antibodies were mouse anti-Pax6, (DSHB, 1:1), mouse anti-Nkx2.1, (Neomarkers, 1:100), mouse anti-Mash1 (gift of Jane Johnson, 1:100), goat anti-Shh (Santa Cruz Biotechnology, 1:1000), rabbit anti-phospho-Smad1/5/8 (gift of Tom Jessell and Ed Laufer, 1:1000), rabbit anti-Gsh2 (Kenneth Campbell, 1:1000), rabbit anti-Prox1 (Axxora, 1:500), mouse anti-Lhx1/5 (DSHB, 1: 10) Since Lhx1 is not expressed in the telencephalon at early stages (71), the staining pattern shown in Figure 1 revealed Lhx5 expression pattern. For Western analysis, protein lysate samples, 200ug each, collected from E13.5 whole brains, were resolved on 6% SDS-polyacrylamide gels. Gli3-190 and Gli3R species were detected by using a Gli3 N-terminal specific antibody as described (Litingtung et al., 2002).

Analysis of cell proliferation and apoptosis

5-BromodeoxyUridine (BrdU) in vivo labeling and TUNEL analysis were performed as previously described (Li et al., 2004). For statistical analysis, three embryos from either wildtype or *ShhN/+* were used to perform BrdU and TUNEL analyses at each developmental stage. At least five stained-sections were randomly selected and counted for each genotype to generate the proliferation and cell death indices shown in Fig. 1. To assess differences among groups, statistical analyses were performed using a one-way analysis of variance (ANOVA) with Microsoft Excel (Microsoft Corporation) and significance accepted at $p < 0.05$. Results are presented as mean +/- SEM.

X-gal staining and transcript detection

X-gal staining for ß-galactosidase was performed according to standard protocol. Whole-mount and section in situ hybridizations were performed as described (Li et al., 2004). The following cDNAs were used as templates for synthesizing digoxygenin-labeled riboprobes: *Shh*, *Lhx5* (H. Westphal, NIH), *Bmp4* (S. Lee, Johns Hopkins), *Bmp7* (E. Robertson, University of Oxford), *Msx1* (R. Mason, University of North Carolina), *Wnt3a* (Image 426103), *Wnt5a* (A. McMahon, Harvard University), *Wnt2b* (L. Zakin, Pasteur Institute), *Lef1* (R. Grossehedl, University of California San Francisco), *Fgf8* (G. Martin, University of California San Francisco), *Foxg1* (E. Lai, Cornell University), *Emx2* (A. Simeone, European School of Molecular Medicine), Ttr (EST#1078224, ATCC).

Skeletal preparation

Cartilage and bones were stained with Alcian blue and Alizarin red as described (Li et al., 2006).

Results

***ShhN/+* telencephalon displays early morphological defects**

Starting from E10.5, *ShhN/+* embryos exhibited several distinct morphological differences compared to wildtype, such as enlarged brain ventricles and widely separated telencephalic ventricles (Fig. 9A, A$^{/}$, C, C$^{/}$). H&E stained coronal sections of E10.5 telencephalon revealed that *ShhN/+* dorsal midline failed to invaginate, which is apparent

in wildtype. In contrast, development of the ventral medial ganglionic eminence, MGE, was morphologically comparable at this stage between wildtype and *ShhN/+* (Fig. 9B, B$^/$). At E12.5, *ShhN/+* telencephalon lacked the characteristic thickened hippocampal neuroepithelium found in the dorsal midline (Fig. 9D, D$^/$). In addition to MGE and LGE at their respective locations, the appearance of a third eminence with LGE character was evident in the mutant (labeled as ** in Fig. 9D$^/$, see below).

ShhN/+ telencephalic roof plate displays increased proliferation and reduced apoptosis

The invagination and remodeling of the telencephalic dorsal midline is normally accompanied by reduced roof plate cell proliferation and increased cell death (Furuta et al., 1997; Nagai et al., 2000). To determine whether these cellular properties are associated with the failure of dorsal midline downgrowth in *ShhN/+*, we performed cell proliferation and apoptosis analysis of the dorsal midline neuroepithelium. At E9.5, a stage prior to dorsal midline invagination, we detected prominent apoptotic activity at the most dorsal-medial tissue in wildtype telencephalon. In contrast, apoptosis was essentially eliminated in *ShhN/+* dorsal midline (Fig. 9F, F$^/$), although cell proliferation was not significantly different from wildtype in this region (Fig. 9E, E$^/$). At E10, differential proliferation was observed in wildtype dorsal telencephalon with reduced proliferation in the roof plate region compared with adjacent neuroepithelium. However, in *ShhN/+*, cell proliferation in the roof region was comparable to adjacent tissues and significantly higher when compared with wildtype (*ShhN/+* roof cell proliferation index

Figure 9. *ShhN/+* **telencephalon displays early dorsal midline defects**

(A, A$^{/}$) Dorsal-frontal views of E10.5 wildtype (A) and *ShhN/+* (A$^{/}$) embryos. Note the widely separated telencephalic ventricles by expanded dorsal midline tissue in *ShhN/+*. (B, B$^{/}$) Coronal sections of E10.5 telencephalons show defective downgrowth of *ShhN/+* dorsal midline (arrowhead in B) compared to wildtype (arrowhead in B$^{/}$). (C, C$^{/}$) Lateral views of E12.5 embryos reveal enlarged brain ventricles in *ShhN/+* mutants (C$^{/}$), indicative of hydrocephalus. (D, D$^{/}$) Coronal sections of E12.5 wildtype (D) and *ShhN/+* (D$^{/}$) telencephalon. In addition to persistent defects in dorsal midline invagination, the presence of a third eminence (labeled as **) positioned between the second ventral eminence (labeled as *) and cortical region is also evident in *ShhN/+* telencephalon (asterisk in D$^{/}$). (E, E$^{/}$, G, G$^{/}$, I, I$^{/}$,H) Roof plate cell proliferation analysis. Proliferation index shown in M is the percentage of BrdU-positive cell numbers over total cell numbers highlighted by DAPI staining. Dorsal midline cell proliferation index was comparable between wildtype (E)and *ShhN/+* (E$^{/}$) at E9.5. Compared to surrounding cortical region, cell proliferation is reduced in the roof region of E10.0 wildtype (G, data not shown). *ShhN/+* roof plate cells show about 1.8-fold higher proliferation index when compared to wildtype control (G$^{/}$, M). Similarly enhanced roof plate cell proliferation was found in *ShhN/+* at E10.5 (I, I$^{/}$, M). White bracket denotes a central region of the roof plate. (F, F$^{/}$, H, H$^{/}$, J, J$^{/}$, N) Roof plate cell death analysis. Cell death index shown in N is the percentage of TUNEL-positive cell numbers over total cell numbers highlighted by DAPI staining. Roof plate cells normally display high apoptotic activity, whereas very little apoptosis is observed in other telencephalic regions (F, H, J and data not shown). However, most *ShhN/+* roof plate cells fail to undergo apoptosis and show significantly

reduced cell death index when compared to wildtype at E9.5, E10.0 and E10.5 (F$^{/}$, H$^{/}$, J$^{/}$, and N). (K, K$^{/}$, L, L$^{/}$,) Yellow spots observed in H, J and J$^{/}$ were auto-flurorescent blood cells. Expression of Lhx5, a roof plate progenitor cell marker, is significantly expanded in E10.0 *ShhN/+* dorsal midline (K$^{/}$, L$^{/}$) when compared to wildtype (K, L).

E10.5   E12.5
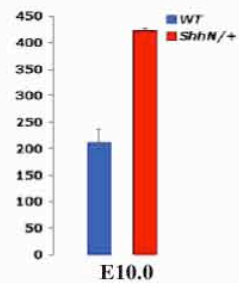
E9.5   E10.0

E10.5   E10.0   E13.5
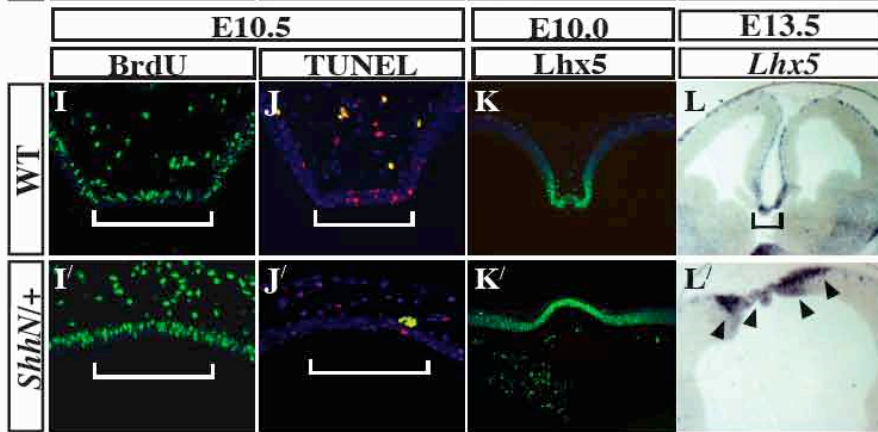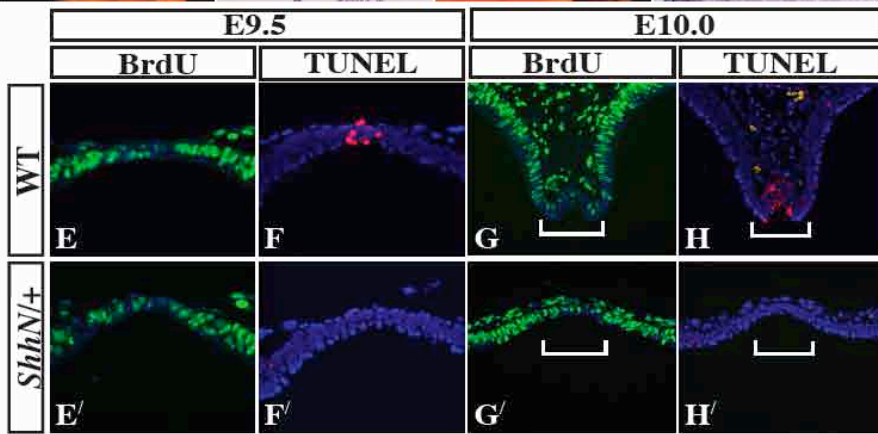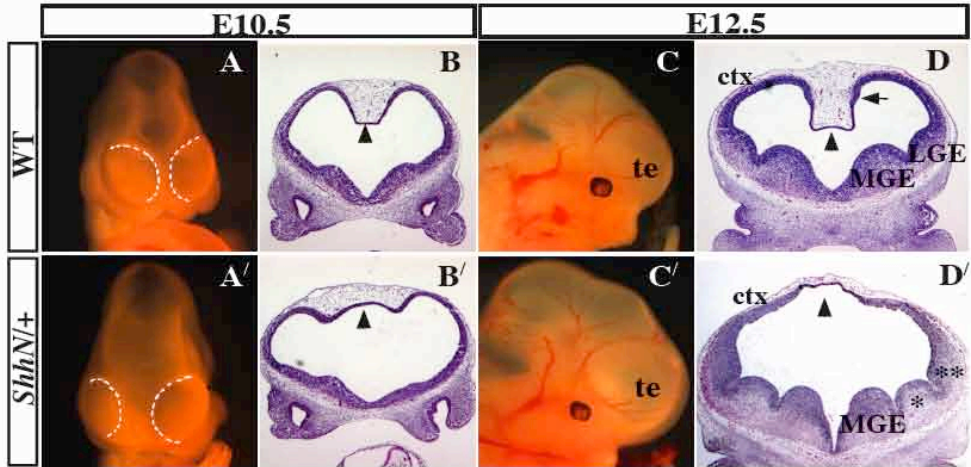
M   Dorsal midline proliferation index
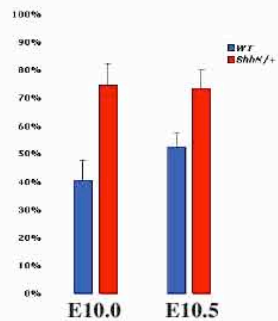
N   Dorsal midline cell death index
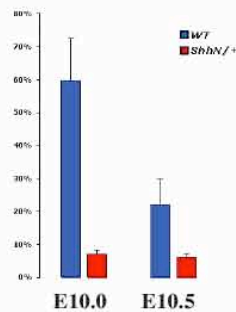
O   Dorsal midline Lhx5-expressing cell number

was approximately 1.8-fold higher) (Fig. 9G, G$^/$, M). Similarly, significantly reduced apoptosis was detected in the *ShhN/+* roof region (more than 7-fold lower) compared with wildtype (Fig. 9H, H$^/$, N). The augmented proliferation and reduced apoptosis in the mutant dorsal midline persisted at E10.5 (Fig. 9I, I$^/$, J, J$^/$, M, N). *Lhx5*, a member of the LIM homeobox gene family encoding a transcription factor, is normally expressed in the roof plate progenitors, but not in the choroid plexus or cortical hem (Shinozaki et al., 2004; Zhao et al., 1999). We found that the Lhx5-expressing domain expanded in *ShhN/+* dorsal telencephalic region as early as E10 with more than 2-fold increase in cell number, which persisted to E13.5, indicating a significant expansion of roof plate progenitor cell population (Fig. 9K, K$^/$, L, L$^/$, O). We conclude that defective dorsal midline development in *ShhN/+* is attributed to increased cell proliferation and reduced cell death in the roof plate region, resulting in expansion of the roof plate progenitor pool. These defects may also lead to failure of tissue invagination.


ShhN/+ telencephalon shows expansion of the basal ganglionic eminences

To examine dorsoventral patterning in *ShhN/+* telencephalon, we performed molecular marker analyses at stages when the telencephalon displays distinct regional patterns. *Pax6*, a homeobox gene that represses *Nkx* expression and is itself repressed by Shh signaling (Ericson et al., 1997), is uniformly expressed in the cortical region of the telencephalon. However, at E12.5, Pax6 expression showed non-uniform and a more dispersed pattern in *ShhN/+* embryos (Fig. 10A, A$^/$). By E13.5, the reduction in Pax6 expression domain became most evident (Fig. 10H, H$^/$). Additional dorsal pallium markers, *Ngn2* and *Emx2,* showed similarly reduced expression domain and intensity,

indicative of severe dorsal patterning defects. In contrast to the loss of cortical progenitors, we observed dorsal expansion of markers indicative of ventral telencephalic progenitors in *ShhN/+*. The expression of Nkx2.1 is normally restricted to the MGE domains (Fig. 10B), but in *ShhN/+* Nkx2.1-positive cells expanded to the ventral portion of the second ganglionic eminence where LGE normally forms (arrowheads in Fig. 10B$^/$). This observation is consistent with the expanded *Shh* expression domain up to the second eminence (see below). *Mash1*, which encodes a pro-neural basic helix-loop-helix transcription factor, is expressed in the pan-ventral telencephalic region, including both MGE and LGE (Casarosa et al., 1999; Horton et al., 1999; Lo et al., 1991). Previous studies have shown that exogenous Shh is capable of eliciting ectopic LGE markers including Mash1 expression in naïve telencephalic explants (Kohtz et al., 1998; Kohtz et al., 2001). We found that Mash1 expression expanded dorsally encompassing the ectopic third eminence and scattered sites within the cortical region of *ShhN/+* telencephalon (Fig. 10C, C$^/$, D, E, E1, E2). Notably, a significant portion of ectopic Mash1-expressing cells also expressed Gsh2 (Fig. 10F1, F2), a Shh-dependent inducible transcription factor normally expressed in the MGE and LGE (Corbin et al., 2000). This is in contrast to wildtype where co-expressing cells were restricted to the basal ganglionic eminences (Fig. 10F). Since Isl1 is expressed in differentiating neurons within the subventricular zone and mantle zone of the LGE (Yun et al., 2001), we further performed Isl1 immunostaining (Fig. 10G, G1, G2), showing that *ShhN/+* cortical region also contained differentiated neurons of LGE identity. Taken together, we conclude that the LGE and, to a lesser extent, MGE are expanded at the expense of the cortical domain in *ShhN/+* telencephalon.

56

Figure 10. MGE and LGE domains are expanded in *ShhN/+* telencephalon

(A, A$^/$) Pax6 expression pattern of E12.5 wildtype and *ShhN/+* cortical region. Pax6+ cells are scattered throughout the *ShhN/+* cortex (A$^/$), while uniform Pax6 expression demarcates the cortical region in wildtype (A). (B, B$^/$) Nkx2.1 expression pattern of E12.5 wildtype and *ShhN/+* MGE region. Nkx2.1, an MGE-specific marker that defines the most ventral-medial eminence in wildtype (B) extends into the ventral portion of the second eminence (*) of *ShhN/+* (B$^/$). (C, C$^/$, D, E, E1, E2) Mash1 expression in wildtype (C) and *ShhN/+* (C$^/$, D, E, E1, E2). Mash1, an LGE marker, is detected in the ectopic third eminence (** in D) and at scattered sites along the cortical region (E, E1, E2), indicative of an expanded LGE territory in *ShhN/+*. E1 and E2 are magnified views of boxed areas 1 and 2 in panel E, respectively. A significant portion of Gsh2 and Mash1 were co-expressed at ectopic sites in the cortical region of *ShhN/+* telencephalon (F1, F2), in contrast to wildtype where co-expressing cells were restricted to the basal ganglionic eminences (F). Differentiated ventral LGE marker Isl1 is also ectopically expressed at the *ShhN/+* cortical region, in contrast to its restricted expression in the differentiating neurons within the subventricular zone and mantle zone in wildtype (Fig. 2G, G1, G2), indicating that *ShhN/+* cortical region also contains differentiated neurons of ventral LGE identity. The locations of F1/G1 and F2/G2 approximately correspond to boxed areas 1 and 2 in panel E, respectively.
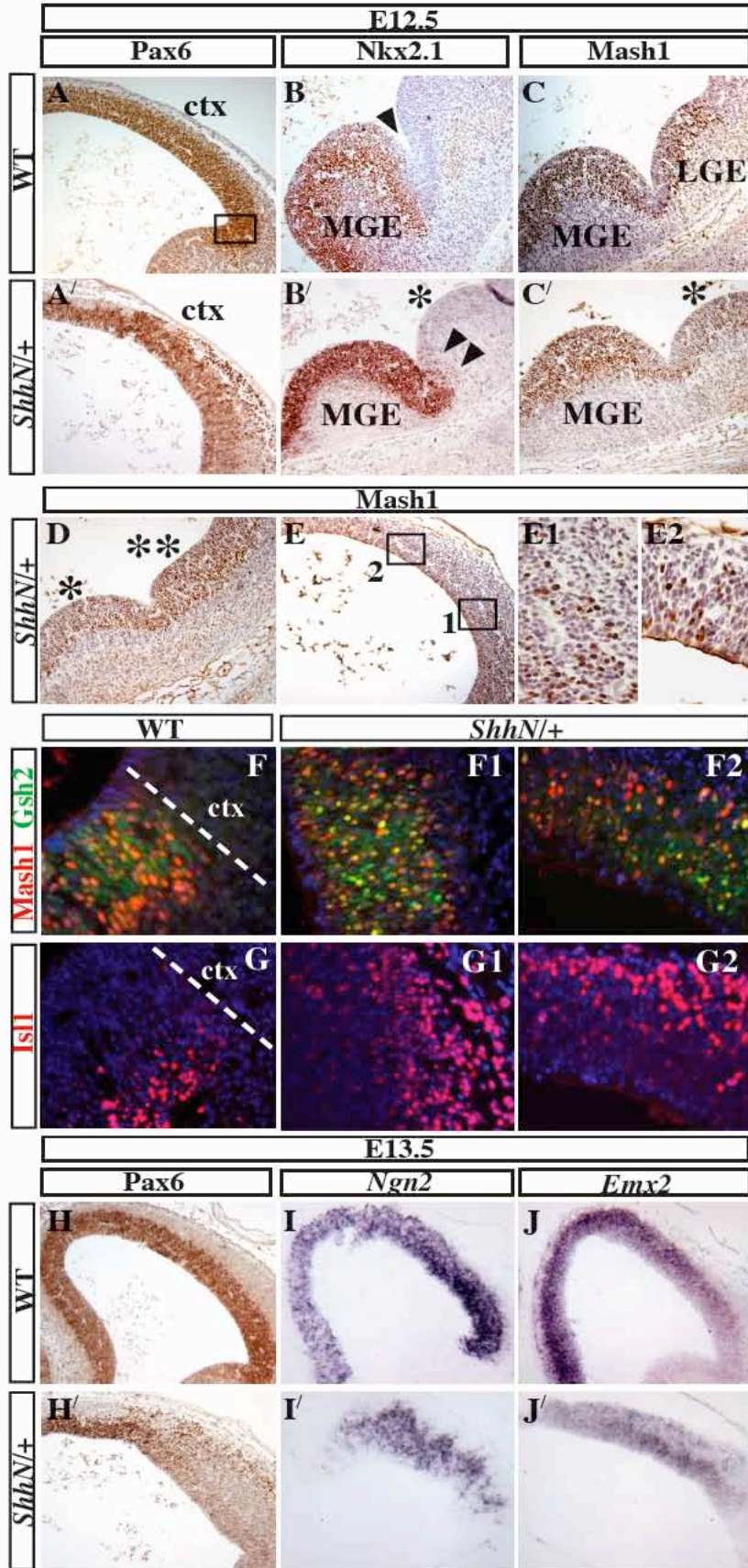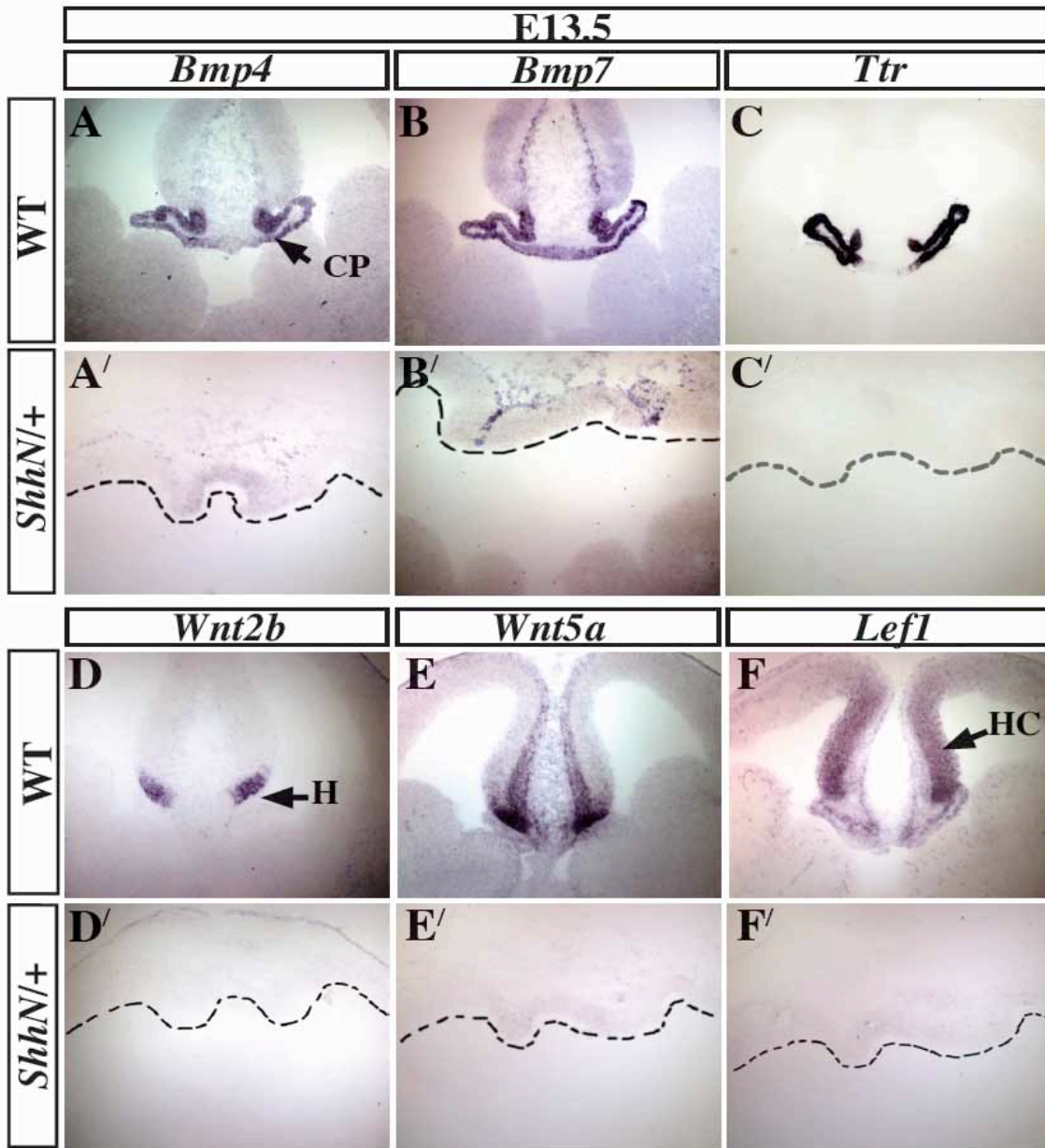
The development of hippocampus, choroid plexus and cortical hem is defective in *ShhN/+* telencephalon

The observation that *ShhN/+* telencephalon failed to invaginate and lacked morphologically distinguishable dorsal midline suggests that the generation of midline-derived structures is affected. To determine the extent of dorsal midline morphogenesis defects, regional marker analyses were performed at E13.5 when dorsal midline structures and their molecular identities are well established. Previous studies demonstrated that *Bmp4* and *Bmp7* expressions normally mark the choroid plexus (Furuta et al., 1997; Grove et al., 1998). We found that expression of these two *Bmp* genes in *ShhN/+* dorsal telencephalic epithelium was barely detectable, while persistent *Bmp7* expression was found in the dorsal medial mesenchyme (Fig. 11A, A$^{/}$, B, B$^{/}$). Also, *ShhN/+* exhibited no expression of definitive choroid plexus marker *transthyretin* (*Ttr*) (Fig. 11C, C$^{/}$), suggesting a failure of choroid plexus specification at this stage. While the expression of *Wnt2b* normally marks the Wnt-rich cortical hem (Grove et al., 1998; Lee et al., 2000b), its transcript was not detectable in *ShhN/+* mutants (Fig. 11D, D$^{/}$). *Wnt5a* expression, which encompasses the cortical hem and mesenchyme underneath the hippocampus and distal cortex, was also severely affected in *ShhN/+* mutants (Fig. 11E, E$^{/}$). Similarly, expression of the Wnt pathway component *Lef1* diminished considerably in *ShhN/+* mutants, in contrast to its normal expression in the choroid plexus and hippocampus (Fig. 11F, F'). Taken together, we conclude that the development of the hippocampal primordium, cortical hem and choroid plexus is significantly compromised in *ShhN/+* mutants.

Figure 11. Loss of telencephalic choroid plexus, cortical hem and hippocampus in *ShhN/+*

(A, B, C) Strong expressions of *Bmp4*, *Bmp7* and *Ttr* are detected in wildtype choroid plexus at E13.5 (A$^/$, B$^/$, C$^/$) Faint or no *Bmp4*, *Bmp7* and *Ttr* transcript signals are detected in *ShhN/+* dorsal midline. (D, D$^/$, E, E$^/$) Strong expressions of *Wnt2b* and *Wnt5a*, which demarcate Wnt-rich cortical hem, are significantly reduced in *ShhN/+*. (F, F$^/$) A hippocampal precursor marker *Lef1* is similarly reduced in *ShhN/+*.

E13.5		
Bmp4	*Bmp7*	*Ttr*

A CP **B** **C** (WT)

A' **B'** **C'** (ShhN/+)

Wnt2b	*Wnt5a*	*Lef1*

D H **E** **F** HC (WT)

D' **E'** **F'** (ShhN/+)

ShhN elicits ectopic signaling throughout *ShhN/+* telencephalic neuroepithelium

In order to assess Shh signaling in wildtype and *ShhN/+* telencephalon, we utilized *Patched-LacZ* mice, in which ß-galactosidase activity indicates Shh signaling activity (Goodrich et al., 1997). At E10.5, coronal sections through the MGE region revealed that while Shh signaling activity was confined within the MGE of wildtype telencephalon, ShhN could evoke signaling activity dorsal to the morphological boundary of MGE in *ShhN/+* mutants (Fig. 12D, D$^/$). However, we could not detect expanded ShhN protein by immunohistochemistry possibly due to a level that is below detection threshold (Fig. 12B, B$^/$). By E13.5, ectopic ShhN signaling activity was detected throughout the *ShhN/+* telencephalic neuroepithelium in contrast with Shh signaling being restricted to the ventral telencephalon in wildtype (Fig. 12E, E$^/$). In addition, we found that the domain of *Shh* transcript in the ventral telencephalic region and zona limitans intrathalamica (zli) at E10.5 appears to be slightly expanded in *ShhN/+* (Fig. 12A, A$^/$). This expansion becomes more evident at E13.5 when we found a small number of Shh-expressing cells extending beyond the morphological boundary of the MGE into the ventral portion of the adjacent eminence (Fig. 12C, C$^/$), consistent with expanded Nkx2.1 expression (Fig. 12B'). Another indicator of Shh pathway activation is the accumulation of the zinc finger transcription factor, Gli3, by inhibiting formation of its repressor forms (Litingtung et al., 2002; Wang et al., 2000). Therefore, we determined the relative amount of Gli3 repressor (Gli3R) to Gli3 full length (Gli3-190) as another readout of Shh signaling. Consistent with widespread *Ptch1* reporter expression, we observed more than 30% reduction in Gli3R/Gli3-190 ratio in E13.5 whole brain extracts of *ShhN/+* mutants compared with

wildtype (Fig. 12F). Taken together, with the ectopic MGE and LGE marker expressions we conclude that the *ShhN/+* telencephalic neuroepithelium is subject to globally expanded ShhN signaling along the dorsal-ventral axis.

Ectopic ShhN signaling impairs dorsal telencephalic Bmp and Wnt signalings through upregulation of *Fgf8*

In order to gain insight into the mechanism by which ectopically enhanced ShhN signaling affects dorsal telencephalic patterning, we examined the expression of multiple essential components of the Fgf, Bmp and Wnt signaling pathways that work in concert to regulate regional identities and growth (Sur and Rubenstein, 2005). Fgf proteins such as Fgf8, Fgf17, Fgf18 and Fgf15, from the anterior telencephalon, have been shown to function as anterior patterning molecules (Bachler and Neubuser, 2001; Crossley et al., 2001; Gimeno et al., 2003; Maruoka et al., 1998). Among these growth factors, the role of Fgf8 has been extensively studied and it has been shown that Shh signaling is required to maintain robust Fgf8 expression (Aoto et al., 2002; Ohkubo et al., 2002). We therefore asked whether *Fgf8* expression is altered in *ShhN/+* telencephalon. As expected, we observed an expansion of *Fgf8* expression domain in the anterior forebrain of *ShhN/+* mutants as early as E9.5 (Fig. 13A, A$^{/}$). At E10.5, the *Fgf8* expression domain encompassed the entire anterior telencephalic midline tissue in *ShhN/+* and even extended into the anterior diencephalon (Fig. 13B, B$^{/}$).

One critical function of Fgf8 in the anterior neural ridge is to restrict Bmp signaling expression to the dorsal midline (Storm et al., 2006). Bmp signaling, in turn, is thought to

63

Figure 12. Widespread activation of Shh signaling in *ShhN/+* telencephalon

(A, A$^{/}$, B, B$^{/}$, C, C$^{/}$) *Shh* transcript and Shh protein expression in wildtype (A, B, C) and *ShhN/+* (A$^{/}$, B$^{/}$, C$^{/}$). Whole-mount *in situ* staining of Shh reveals a generally similar pattern between wildtype and *ShhN/+*; however, a modest expansion of *Shh* expression in MGE and zona limitans intrathalamica is observed in *ShhN/+* when compared to wildtype (arrows in A and A$^{/}$). Consistently, *Shh*-expressing domain extends into the ventral portion of the second ventral eminence in *ShhN/+* (C$^{/}$), while *Shh* transcript signal is confined within the MGE domain in wildtype (C). (B and B$^{/}$) Shh protein signal is detected mainly within the MGE region in both wildtype and *ShhN/+*. At E10.5, Shh signaling activity, as evidenced by *Ptch1-LacZ* expression, is confined within the MGE region in wildtype (D), but is extended in *ShhN/+* (D$^{/}$). At E13.5, *Ptch1-LacZ* expression is strongly expressed in the MGE and only weakly in the LGE (E), but in *ShhN/+,* the weak LGE expression extends to the entire cortical region including dorsal midline (E$^{/}$). (F) Immunoblotting of whole brain protein extracts from E13.5 wildtype and *ShhN/+* followed by incubation with Gli3-specific antibody recognizing Gli3 full-length (Gli3190) and repressor forms (Gli3R); *Gli3*$^{-/-}$ brain extract is used as negative control. Histogram shows relative Gli3R/Gli3190 ratio.
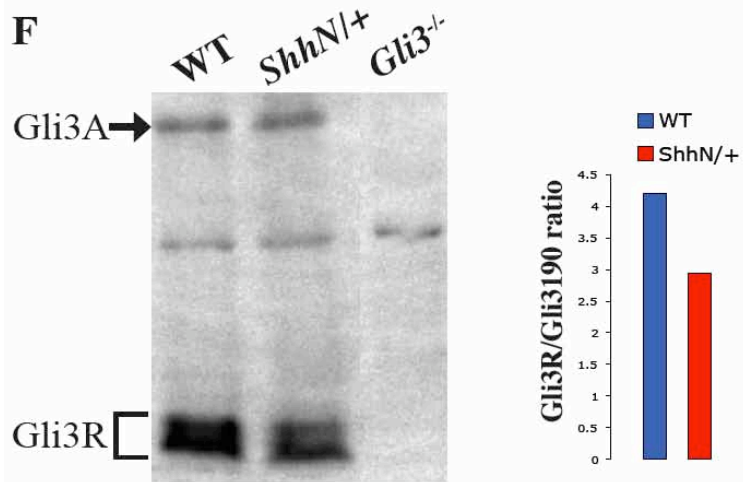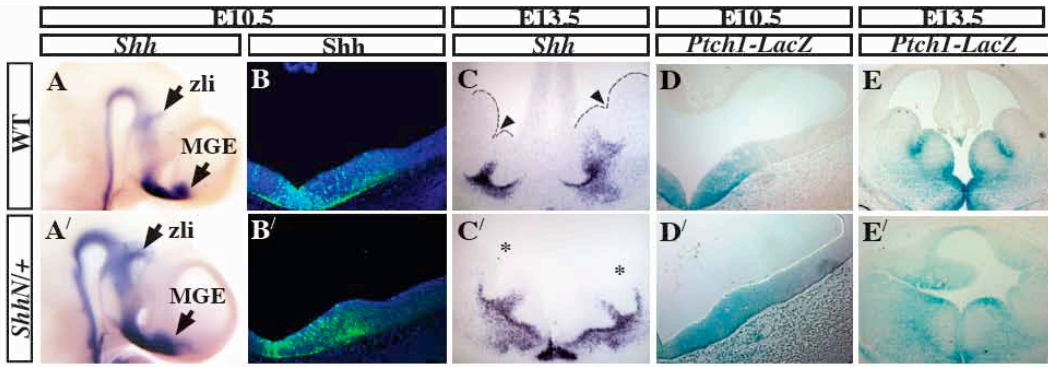
promote localized cell death and the differentiation of a dorsal midline derivative, the choroid plexus, from roof plate progenitors (Furuta et al., 1997; Hebert et al., 2002). Thus, defective Bmp signaling could explain some of the midline defects observed in *ShhN/+* telencephalon despite expansion of roof plate progenitors. To test this possibility, we compared *Bmp4* expression and Bmp signaling activity in early wildtype and *ShhN/+* telencephalon. *Bmp4* expression was monitored using a sensitive *lacZ* reporter driven by the endogenous *Bmp4* promoter (Weaver et al., 2000). At E9.5, a stage at which there was no evident morphological dorsal midline defect in *ShhN/+* (Fig. 9E, E', F, F'), a reduction in *Bmp4*-expressing domain was already apparent in the dorsal telencephalic midline (arrowhead in Fig. 13C, C$^/$). This reduction of *Bmp4* expression appeared to correlate with the lack of cell death at this stage (Fig. 9F'). By E10.5, the *Bmp4* reduction was more pronounced and extended to the rostral diencephalon (Fig. 13D, D$^/$). Similarly, *in situ* analysis of *Bmp4* transcript also showed barely detectable level in the dorsal-medial telencephalon of *ShhN/+* mutants, in contrast to its robust expression in wildtypes (Fig. 13E, E$^/$). Concomitantly, the expression of *Msx1,* which correlates with sites of elevated Bmp signaling (Furuta et al., 1997; Shimamura and Rubenstein, 1997b), was also significantly reduced in *ShhN/+* mutants (Fig. 13F, F$^/$). Since it has been shown that nuclear accumulation of phosphorylated forms of Smad1, 5, 8 proteins (pSmads) is an indication of active Bmp signaling (Feng and Derynck, 2005), we also determined pSmads expression by immunostaining. At E10.5, we observed significant accumulation of nuclear pSmads in the neuroepithelium of wildtype hippocampal primordium (white arrows in Fig. 13G) in contrast to its low level in the roof plate region. However, we did not detect high level of pSmads in *ShhN/+* dorsal telencephalic neuroepithelium,

66

suggesting a severe loss of Bmp signaling. Notably, *ShhN/+* dorsal telencephalic mesenchymal cells also showed significantly reduced pSmads staining (Fig. 13G, G$^/$, data not shown). Taken together, these findings indicate that deficient Bmp signaling at the dorsal midline likely accounts for the reduced cell death and defective choroid plexus formation in *ShhN/+* telencephalon.

The cortical hem, a developmentally transient structure positioned ventral to the hippocampus and dorsal to the telencephalic choroid plexus, is a source of multiple Wnt proteins that have also been implicated in dorsal midline development (Grove et al., 1998; Lee et al., 2000b). Expanding the *Fgf8* expression domain by *in utero* electroporation suppressed the expression of *Wnts* (*Wnt2b*, *Wnt3a*, *Wnt5a*) in the cortical hem and led to a hypoplastic hippocampus. Thus, constraining the *Fgf8* expression boundary is vital for the maintenance of hem Wnt signaling and hippocampus development (Shimogori et al., 2004). Therefore, we asked whether expanded *Fgf8* expression and loss of high level Bmp signaling would impair Wnt signaling in *ShhN/+* dorsal telencephalon. *In situ* hybridization analyses showed that, while *Wnt2b*, *Wnt3a*, *Wnt5a* delineated the Wnt-rich hem of wildtype dorsal midline at E10.5 and E11.5, their expressions were markedly diminished in *ShhN/+* mutants (Fig. 13H, H$^/$, J, J$^/$, K, K$^/$). Notably, comparable expression of *Wnt7a* that is normally expressed at the lateral and dorsal cortex (Grove et al., 1998), but not the cortical hem, was observed in wildtype and *ShhN/+* (data not shown), indicating a specific loss of *Wnt* genes in the dorsal midline region. The severe loss of Wnt signaling activity in *ShhN/+* dorsal telencephalon was confirmed using TOPGAL reporter mice which express β-galactosidase under the control of multimerized LEF/TCF consensus binding sites (Fig. 13I, I$^/$, L$^/$, L). The

absence of apparent Wnt signaling activity may account for the severely defective hippocampal development in *ShhN/+* mutants.

Taken together, we conclude that ectopic ShhN signaling in the dorsal telencephalic region specifically impaired Bmp and Wnt signaling from dorsal patterning centers, likely via upregulation of *Fgf8* expression.

***ShhN/+* mice display a spectrum of phenotypic features mimicking the human HPE**

Next, we characterized the *ShhN/+* forebrain and craniofacial defects at perinatal stages. Surprisingly, *ShhN/+* mice showed relatively normal external craniofacial morphological defects, although a bulging cranium, which is generally associated with hydrocephalus (Banizs et al., 2005), was clearly evident in more than 10 embryos examined (Fig. 14A, A$^/$). Gross analysis of brains indicated an enlarged forebrain (and midbrain) and lack of olfactory bulbs in mutants (Fig. 14B, B$^/$). H&E staining of coronal sections revealed that the enlarged ventral eminences in *ShhN/+* were well separated (Fig. 14C, C$^/$), whereas the dorsal midline of *ShhN/+* telencephalon was severely hypoplastic and lacked conjunction of corpus callosum and septum that normally separated anterior cerebral hemispheres (Fig. 14C, C'). Dorsal interhemispheric cyst-like structure was occasionally observed in *ShhN/+* telencephalon (arrow in Fig. 14C$^/$). In addition, the dorsal telencephalon of *ShhN/+* mutants lacked middle anterior commissure and characteristic choroid plexuses and hippocampal structures seen in wildtypes (Fig. 14E, E$^/$). Nevertheless, a small region of simplified epithelium with *Ttr* expression in the dorsal midline of the anterior forebrain in the newborn mutant was observed (Fig. 14F,

Figure 13. Up-regulation of *Fgf8* in rostral midline accompanies loss of Bmp and Wnt signalings from dorsal organizing centers in *ShhN/+* telencephalon

(A, A$^/$, B, B$^/$) Expansion of *Fgf8* expression. *Fgf8* expression is normally confined to the ventral anterior telencephalic midline at E9.5 (A) and E10.5 (B). However, in *ShhN/+*, *Fgf8* expression expands gradually to the entire dorsal-ventral axis of the anterior telencephalic midline (A$^/$, B$^/$). (C, C$^/$, D, D$^/$, E, E$^/$, F, F$^/$, G, G$^/$) Loss of high-level Bmp4 expression and Bmp signaling in *ShhN/+* telencephalic dorsal midline. *Bmp4-LacZ* expression is detected in rostral diencephalons, but largely absent in the *ShhN/+* telencephalic dorsal midline at E9.5 (C$^/$), while its expression is prominent in wildtype dorsal telencephalon (bracket in C) Arrowheads in C and C$^/$ indicate telencephalic-diencephalic boundary. *Bmp4-LacZ* expression is essentially abolished in *ShhN/+* dorsal midline and rostral diencephalic region at E10.5(D, D$^/$). *In situ* staining of *Bmp4* also reveals drastically reduced expression in *ShhN/+* (E$^/$), in contrast to its robust expression in dorsal midline neuroepithelium of wildtype (E). Similar downregulation of *Msx1* is also observed (compare F and F$^/$). Accordingly, nuclear accumulation of phosphorylated-forms of Smad1, 5, 8 is largely abolished in *ShhN/+* dorsal neuroepithelium and adjacent mesenchymal cells (G, G$^/$). (H, H$^/$, I, I$^/$, J, J$^/$, K, K$^/$, L, L$^/$) Loss of multiple Wnt ligand expressions and canonical Wnt signaling in *ShhN/+* dorsal telencephalons. Dorsal midline tissue-specific expressions of Wnt ligands, including *Wnt2b*, *Wnt3a* and *Wnt5a*, are largely absent in *ShhN/+* (H, H$^/$, J, J$^/$, K, K$^/$). As a result, canonical Wnt signaling, revealed by β-galactosidase activity in TOPGAL reporter mice (I, L), is largely abolished

except in the small region of the posterior telencephalon (I', L'). Dashed lines in K and K'

indicate sectioning planes shown in L and L', respectively.
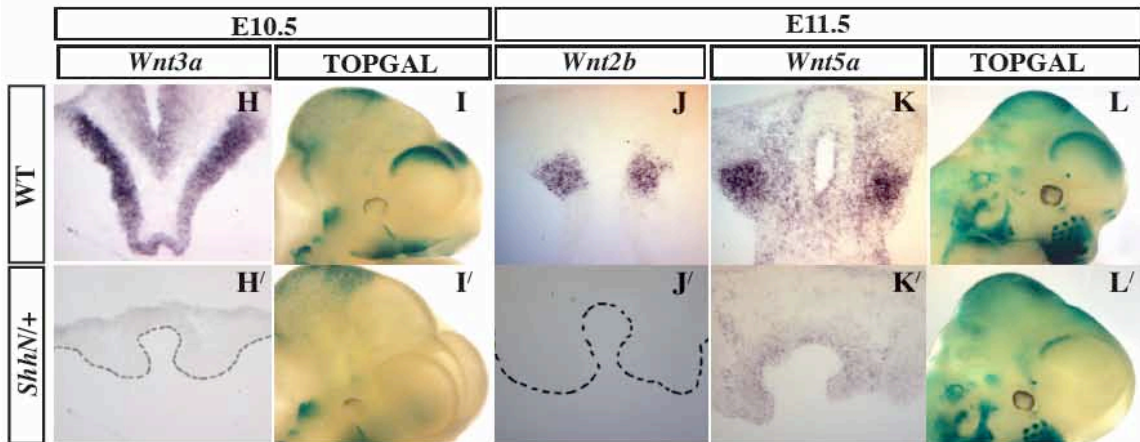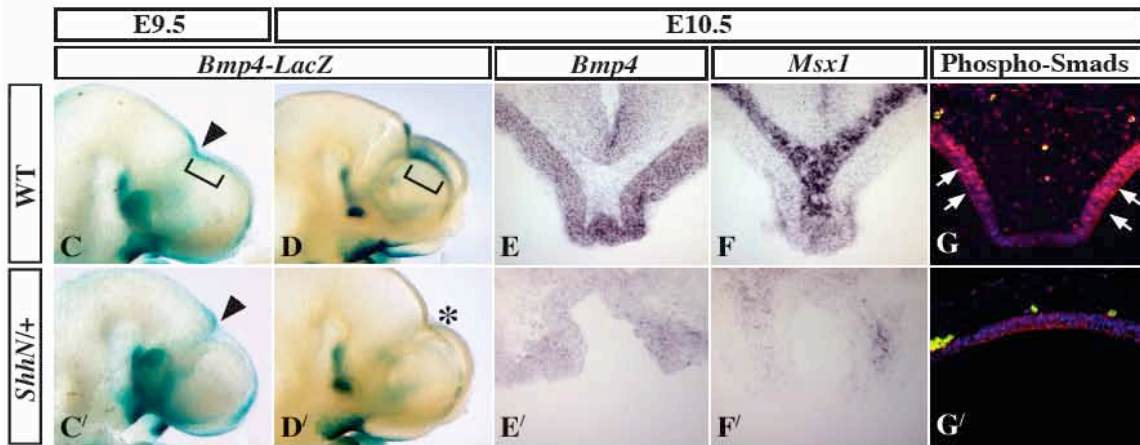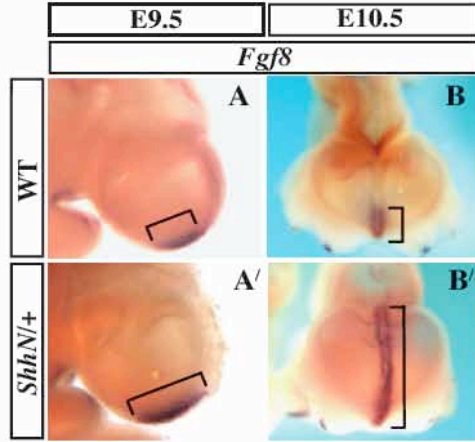
F$^{/}$). Since *Ttr* expression was absent in E13.5 *ShhN/+* mutants, this observation suggests either delayed/defective choroidal fate specification or a diencephalic origin of the choroid plexus. Regardless, the presence of low but persistent level of Bmp signaling in the roof region (shown as residual Bmp4 and Bmp7 expressions at E10.5 in Fig. 13E, E$^{/}$ and at E13.5 in Fig. 11A, A$^{/}$, B, B$^{/}$) likely contributed to the reduced choroidal fate in the mutant. Similarly, the development of the hippocampus was also significantly compromised. The expression of Prox1 marks the characteristic V-shape dentate gyrus of the hippocampus; we observed few and scattered Prox1+ cells at the distal cortical neuroepithelium in *ShhN/+* (Fig. 14G, G$^{/}$), consistent with significantly reduced *Lef1* expression in the hippocampal precursors (Fig. 11F').

In contrast to a monoventricle in the anterior telencephalon, the ventricles in the posterior telencephalon are clearly separated by an enlarged thalamus (Fig. 14D, D$^{/}$). Although external craniofacial morphology appeared relatively unaffected, *ShhN/+* mutants developed cleft palate (CLP). The palatal shelves failed to fuse in *ShhN/+* at E15.5 (Fig. 14H, H$^{/}$), leading to a cleft secondary palate in newborn pups (Fig. 14I, I$^{/}$, J, J$^{/}$). Strikingly, some of the phenotypic features including partial separation of the forebrain ventricles, hydrocephalus and cleft palate are similar to those found in a human patient with milder HPE carrying a truncation mutation (CAG->TAG, Q209X) in one *SHH* allele that was predicted to produce SHHN protein due to failure to catalyze cholesterol transfer; the other *SHH* allele was normal, thus indicating that the genotype of this patient is *SHHN/+* (Nanni et al., 1999).

Figure 14. *ShhN/+ mice mimic human HPE phenotypes*

(A, A$^{/}$) Wildtype and *ShhN/+*, both showing relatively normal external craniofacial morphologies except bulging forehead characteristic of hydrocephalus in mutant (white bracket in A$^{/}$). (B, B$^{/}$) Gross analysis of brains indicating lack of olfactory bulbs in mutant. (C, C$^{/}$, D, D$^{/}$) Coronal sections of wildtype and *ShhN/+* telencephalons shown in B and B$^{/}$. In the rostral telencephalon, the corpus callosum (CC) and septum (s) that normally connect with each other to divide the telencephalic lobes into two lateral ventricles are either missing or defective in the mutant resulting in a single ventricle (compare C and C$^{/}$). The mutant dorsal midline is severely hypoplastic with simplified epithelium and cyst like structure (arrow). Note the presence of normally separated ventral eminences in *ShhN/+*. (C$^{/}$). Caudally, *ShhN/+* telencephalon lacks well-formed U-shape hippocampus and the ventricles are separated by enlarged thalamus (D$^{/}$). (E, E$^{/}$) Brain cross sections further show that the mutant lacks dorsal midline fissure, telencephalic choroid plexuses (CP) and anterior commissure (AC), while the separation of the thalamus (TH) is not affected. The simplified epithelium at the dorsal midline in *ShhN/+* exhibits *Ttr* expression (F$^{/}$), similar to the normal telencephalic choroid plexus in wildtype (F). G and G$^{/}$ were zooned-in view of boxed-area shown in D and D$^{/}$. While Prox1+ cells mark the characteristic V-shape dentate gyrus of the wildtype hippocampus (G), few and scattered Prox1+ cells are found at the most distal *ShhN/+* cortical neuroepithelium (G$^{/}$) (H, H$^{/}$, I, I$^{/}$, J, J$^{/}$) *ShhN/+* mutants exhibit cleft secondary palate (CLP). E15.5 coronal section through the palatal region shows failure of palatal fusion in *ShhN/+* (compare H to H$^{/}$). A direct view of the secondary palate region with mandible removed shows cleft palate in *ShhN/+* (compare I to I$^{/}$). Skeletal staining further shows

the presence of widely-separated palatal shelves ($J^/$), allowing direct view of the presphenoid bone (psp) underneath the otherwise fused palatine shelves. Note that the maxillary shelves are not fully mineralized in the mutant (asterisks) (J).
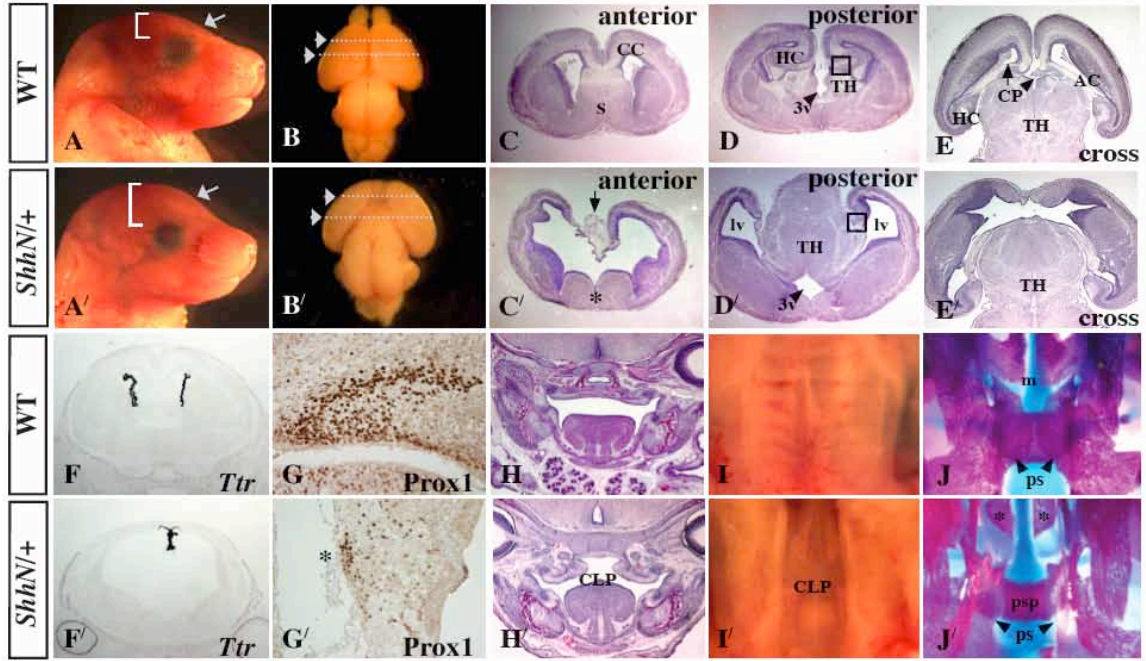
Discussion

HPE is the most common developmental anomaly of the human forebrain (Cohen, 2006). Considerable amount of effort has been exerted to understand the pathogenesis of HPE, and several animal models that are generally associated with loss of Shh signaling have been established, showing severely disrupted ventral forebrain as a phenotypic hallmark. Our finding that *ShhN/+* mice exhibit many aspects of forebrain defects observed in a human patient with a milder form of HPE with a similar genotype, implicates a novel mechanism by which ectopic Shh signaling impairs dorsal forebrain development, resulting in non-cleavage of midline structures. Additionally, our study may shed light on the molecular pathogenesis of MIH, a variant of HPE that preferentially shows disruption of telencephalic dorsal midline structures.

Ectopic Shh signaling impairs dorsal organizing center function

Early telencephalic regionalization is mediated by diffusible morphogenic ligands and graded transcription factor expressions (Campbell, 2003; Grove and Fukuchi-Shimogori, 2003; Sur and Rubenstein, 2005). It has long been established that Shh signaling is essential for ventral telencephalic patterning (Chiang et al., 1996). Recent studies indicate that this requirement appears to be mediated through Fgf signaling, as deletion of Fgf8 or multiple Fgf receptors in the telencephalon leads to loss of ventral cell fates analogous to that of $Shh^{-/-}$ mutants (Gutin et al., 2006; Storm et al., 2006). Thus, the expansion of *Fgf8* expression to the dorsal midline in *ShhN/+* mutants is consistent with long-range activation of Shh signaling. Because Fgf signaling normally promotes cell survival by restricting *Bmp4* expression in the dorsal midline (Furuta et al., 1997; Storm

76

et al., 2003), the decrease in cell death in *ShhN/+* is in agreement with significantly reduced Bmp signaling. Additionally, impaired choroid plexus formation can also be attributed to defective Bmp signaling as Bmpr1a gain- and loss-of-function studies reveal that Bmpr1a is required for promoting choroidal fate by antagonizing cortical specification (Hebert et al., 2002). The hippocampus is another midline-derived structure that is defective in *ShhN/+* telencephalon. Studies of *Wnt3a* or *Lef1* mutants have demonstrated that high level of canonical Wnt signaling close to the hem is vital for normal hippocampus development (Galceran et al., 2000; Lee et al., 2000b; Zhou et al., 2004). The ability of ectopic *Fgf8* to suppress *Wnt2b*, *Wnt3a* and *Wnt5a* expressions at the cortical hem (Shimogori et al., 2004) is also consistent with hippocampus hypoplasia observed in *ShhN/+* telencephalon. While altered dorsal patterning centers in *ShhN/+* can be logically connected to the expanded *Fgf8* expression via ectopic Shh signaling, considering the prominent role of Shh in promoting neuroepithelial cell proliferation (Ho and Scott, 2002; Stecca and Ruiz i Altaba, 2005), it remains possible that Shh signaling can also directly contribute to increase cell proliferation and reduced cell death observed at the dorsal midline, resulting in defective roof plate progenitor cell differentiation, and subsequently dampening roof signaling activities (Fig. 15).

ShhN/+ as a novel mouse model of human HPE

HPE is characterized by a spectrum of brain malformations in which the bilateral cerebral hemispheres fail to separate along the midline. One of the principle underlying mechanisms of HPE pathogenesis is the disruption of basal forebrain patterning associated with impaired Shh signaling during early embryogenesis

Figure 15. Proposed mechanism of dorsal midline dysgenesis and HPE mediated by ectopic Shh signaling.

During normal development, Bmp and Wnt signals generated from the roof plate (RP) and its neighboring neuroepithelium are thought to pattern the dorsal midline structures such as choroid plexus, cortical hem and hippocampus (Grove and Fukuchi-Shimogori, 2003). Shh secreted from the ventral telencephalic midline is required to maintain *Fgf8* expression in the anterioventral midline (anterior neural ridge, ANR). In turn Fgf8 restricts Bmp and Wnt signals to the dorsal midline (Sur and Rubenstein, 2005). In *ShhN/+* mutants, widespread activation of Shh signaling activity leads to expansion of *Fgf8* expression to the dorsal midline, which in turn downregulates Bmp and Wnt signalings. In addition, long-range ShhN signaling may also directly promote cell proliferation and reduce cell death at the dorsal midline.
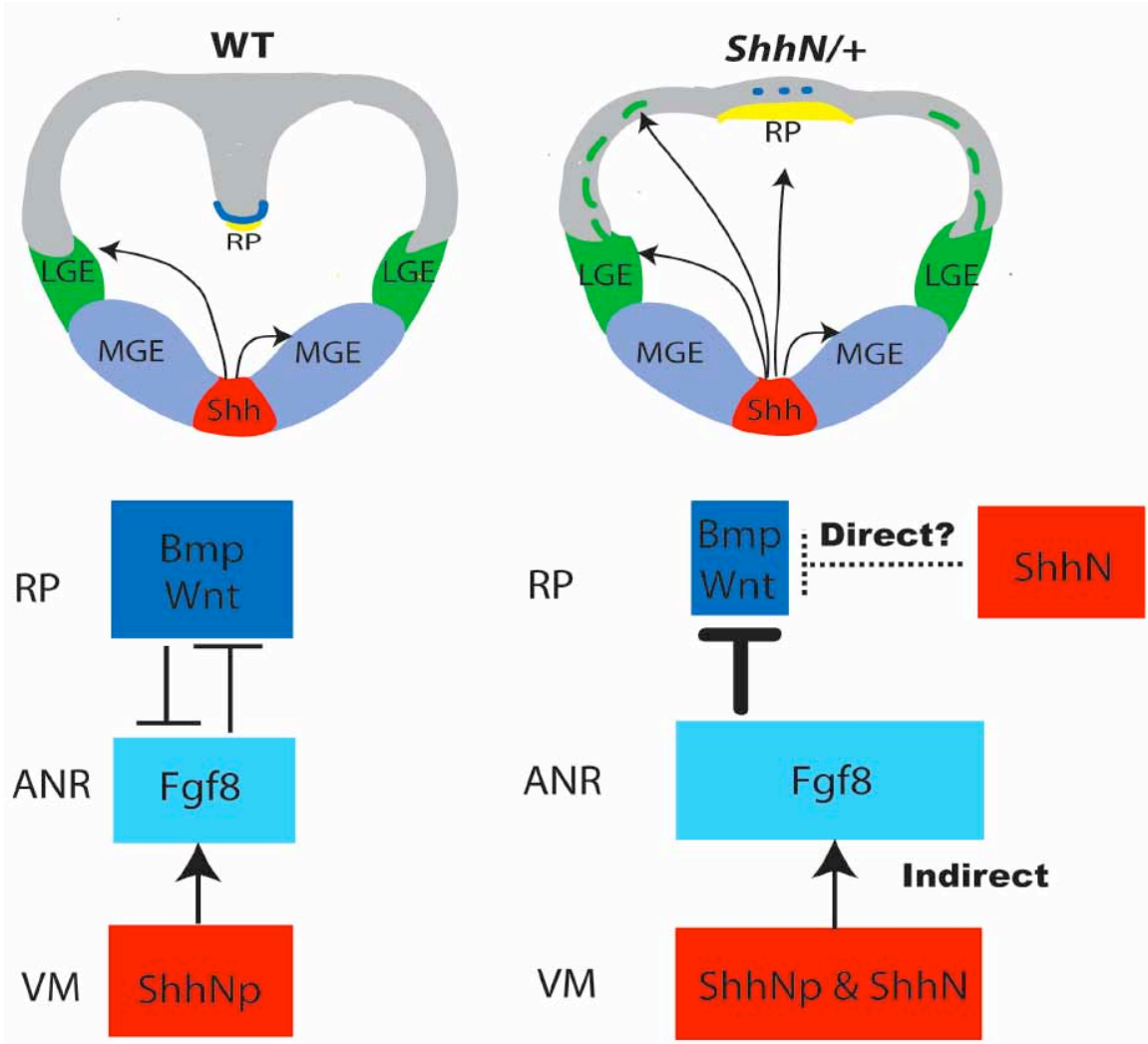
(Muenke and Beachy, 2000). Indeed, molecular genetic analyses have identified numerous SHH mutations in HPE patients, including a Q209X truncation mutation in one *SHH* allele that is predicted to produce SHHN protein (Nanni et al., 1999). The Q209X patient was previously diagnosed with semi-lobar HPE, a milder form of HPE in which the brain is divided with two distinct hemispheres only in the caudal but not rostral region of the telencephalon (Cohen, 2006; Hayhurst and McConnell, 2003; Kinsman et al., 2000). This patient also exhibited hydrocephalus and cleft palate; all of these phenotypic features are reproduced in the *ShhN/+* mutant embryos. However, unlike "classical" HPE, Shh signaling is ectopically activated and the basal forebrain is well separated in *ShhN/+* mutants. Molecular analysis further revealed that the lack of regional cerebral hemispheric separation in *ShhN/+* mutants is largely attributed to the disruption of dorsal midline signaling center. In this context, it is also interesting to note that dorsal midline defects have been reported in some patients with semi-lobar HPE (Takahashi et al., 2003). These observations suggest a novel mechanism by which ectopic Shh signaling could be associated with milder HPE.

Recent brain images and genetic studies in human have implicated an association of impaired embryonic roof plate development with MIH, a peculiar subtype of HPE, displaying non-cleavage of the cerebral hemisphere in the posterior frontal and parietal region. Notably, *ShhN/+* mutants share several features observed in MIH patients, including 1) largely normal craniofacial structures; 2) frequent agenesis of the dorsal corpus callosum while ventral forebrain nuclei are generally separated; 3) midline third

80

ventricle is separated by hypothalamus at the posterior frontal lobe; 4) dysgenesis of dorsal midline-derived structures including absence or reduced choroid plexus and hypoplastic hippocampus (Lewis et al., 2002; Pulitzer et al., 2004; Simon et al., 2002). We are only beginning to understand the molecular pathogenesis of MIH. The mechanism underlying the failure of hemispheric bifurcation in MIH appears to be different from that of classical HPE (Muenke and Beachy, 2000; Simon et al., 2002). In MIH, the defective functions of genetic factors impair roof plate development, whereas in classical HPE the floor plate is mostly affected. To date, the only gene implicated in MIH pathogenesis has been linked to mutations in *ZIC2*, which encodes a zinc finger protein that is homologous to *Drosophila* odd-paired (Brown et al., 2001). Reduced *Zic2* expression in mice results in failure of roof plate invagination and fusion of cerebral hemispheres with relatively normal ganglionic eminence development (Nagai et al., 2000). Indeed, it has been hypothesized that haplo-insufficiency in *ZIC2* underlies MIH in humans, and the absence of craniofacial malformation, which is normally observed in mutants with loss of Shh signaling (Brown et al., 2001; Simon et al., 2002), argued that this anomaly may arise by a SHH-independent pathway. However, predominant ZIC2 mutations are associated with classical HPE (Brown et al., 2001; Brown et al., 1998). The fact that *Zic2* ablation in mice does not faithfully reproduce MIH phenotypes (Nagai et al., 2000), indicates that the molecular pathogenesis of MIH could be heterogeneous. Bmp and Wnt ligands derived from the roof region are thought to organize dorsal structures. Roof plate cell ablation leads to loss of dorsal midline-derived structures as well as associated Bmp signaling and thus, it has been proposed that *Bmp*s expressed in the roof plate are candidate genes for MIH (Cheng et al., 2006). However, fate-mapping

81

studies indicate that cells of the choroid plexus and Wnt-rich cortical hem are descendents of roof plate progenitors (Currle et al., 2005). Therefore, defective dorsal midline development could arise secondary to the depletion of roof plate cell population rather than a consequence of reduced Bmp signaling. Furthermore, studies of *Gdf7* (*Bmp12*) and telencephalon-specific conditional *Bmp4* and *Bmpr1a* mutants implicate a role of Bmp signaling primarily in choroid plexus specification and differentiation (Currle et al., 2005; Hebert et al., 2003; Hebert et al., 2002). Therefore, it remains an open question as to whether and how impaired Bmp signaling affects the intricate signaling network involved in dorsal telencephalic patterning that result in severe defects in multiple midline structures such as the choroid plexus, cortical hem and hippocampus observed in roof plate-depleted mutants. Our study demonstrates that reduced Bmp signaling coupled with impaired Wnt signaling appear to synergistically affect dorsal midline development. Thus, reduction in hem-enriched Wnt or its pathway activity should be considered as an integral part of MIH pathogenesis.

An intriguingly consistent phenotype of *ShhN/+* mice that parallels the phenotype observed in some human HPE patients, including MIH, is the cleft palate (CLP). Studies on *Fgf10$^{-/-}$*, *Fgfr2b$^{-/-}$* and *Shh$^{-/-}$* conditional mutant mice, which all exhibit CLP, demonstrate that palatal epithelial *Shh* expression is a downstream target of *Fgf10* expressed in the palatal mesenchyme (Rice et al., 2004). Thus, loss of Shh signaling is generally associated with induction of CLP. However, *ShhN/+* mice exhibit Shh gain-of-function signaling in many developmental contexts such as in the telencephalon, spinal cord and limb bud (Li et al., 2006) (this study and data not shown). Thus, the notion that Shh gain-of-function could also lead to CLP is particularly interesting. Recent

investigation into *Insig1* and *Insig2* knockout mice also postulates that excess Shh signaling may cause CLP (Engelking et al., 2006). Furthermore, hydrocephalus and CLP have been reported in several patients with a duplication of distal chromosome 7q, which contains the *SHH* gene locus, raising the possibility that over-expression of SHH may contribute to these craniofacial defects (Morava et al., 2003). Consistent with this notion, approximately 5% of Gorlin syndrome patients with PTCH1 mutations, in which Shh pathway activity is elevated, develop cleft palate (Evans et al., 1993). Further studies are required to determine the mechanism by which dysregualtion of Shh signaling in *ShhN/+* leads to cleft palate formation. Similarly, how dysregulation of Shh signaling leads to absence of olfactory bulb in *ShhN/+* mutants remains to be determined. However, olfactory bulb aplasia has been observed in *Gli3* loss-of-function mutants (Franz, 1994) (Naruse and Keino, 1993; Tomioka et al., 2000), suggesting a causative link between loss of Gli3 repressor activity and failure of olfactory bulb development. Interestingly, olfactory bulb hypoplasia has also been reported in MIH patients (Simon et al., 2002).

CHAPTER IV

SONIC HEDGEHOG SIGNALING REGULATES A NOVEL EPITHELIAL

PROGENITOR DOMAIN OF THE HINDBRAIN CHOROID PLEXUS

Introduction

Choroid plexuses (ChPs) are heavily vascularized secretory organs in the brain, which serve as sites of cerebrospinal fluid (CSF) production and are also known to generate chemicals and polypeptides with neuroprotective, surveillance and repair functions. The ChP epithelium has been the focus of extensive studies as it serves as the blood-CSF barrier (Redzic et al., 2005; Segal, 2000). ChPs originate from four focal sites at the roof of the brain ventricles: two in the lateral ventricles of the telencephalon, one in the third ventricle of the diencephalon, and one in the fourth ventricle of the hindbrain (hChP). Among all ChPs, hChP emerges earliest during embryogenesis and is conspicuously large. Outgrowth of the hChP is clearly evident at E12.5 as a pair of bilateral ridges protruding from the roof of the hindbrain, gradually developing into a highly convoluted organ with extensive epithelial folding. hChP consists of an outer epithelial layer and an inner core of stromal cells that are surrounded by a dense vascular network. The hChP epithelium (hChPe) initially emerges as a single sheet of pseudostratified cells, but by E13.5 the hChPe adopts a simple columnar morphology with defined brush borders and numerous microvilli at the surface (Sturrock, 1979).

Previous studies suggest that the rhombic lip, a germinal zone, first gives rise to the hindbrain roof plate epithelium (hRPe), which is further specified, potentially by high levels of Bmp signaling (Hebert et al., 2002), into definitive hChPe (Thomas and Dziadek, 1993). Genetic fate-mapping studies have shown that hChPe cells are derived from progenitor cells residing in the anterior lower rhombic lip (LRL) which is positioned between the developing hChP and medulla, with expression of secreted growth factors Wnt1, Gdf7 and Lim-domain transcription factor Lmx1a (Awatramani et al., 2003; Chizhikov et al., 2006; Currle et al., 2005). A recent study indicates that Wnt1-expressing LRL cells can directly contribute to hChPe from E10-E14 but this contribution ceases around E14 (Hunter and Dymecki, 2007). However, continued growth of the hChP beyond E14 suggests contribution by other hChPe progenitor source besides early contribution by the hRPe and anterior LRL.

The *Shh* gene encodes a secreted signaling molecule that is indispensable for animal development. Patched1 (Ptch1), a twelve-pass transmembrane receptor for Shh, functions as a negative regulator of Shh signaling by suppressing the activity of a seven-pass transmembrane protein, Smoothened (Smo). Shh binding to Ptch1 relieves Smo from inhibition, hence triggering Shh signaling and subsequent activation of downstream target gene expression mediated by the Gli family of transcription factors (Ingham and McMahon, 2001). *Gli1* is the only member whose expression is directly regulated by Shh signaling at the transcriptional level, and like *Ptch1* expression, it serves as a direct readout of Shh pathway activation (Ahn and Joyner, 2004; Goodrich et al., 1996).

In the central nervous system (CNS), Shh is well recognized for its role in patterning different ventral neuronal cell types during early embryogenesis and in promoting

cerebellar granule precursor cell proliferation (Goodrich et al., 1997; Wallace, 1999b; Wechsler-Reya and Scott, 1999a). However, the role of Shh signaling during early embryonic CNS development is largely confined to the ventral regions. Interestingly, a recent study reported that Shh functions as an indispensable mitogen during dorsal telencephalic development (Komada et al., 2008). Nevertheless, a definitive dorsal role of Shh has not been generally appreciated. Here we have identified a distinct proliferating hChPe progenitor domain, adjoining the anterior LRL, displaying Shh signaling. While contribution to the hChPe directly by cells of the LRL may have ceased by E14 (Hunter and Dymecki, 2007), our finding indicates that Shh signaling promotes proliferation of cells in the hChPe progenitor domain, thus contributes to the continual growth and expansion of the dorsally-situated hChP, throughout embryonic development.

Experimental procedures

Mice

Wnt1-cre (Jiang et al., 2000), *Gdf7-cre* (Lee et al., 2000a), *Shh$^{f/f}$* (Lewis et al., 2001), *SmoM2* (Jeong et al., 2004), *Patched1$^{lacZ/+}$* (Goodrich et al., 1997), *Gli1-cre^{ERT2}* (Ahn and Joyner, 2004)*, ROSA26-LacZ* (Soriano, 1999) and *ROSA26-eYFP* (Srinivas et al., 2001) mice have been described previously.

Immunohistochemistry

All immunohistochemistry analyses were performed on tissue sections collected from OCT- or paraffin-embedded embryos as previously described (Huang et al., 2007a).

86

The primary antibodies were rabbit anti-Shh (Santa Cruz Biotechnology, 1:1000), rabbit anti-ß gal (Cappel, 1:100), rabbit anti-Aquaporin1 (Chemicon, 1:500), rabbit anti-Lmx1a (gift of Dr. Michael German, 1:200), mouse anti-BrdU (Roche Diagnostics, 1:50), rabbit anti-GFP (Molecular Probes, 1:500) and rabbit anti-Cleaved Caspase3 (Cell signaling, 1:100)

Analysis of cell proliferation and apoptosis

5-Bromodeoxyuridine (BrdU) *in vivo* labeling and terminal deoxynucleotidyl transferase dUTP nick end labeling (TUNEL) analyses were performed as previously described (Huang et al., 2007a).

Cell imaging, counting and statistics

Confocal microscopy was performed on immunofluorescent-stained sections at 1 μm optical slices. Independent stainings were performed on at least three animals for each marker and at least ten non-overlapping sections were counted to generate statistical comparisons. For one-hour short-term BrdU pulse, Lmx1a$^+$; BrdU$^+$ cells in the developing hChP region were located between the LRL and AQP1-expressing differentiated hChPe. For quantifying proliferating hChPe progenitor cell numbers shown in Fig.3, Fig.6, total number of Lmx1a$^+$; BrdU$^+$ cells were counted that spanned the putative hChPe progenitor domain adjoining the anterior LRL, identified by a characteristic bulge. For quantifying number of BrdU$^+$ cells, after 3-day pulse, contributing to the maturing hChPe shown in Fig.4, total numbers of BrdU$^+$; AQP1$^+$ hChPe cells, but not BrdU$^+$; AQP1- hChPm cells, were counted in randomly selected

87

fields under 400X magnification. Only cells with purple-stained AQP1+ membrane contacting brown-stained BrdU+ nucleus were scored. To assess differences among groups, statistical analyses were performed using a one-way analysis of variance (ANOVA) with Microsoft Excel and significance accepted at $p<0.05$. Results are presented as mean $\pm$ standard deviation (sd).

Tamoxifen treatment for temporal fate-mapping studies

Tamoxifen powder (Sigma T-5648) was dissolved in corn oil (Sigma C-8267) at a final concentration of 20 mg/ml. Pregnant females with E13 or E15 embryos from matings between *Gli1-Cre^{ERT2}* and *ROSA26-LacZ* or *ROSA26-eYFP* conditional reporter mice, respectively, were each intraperitoneally injected with 4 mg tamoxifen. Females with E15 embryos were re-injected with 4 mg tamoxifen at E17. Embryos were then harvested and genotyped at E16 (injection at E13) and at newborn stage (P0) for injections at E15/E17. *Gli1-Cre^{ERT2}; ROSA* embryos were processed for b-galactosidase activity or YFP staining followed by confocal microscopy.

X-gal staining and transcript detection

X-gal staining for ß-galactosidase was performed according to standard protocol. The following cDNAs were used as templates for synthesizing digoxygenin-labeled riboprobes: *Shh, Gli1, Patched1, Patched2, Gli3, Ttr, Bmp4, Msx1, Tgfß1, Tgfß3, Sprouty1 and Sprouty2.*

Results

Shh expression and signaling fields in the hindbrain choroid plexus

The hChP is generated bilaterally, protruding into the fourth ventricle, and is clearly evident at E12.5 (Fig.16A, B). It undergoes dramatic growth and expansion as development progresses and joins at the midline (Fig.16D-I). By E16.5, the hChP has developed into a highly convoluted epithelial structure enveloping a vascularized stroma (Fig.16G, H). We observed strong *Shh* mRNA expression in the developing hChP epithelium (hChPe) starting at ~E12.5 and its expression persisted through E18.5, the latest stage analyzed (Fig.16C, F, I and data not shown). In agreement, Shh protein is also highly expressed in the hChPe with localization to both the apical and basolateral sides (Fig.16J, K and L). Interestingly, a small subset of hChPe cells appeared to express low or no *Shh* transcript at various developmental stages (red arrows in Fig.16C). We detected strong Shh signaling in the underlying hChP mesenchyme (hChPm) as shown by Shh signaling targets *Gli1* and *Ptch1* expressions (Fig. 16M, N, O). Notably, we also identified a novel Shh target field within the developing hChP region, a restricted epithelial domain intercalated between the anterior LRL and the differentiated hChPe (Fig.16, red dotted lines). This Gli1$^+$ hChPe domain does not express Shh (arrows in Fig.16C, J). In contrast, the differentiated hChPe expresses Shh but does not display apparent Shh signaling activity (Fig.16, black dotted lines). We did not detect apparent *Ptch2* expression in the developing hChP (Motoyama et al., 1998). Interestingly, *Gli3,* a transcriptional repressor in the absence of Shh pathway activity, is expressed in the adjoining LRL but excluded from the putative hChPe progenitor domain (Fig.16P). We barely detected *Gli1* signal in the telencephalic and diencephalic ChP regions at various

developmental stages (data not shown), consistent with the fact that during embryogenesis only the hindbrain ChP expresses *Shh* while the telencephalic and diencephalic ChPs do not (Tannahill et al., 2005) (data not shown).

Conditional abrogation of Shh signaling in *Wnt1-cre; Shh^{f/-}* mutants leads to impaired hChP development

To determine the functional role of Shh signaling during hChP development, we employed the Cre/loxP strategy to conditionally remove Shh in the hChPe. Previous genetic fate mapping studies indicated that the hChP consists entirely of descendants of Wnt1-expressing cells that localize to the LRL (Hunter and Dymecki, 2007). Indeed, we detected ß-galactosidase activity uniformly in the hChPe when the *Wnt1-cre* driver line was crossed to the *ROSA26-lacZ* reporter strain (Fig. 17A and B). Therefore, the *Wnt1-cre* driver line is suitable for deleting *Shh* in the hChPe. The effectiveness of *Wnt1-cre* deletion of *Shh* was confirmed by essentially ablated *Shh* and *Gli1* expression in the *Wnt1-cre; Shh^{fl/-}* mutant hChP region (compare Fig. 17C, D and Fig.16C, M). Significant loss of Shh signaling in both the epithelial and mesenchymal target fields of the hChP resulted in severe defects in hChP development by E16.5. The *Wnt1-cre; Shh^{fl/-}* mutant hChPs were hypoplastic with markedly reduced epithelial folding at E16.5 (compare Fig. 17 E, F to G, H). The underdeveloped *Wnt1-cre; Shh^{fl/-}* mutant hChPm also showed decreased vascularity (compare Fig. 17 E, F to G, H). However, *Wnt1-cre; Shh^{fl/-}* mutant hChPe maintained its molecular identity as evidenced by expression of differentiated hChPe marker *Transthyretin (Ttr)* and water channel aquaporin1 (AQP1), expressed apically (Fig. 17 I-L). Furthermore, abrogating Shh signaling in the hChP did not appear

90

Figure 16. Differentiated hChPe expresses Shh that signals to the underlying mesenchyme (hChPm) and to a distinct epithelial domain adjoining the lower rhombic lip (LRL).

(A-I) Rapidly expanding hChPe expresses *Shh* in its differentiated epithelial domain. Concomitant with hChP development and epithelial folding (A-I), hChPe cells strongly express *Shh* RNA (C, F, I). Note that Shh expression is either low or absent in a subset of hChPe cells as indicated by red arrows in C. Black arrows in C point to the hChPe region adjoining the LRL that does not express *Shh* RNA. (J, K, L) Shh protein localizes to both apical and basolateral domains of hChPe cells. Again, white arrows in J indicate hChPe domain adjoining the LRL lacking Shh protein expression. (M, N, O) Shh signaling is robust in the developing hChPm, as well as in a distinct hChP epithelial domain adjoining the LRL as indicated by red dotted lines (Gli1^{+}); black dotted lines are continuous with the rest of hChPe (Shh+ and Gli1-) (M, N, O). (P) Gli3 is strongly expressed in the LRL, but not in the putative Gli1^{+} hChPe progenitor domain (red dotted line). Size bar is 20 micron.
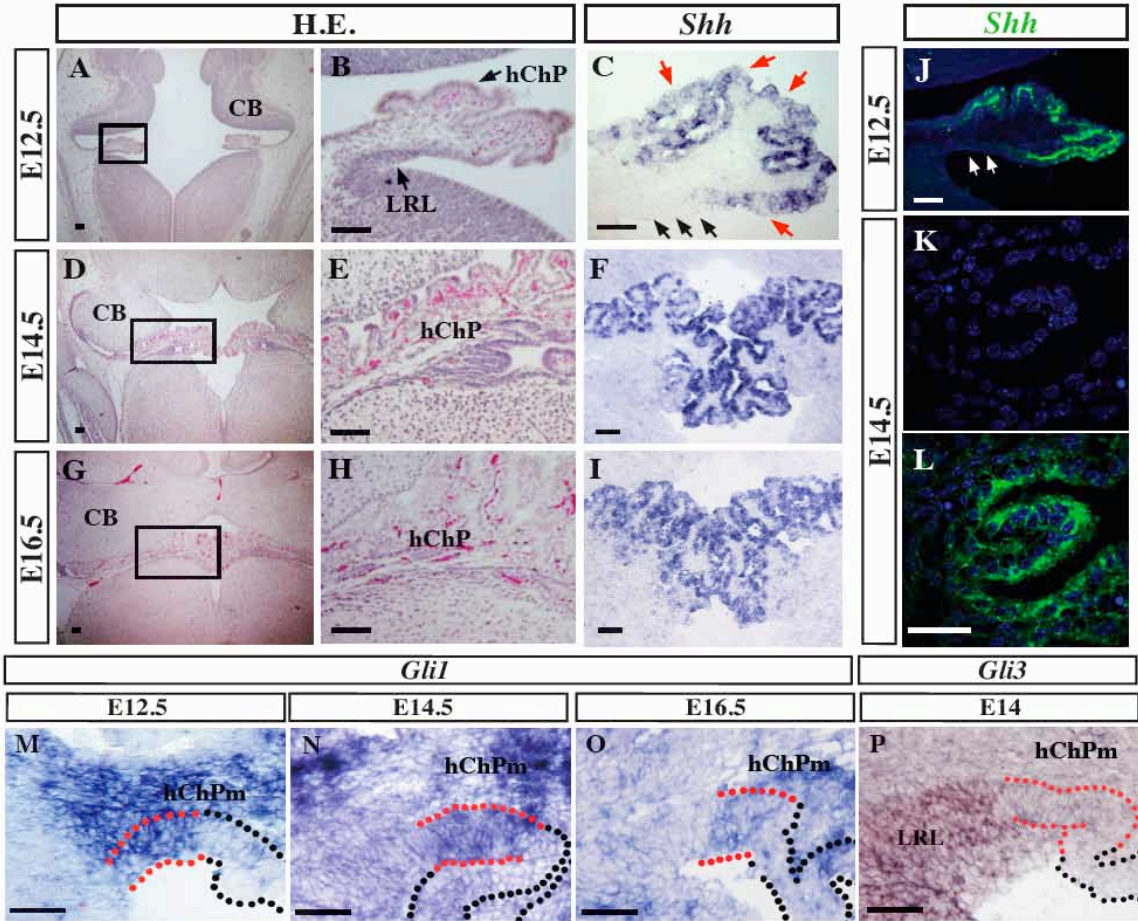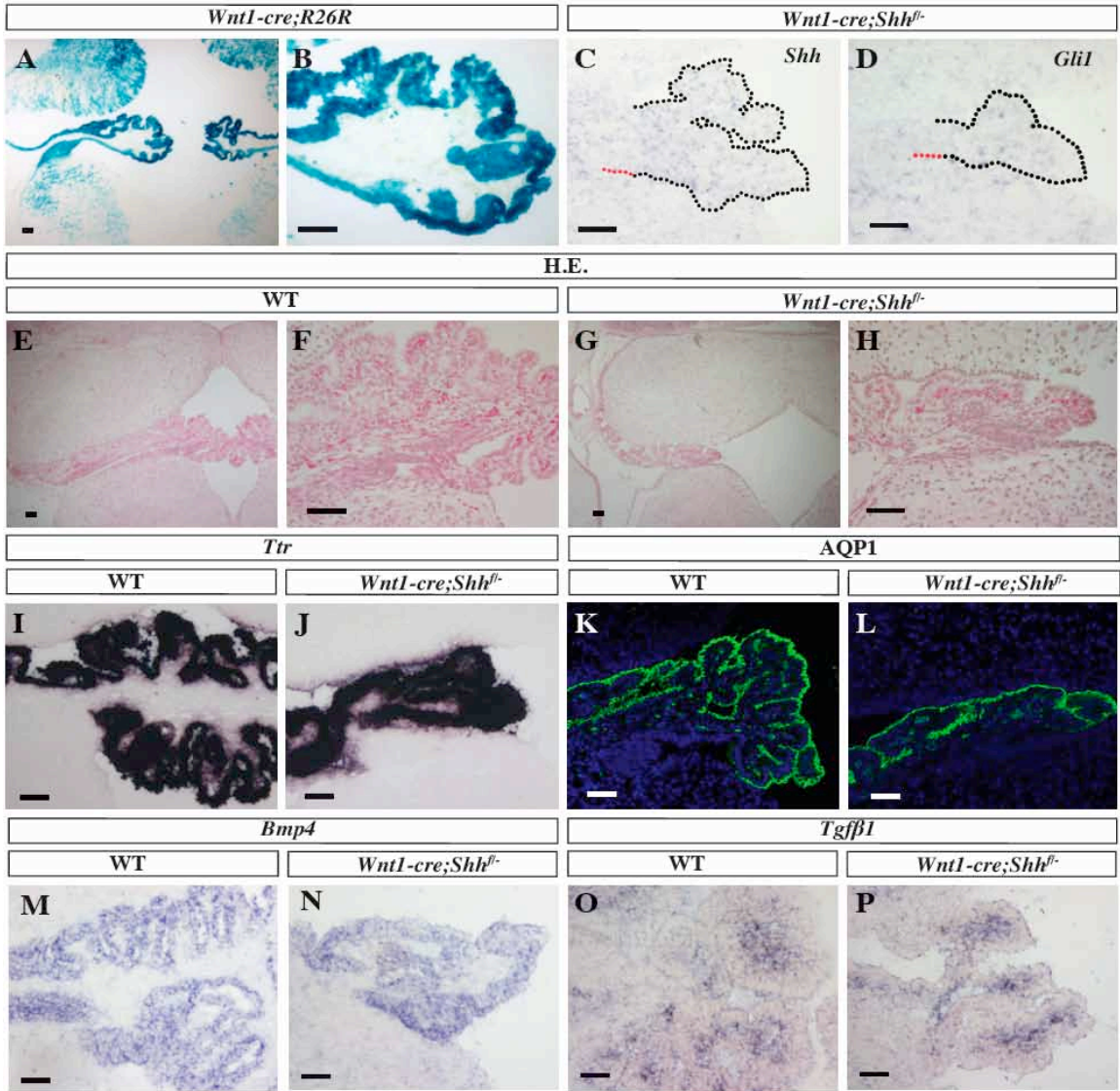
to alter its ability to produce other growth factors, such as *Bmp4* and *Tgfß3* in the hChPe or *Tgfß1* in hChPm (Fig. 17 M-P and data not shown). The Fgf signaling pathway does not appear to regulate hChP development directly, as we did not detect appreciable expression of *Sprouty1* and *2,* target genes of the Fgf signaling pathway (Minowada et al., 1999) (data not shown). These findings indicate that the growth defects seen in *Wnt1-cre*; *Shh$^{fl/-}$* mutant hChP are primarily due to inability to perceive Shh signaling. Therefore, Shh production in the differentiated hChPe domain and Shh signaling within the hChP including the distinct epithelial domain adjoining the LRL are critical for hChP development.

Shh signaling promotes proliferation of a distinct hChP epithelial progenitor domain

Next, in order to elucidate the molecular mechanism of hChPe growth during development, we focused on determining the function of Shh signaling in the hChP epithelial target field. As mentioned above, while the Gli1^{-} differentiated hChPe expressing AQP1 did not appear to display Shh signaling (Fig.16, 3A, B, black dotted lines), we observed distinct Shh signaling (Gli1^{+}) in a restricted epithelial domain adjoining the anterior edge of the LRL extending towards the hChPe (Fig. 16M, N, O, and Fig. 18 A, B; red dotted lines). As we observed marked reduction in hChP growth in *Wnt1-cre*; *Shh$^{fl/-}$* mutants, we asked whether this Gli1^{+} hChPe region defined an hChPe

93

Figure 17. Genetic removal of Shh signaling impairs hChP biogenesis

(A-D) The transgenic *Wnt1-cre* line effectively drives gene deletion in hChPe cells, as indicated by strong LacZ staining signal in E13.5 *Wnt1-Cre; R26R* embryo (A, B) and abrogated Shh expression and signaling in *Wnt1-cre*; *Shh*$^{fl/-}$ mutant hChP (C, D). (E-H) E16.5 *Wnt1-cre*; *Shh*$^{fl/-}$ mutants display severely affected hChP development as indicated by apparent reduction in epithelial and mesenchymal mass and vascularity. (I-P) hChPe cell differentiation and ability to produce other signaling factors appear to be unaffected by loss of Shh signaling. E14.5 *Wnt1-Cre*; *Shh*$^{fl/-}$ mutant hChPe cells maintain expression of differentiation marker *Ttr* (I and J), apical marker AQP1 (K and L), and signaling molecules *Bmp4* (M and N) and *Tgfß1* (O and P). Size bar is 20 micron.

Wnt1-cre;R26R	*Wnt1-cre;Shh^{fl-}*

A   B   C   *Shh*   D   *Gli1*

H.E.

WT	*Wnt1-cre;Shh^{fl-}*

E   F   G   H

Ttr	AQP1
WT	*Wnt1-cre;Shh^{fl-}*	WT	*Wnt1-cre;Shh^{fl-}*

I   J   K   L

Bmp4	*Tgfβ1*
WT	*Wnt1-cre;Shh^{fl-}*	WT	*Wnt1-cre;Shh^{fl-}*

M   N   O   P

progenitor domain. We used Lmx1a expression to mark all cells in the hChPe (Chizhikov et al., 2006). Indeed, in *Patched1$^{LacZ/+}$* embryo, LacZ$^+$ Shh signaling domain overlapped with the Lmx1a-expressing domain adjoining the LRL (Fig. 18C-I, white arrows in E and F, G-I is representative of the red boxed region shown in C) indicating that Shh signaling occurred in this critical domain. We determined that this specific Lmx1a+ hChPe domain also displayed proliferative activity as indicated by its rapid incorporation of BrdU and expression of Ki67 (Fig. 18J-M and data not shown). In contrast, the rest of the hChPe was *Ptch1$^-$* and *Gli1$^-$* (Fig. 16M-O, Fig. 18A, B, black dotted lines) and post-mitotic as these cells did not show BrdU incorporation (after one-hour short-term pulse) or Ki67 expression (Fig. 18J-M, data not shown). Therefore, we propose that Shh pathway activity in the proliferating domain is a distinct hChPe domain harboring progenitor cells that gives rise to nascent differentiated hChPe as development progresses. In agreement, we observed more than 2-fold reduction in proliferating cells in this hChPe progenitor region in *Wnt1-cre*; *Shh$^{fl/-}$* mutants compared with control at E12.5 (44.4$\pm$8.5% vs 100$\pm$11.7%, p<0.001, N=3, Fig. 18J, K, N), and a more pronounced decline in BrdU+ cells (about 7-fold) at E14.5 (15.3$\pm$5.2% vs 100$\pm$18.3%, p<0.001, N=3, Fig. 18L,M, N). We have also generated conditional *Gdf7$^{cre/+}$*; *Shh$^{fl/-}$* mutants using mice with Cre expression driven by the endogenous *Gdf7* promoter which is expressed in all ChPe (Currle et al., 2005). However, we found that the knock-in *Gdf7$^{cre/+}$* line (Lee et al., 2000a) is not as robust as the transgenic *Wnt1-cre* deleter line (Jiang et al., 2000) in driving complete Shh deletion in the hChPe (data not shown). In agreement, we observed a relatively milder, but significant, hChP phenotype in *Gdf7$^{cre/+}$*; *Shh$^{fl/-}$* compared to *Wnt1-cre*; *Shh$^{fl/-}$* mutants at E14.5 (data not shown). The finding that *Gdf7$^{cre/+}$*; *Shh$^{fl/-}$*

mutants exhibited impaired proliferation in the Lmx1a+ hChPe progenitor domain is consistent with our *Wnt1-cre*; *Shh*$^{fl/-}$ mutant studies, lending further support for the essential role of Shh signaling in regulating hChPe progenitor proliferation. Shh signaling did not appear to be required for maintaining cell survival in the hChPe progenitor region as neither control nor *Wnt1-Cre*; *Shh*$^{fl/-}$ mutant displayed apparent apoptotic activity as shown by TUNEL assay (data not shown), or cleaved-Caspase 3 immunolabeling (Fig. 18O-R), while apoptotic signals in the same sections were detected in peripheral nerve or muscle tissues between the developing ribs (data not shown). Previous studies have shown direct LRL cell contribution to the hChPe but production appears to cease around E14. Here, we reveal the essential role of Shh signaling in promoting the proliferation of a distinct pool of hChPe progenitor cells in a domain adjoining the LRL starting ~E12.5 through late embryonic development for the continual expansion of the hChP.

Shh signaling promotes proliferation of hChPe progenitor cells and hChPe biogenesis

To further define the role of Shh signaling in the production of hChPe cells, we performed BrdU pulse-chase labeling, for short and long periods, to compare the temporal contribution of nascent epithelial cells to the hChPe. By co-labeling 1-hour pulsed BrdU with differentiated hChPe apical marker AQP1, we observed a BrdU$^-$AQP1$^-$ region between the hChPe progenitor and differentiated hChPe domains (Fig. 19A and A$^{/}$). Ki67 and AQP1 double-labeling demonstrated that this "gap" region is non-mitotic (Fig. 19C, D). After a 24 hour-pulse, the BrdU$^+$ cells have migrated to the region just adjoining the AQP1$^+$ domain (Fig. 19B and B$^{/}$, white arrow), suggesting a rather slow

97

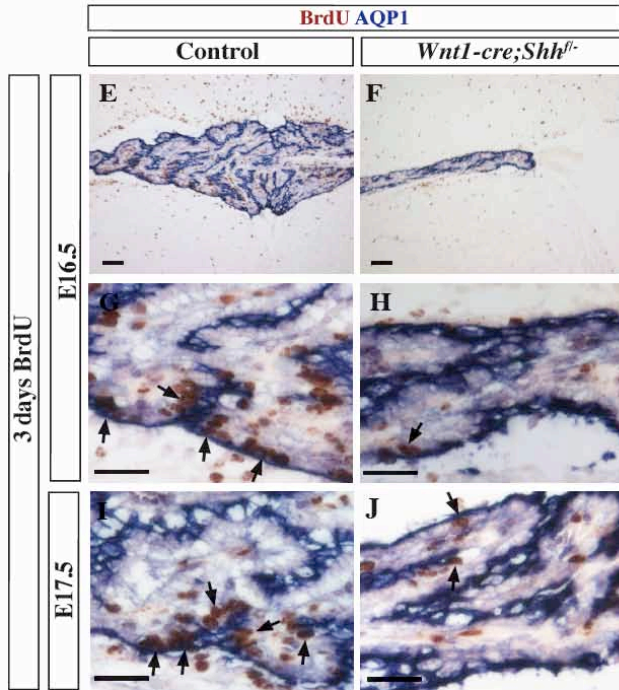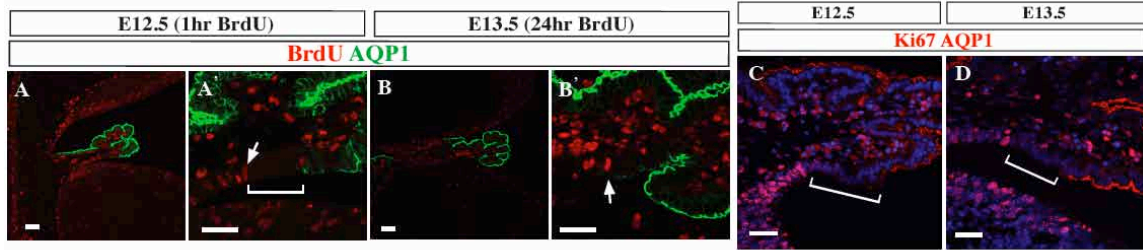**Figure 18. Shh signaling defines an Lmx1a^{+} hChPe progenitor domain and promotes its proliferation**

(A-I) Shh signals to a distinct Lmx1a^{+} domain adjoining the anterior LRL. Shh signaling activity, as evidenced by *Gli1* and *Ptch1*-LacZ expressions, overlaps with this distinct Lmx1a+ domain (compare A-D to E and F), which is confirmed by co-labeling of Lmx1a and ß-gal in *Ptch1*$^{LacZ/+}$ embryos (G, H and I). hChPe progenitor domain adjoining LRL is highlighted by red dotted lines and arrows in A and B. Black dotted lines demarcate the rest of the hChPe (Gli1^{-}). (J-N) Genetic deletion of Shh signaling results in severe proliferation defect in the progenitor domain. Co-labeling of BrdU and Lmx1a in one-hour BrdU-pulsed control and *Wnt1-cre*; *Shh*$^{fl/-}$ embryos reveals a profound proliferation defect at E12.5 (J-K, N) and E14.5 (L-M, N). The proliferation defect is even more severe at E14.5 (N). (O-R) Loss of Shh signaling does not appear to affect cell survival in the hChP, as indicated by absence of cleaved-caspase 3 activity in E12.5 or E14.5 control and *Wnt1-cre*; *Shh*$^{fl/-}$ embryos. Size bar is 20 micron.
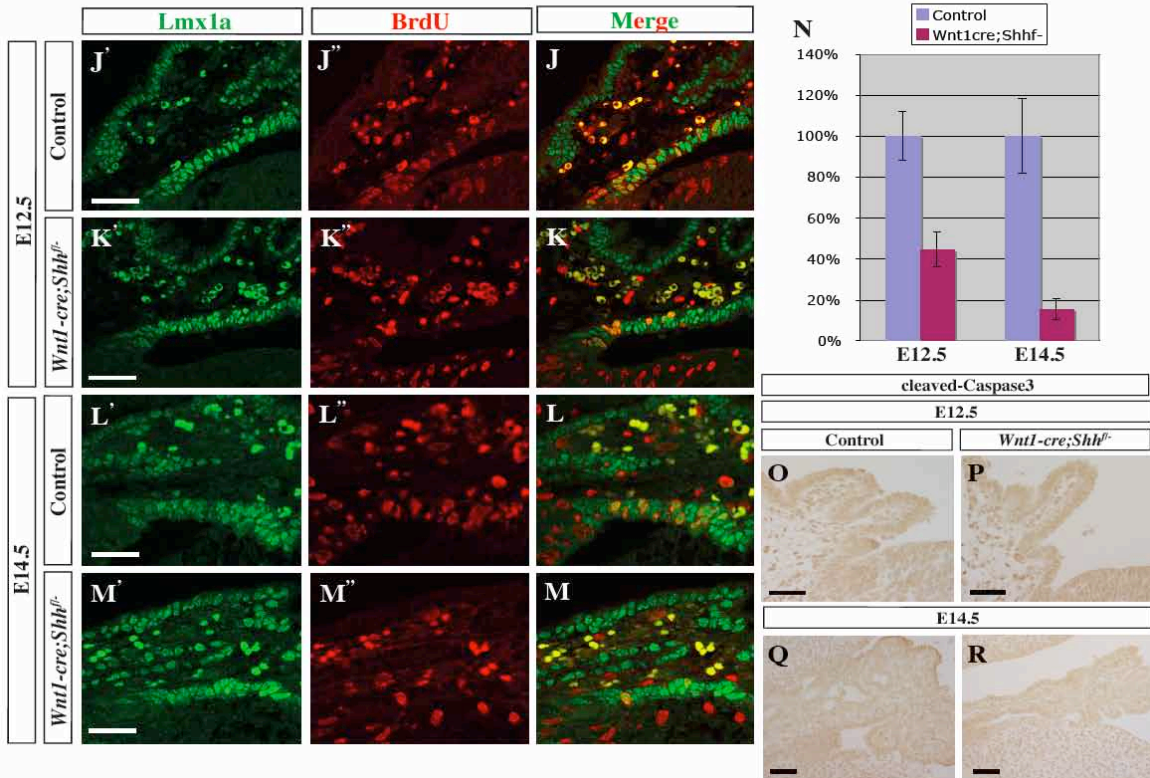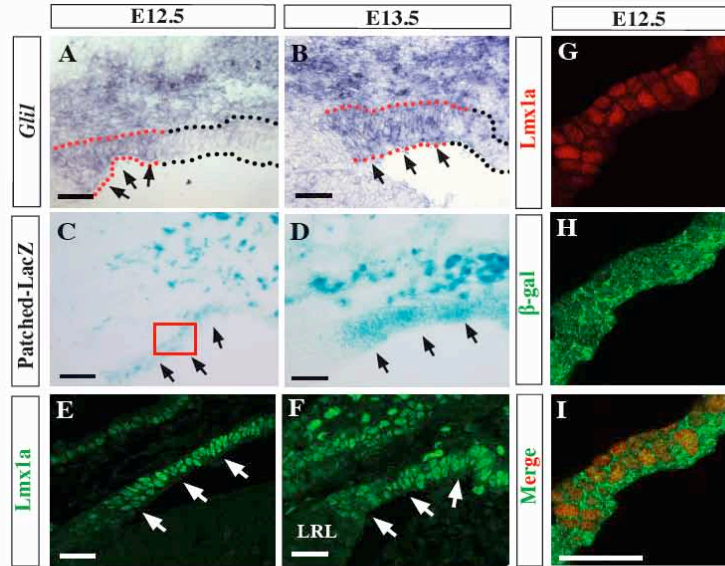
rate of progenitor contribution to the hChPe. However, after 3-day BrdU pulse, starting at E13.5 or14.5, we observed extensive contribution of nascent BrdU+ cells well into the differentiated hChPe (Fig. 19E, G, I). The BrdU$^+$ cell contribution to the hCPe in *Wnt1-cre; Shh$^{fl/-}$* mutants was evidently decreased by about 5-fold compared to control upon analysis at E16.5 (22.1±4.8% vs 100±20.5%, p<0.001, N=3, Fig. 19E-H, K) and E17.5 (24.6 ±7.5% vs 100±15.2%, p<0.001, N=3, Fig. 19I, J, K). These results clearly indicated that hChPe progenitor proliferation in mutants had been compromised in the absence of Shh signaling. To follow the fate of Gli1$^+$ cells in the hChPe progenitor domain, we performed tamoxifen injections on pregnant females from matings between *Gli1cre^{ERT2}* and *ROSA-LacZ* or *ROSA-eYFP* reporter mice at E13 or E15/17, respectively and harvested embryos at E16 or P0. These temporal fate-mapping studies demonstrated that indeed cells derived from the Gli1$^+$ hChPe progenitor domain are incorporated into the mature hChPe (Fig. 20A-D, arrows). The later-stage tamoxifen injection appeared to label fewer cells in the hChPe, consistent with our finding that the Lmx1a+ hChPe progenitor domain displayed reduced proliferative activity at late developmental and postnatal stages (Fig.21, data not shown). We have observed extensive *Gli1-cre* activated gene recombination in the cerebellar external granule layer in the same embryo, indicating the efficacy of tamoxifen treatment (data not shown). As tamoxifen usually begins to be effective in driving gene recombination ~12-24 hours post-injection, our data reveal that *Gli1*-expressing cells between ~E14-18 within the hChPe progenitor domain continue to be incorporated into the expanding hChPe. Taken together, these data demonstrate that Shh signaling is required to maintain a pool of proliferating cells in the hChPe progenitor

Figure 19. Loss of Shh signaling leads to reduced hChPe production

(A-B) Nascent hChPe cells from the progenitor domain appear to be incorporated at a slow rate into the differentiated hChPe region (AQP1+). 1-hour BrdU pulse labeling reveals a BrdU$^-$ and AQP1$^-$ "gap" region intercalated between the hChPe progenitor and differentiated domains (A and A$^/$); this gap region is non-mitotic as indicated by lack of Ki67 expression (C, D). (B and B$^/$) 24-hour BrdU pulsed cells now abut (indicated by white arrow) the AQP1+ hChPe domain indicating a rather slow process by which nascent hChPe cells become incorporated into the differentiated zone. (E-K) Loss of Shh signaling results in largely reduced hChPe cell production in *Wnt1-cre*; *Shh*$^{fl/-}$ mutants. Black arrows indicate 3-day pulsed BrdU+ cells in the differentiated hChPe domain highlighted by AQP1. Size bar is 20 micron.

E12.5 (1hr BrdU)	E13.5 (24hr BrdU)
BrdU AQP1	

E12.5	E13.5
Ki67 AQP1	

BrdU AQP1

Control	Wnt1-cre;Shh$^{f/-}$

3 days BrdU

E16.5

E17.5
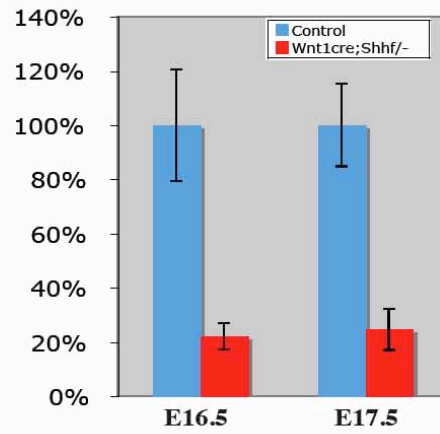
K Comparison of BrdU+;AQP1+ cells

Figure 20. Gli1+ cells from the hChPe progenitor domain contribute to hChPe growth.

Temporal fate-mapping of Gli1$^+$ Shh-responding cells in E16 and P0 hChPe domains with tamoxifen injections at E13 and E15/17, respectively. Black arrows (A, B) and white arrows (C and D panels) point to Gli1-marked hChPe cells. Cells of the Gli1$^+$ lineage are also evident in hChPm. Size bar is 20 micron.
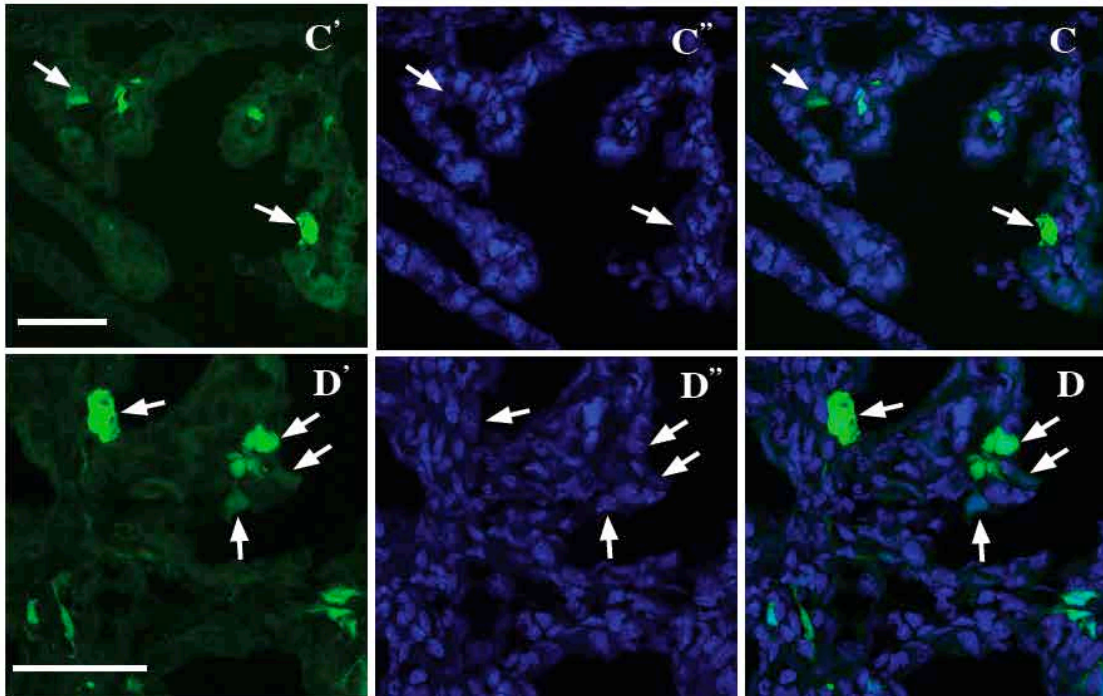
Gli1-creER^{T2};R26R

E16 (Tm at E13)
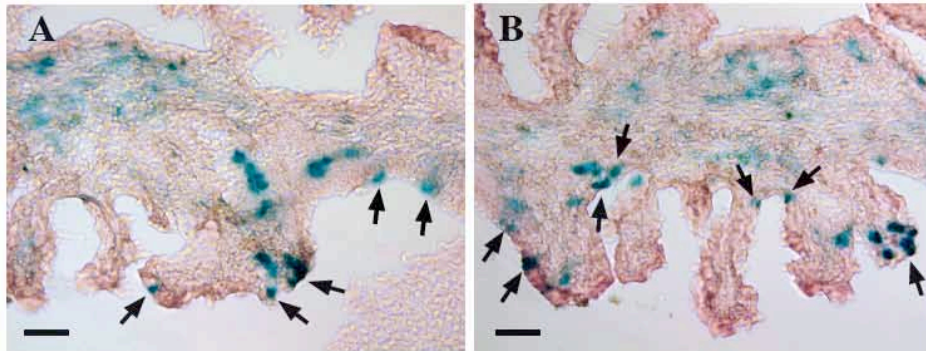
Gli1-creER^{T2};R-eYFP

P0 (Tm at E15 and E17)

domain and that these Gli1^{+} cells appear to contribute to hChPe expansion beginning at ~E12.5 through late developmental stages.

To further support the critical proliferative role of Shh signaling during hChPe development, we generated *Wnt1-cre; SmoM2* and *Gdf7*[cre/+]*; SmoM2* mutants, in which constitutively active SmoM2 (Jeong et al., 2004) is expressed in all hChPe cells. As *Wnt1-cre* is also expressed in the neural crest lineage and widespread Shh pathway over-activation led to profound craniofacial and neural tube defects including excencephaly, all subsequent analyses were performed using the *Gdf7*[cre/+] driver line. Interestingly, while ectopic Notch signaling has been reported to elicit persistent proliferation in many mature hChPe cells (Dang et al., 2006; Hunter and Dymecki, 2007), we observed enhanced mitotic activity that appeared to be confined to the putative hChPe progenitor region adjoining the anterior LRL in *Gdf7*[cre/+]*; SmoM2* mutants at E14.5 and at birth (Fig. 21). By 1-hour pulse, we did not observe BrdU^{+} cells within the AQP1-expressing differentiated hChPe in either control or *Gdf7*[cre/+]*; SmoM2* mutants (Fig. 21F, G). This observation suggests distinct regulatory mechanisms by which Notch and Shh pathways expand the hChPe cell population. Although the number of proliferating Lmx1a^{+} hChPe progenitor cells appeared to dwindle at birth (Fig. 21C, D), we observed enhanced proliferative activity in the hChPe progenitor domain in *Gdf7*[cre/+]*; SmoM2* mutants compared with control at E14.5 ($188.8\pm21.1\%$ vs $100\pm10.9\%$, $p<0.001$, N=3, Fig. 21A-B, E) and P0 ($161.2\pm25.9\%$ vs $100\pm25.4\%$, $p<0.001$, N=3, Fig. 21C-D, E). These gain-of-function studies further support our finding that Shh signaling is both necessary and sufficient to drive proliferation of hChPe progenitor cells. Most *Gdf7*[Cre/+]*; SmoM2* mutants do not survive beyond 3 weeks after birth. All mutants were runted and exhibited

Figure 21. Ectopic Shh signaling drives excessive Lmx1a+ hChPe progenitor cell proliferation

(A-E) *Gdf7$^{cre/+}$; SmoM2* gain-of-function mutants display augmented proliferative activity in the Lmx1a$^+$ hChPe progenitor domain at E14.5 (A-B, E) and P0 (C-D, E), further supporting a proliferative role of Shh signaling during hChPe production. (F, G) Ectopic Shh signaling did not render the differentiated AQP1+ hChPe cells mitotic as evidenced by lack of BrdU signal after 1-hour pulse. BrdU+ cells are present within the mesenchymal compartment of both control and *Gdf7$^{cre/+}$; SmoM2* mutant. Size bar is 20 micron.
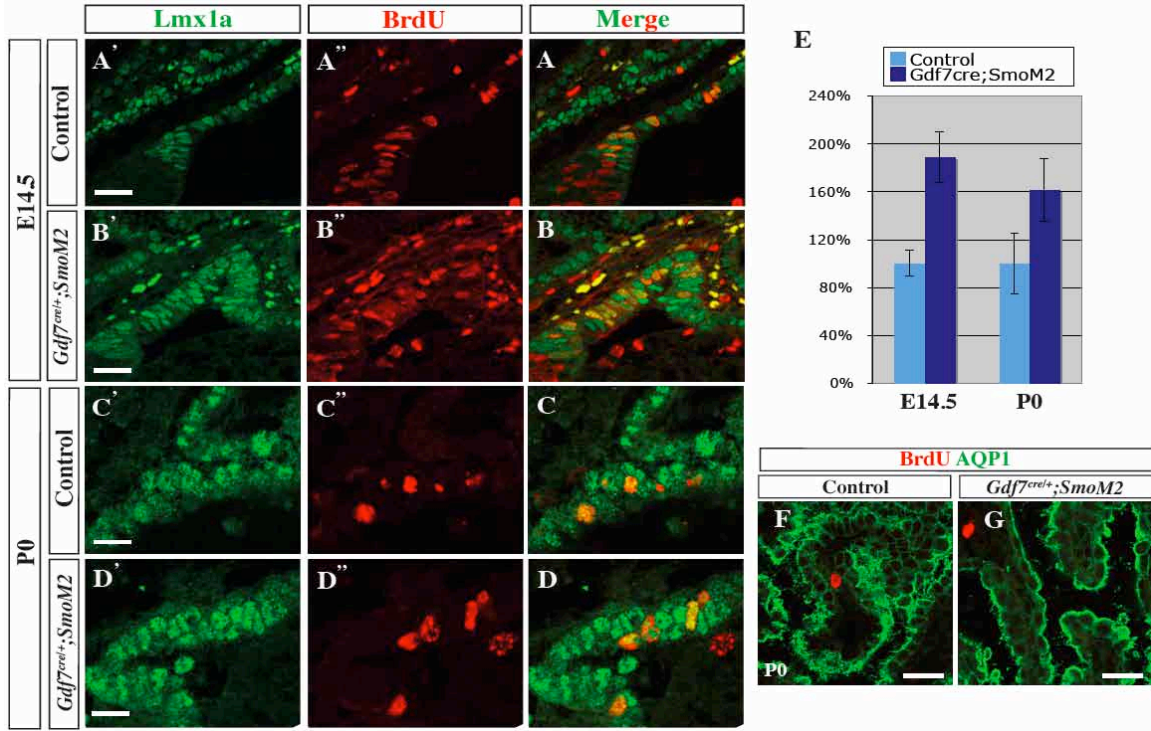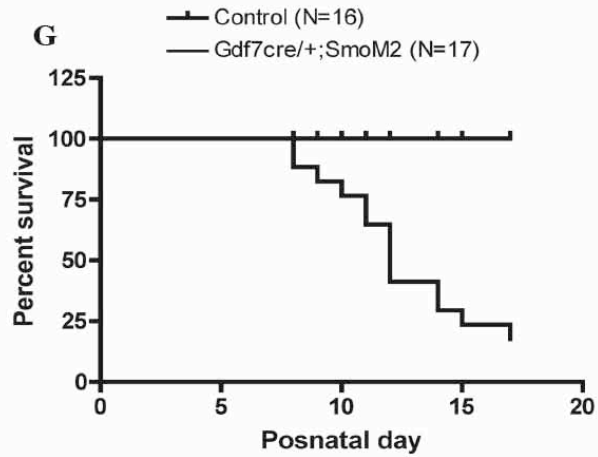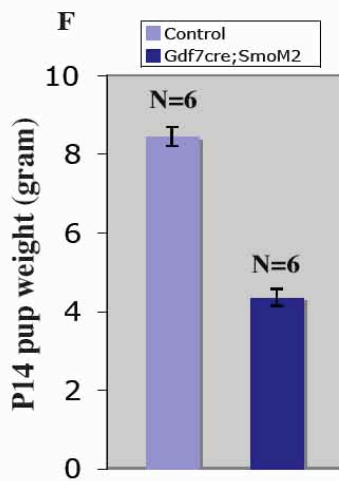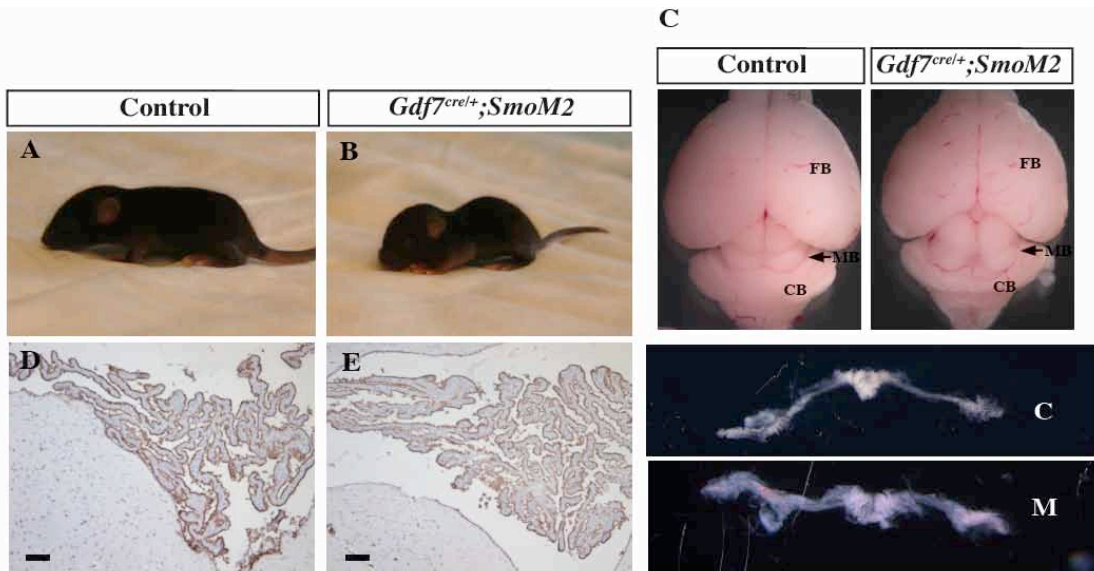
neurological defects reflected by their relative immobility compared with control littermates. Consistent with enhanced proliferation at the progenitor domain, the hChPs of $Gdf7^{Cre/+}$; $SmoM2$ mutants appeared larger in size, displaying more epithelial foldings (Fig. 22). ChPs of the diencephalon and telencephalon may also be affected by expression of SmoM2 since the Gdf7 lineage maps to these choroid plexus epithelia. Therefore, the severe phenotype of $Gdf7^{Cre/+}$; $SmoM2$ mutant neonates may be due to the combined aberrant function of ChPs and disruption in CNS homeostasis.

Discussion

ChPs are secretory organs in the brain and they serve as sites of CSF production and function as blood-CSF barriers to maintain CNS homeostasis. While Bmp signaling in the dorsal midline has been implicated in the specification of ChP epithelial fate (Cheng et al., 2006; Hebert et al., 2002), signaling mechanisms that regulate ChP epithelium production and expansion remain poorly understood. It has been reported that the hChP expresses many morphogens such as Bmps, Fgfs, Tgfßs and Shh (Bitgood and McMahon, 1995; Emerich et al., 2005; Redzic et al., 2005). However, surprisingly little is known about the developmental mechanism or molecular pathway that regulates hChP biogenesis. Interestingly, choroid plexus tumor is a pediatric neoplasm characterized by uncontrolled growth of the ChP epithelium and 40% of ChP tumors arise in the hindbrain ventricle (Gopal et al., 2008). Considering that Shh expression in the CNS is restricted to the ventral axial midline of floor plate and the neuroectoderm before/at midgestation, it is quite unique that a dorsal roof plate-derived hChP exhibits robust Shh expression. Here we show that Shh signaling plays an essential role in regulating hChPe progenitor cell

108

Figure 22. Postnatal studies of gain-of-function *Gdf7$^{Cre/+}$; SmoM2* mutants

(A-B) External view of postnatal day 10 control (A) and *Gdf7$^{Cre/+}$; SmoM2* mutant (B) pups. The *Gdf7$^{Cre/+}$; SmoM2* mutant is severely runted and relatively immobile. (C) *Gdf7$^{Cre/+}$; SmoM2* mutant and control brains appear comparable in size yet wholly dissected hChP of the mutant (M) appears enlarged relative to control (C). (D-E) Despite the much smaller body size of *Gdf7$^{Cre/+}$; SmoM2* mutants, their hChPs appear to be larger displaying more epithelial folds than control. (F) *Gdf7$^{Cre/+}$; SmoM2* mutants are significantly smaller than control. (G) Most of *Gdf7$^{Cre/+}$; SmoM2* mutants do not survive beyond three weeks after birth. Size bar is 20 micron.

Control	Gdf7*cre/+*;SmoM2

A **B**

C

Control	Gdf7*cre/+*;SmoM2

FB · FB · MB · CB · MB · CB

D **E**

C

M

F

P14 pup weight (gram)

Control
Gdf7cre;SmoM2

N=6

N=6

G

Control (N=16)
Gdf7cre/+;SmoM2 (N=17)

Percent survival

Posnatal day

proliferation and thus, expansion of the hChP throughout embryogenesis (Fig. 23).

The hChP exhibits complex epithelial folding during development that vastly enlarges its surface area necessary for secretory functions. Therefore, it is essential to ensure adequate production of epithelial cells throughout hChP development. Previously, Bmp signaling has been identified to specify the primitive pseudostratified epithelial domain into a definitive ChPe fate, demonstrated by specific loss of ChP after telencephalic inactivation of Bmp receptor 1a (Bmpr1a) (Hebert et al., 2002). Genetic fate-mapping studies suggested that the hChPe progenitor resides in the anterior LRL domain expressing Gdf7 and Lmx1a. The Notch signaling pathway has been shown to promote hChPe proliferation, as retrovirus-driven expression of Notch3 ligand (Dang et al., 2006) and *Gdf7^{Cre}*-driven ectopic expression of activated Notch1^{ICD} ligand (Hunter and Dymecki, 2007) all led to persistent proliferation of hChPe cells. Conversely, global inactivation of Notch signaling in zebrafish resulted in defective ChP development (Bill et al., 2008; Garcia-Lecea et al., 2008). However, these over-expression and global gene inactivation analyses yielded limited information as to whether Notch signaling regulates the proliferative capacity of hChPe progenitor domain in a physiologically unperturbed situation, and what cell population Notch signaling directly targets. Indeed, we observed that Notch1 expression encompasses the entire LRL (unpublished observation), indicative of a broader function of Notch signaling rather than specifically acting on expanding the hChPe progenitor domain. Here, our study identifies a Shh signaling hChPe progenitor domain adjoining the anterior LRL. Loss- and gain-of-function analyses demonstrated that Shh signaling

111

Figure 23. Compartmentalization of Shh expression and signaling in the hChP

Shh expression in the differentiated hChPe (yellow, Gli1⁻ BrdU⁻) activates Shh signaling in two hChP target fields, the hChPe progenitor domain (red, Gli1⁺ BrdU⁺) and the mesenchyme (blue). Since Shh protein is distributed in both apical and basal membranes of the differentiated hChPe, Shh movement to the hChPe progenitor domain could potentially occur via either or both routes (curved arrows).
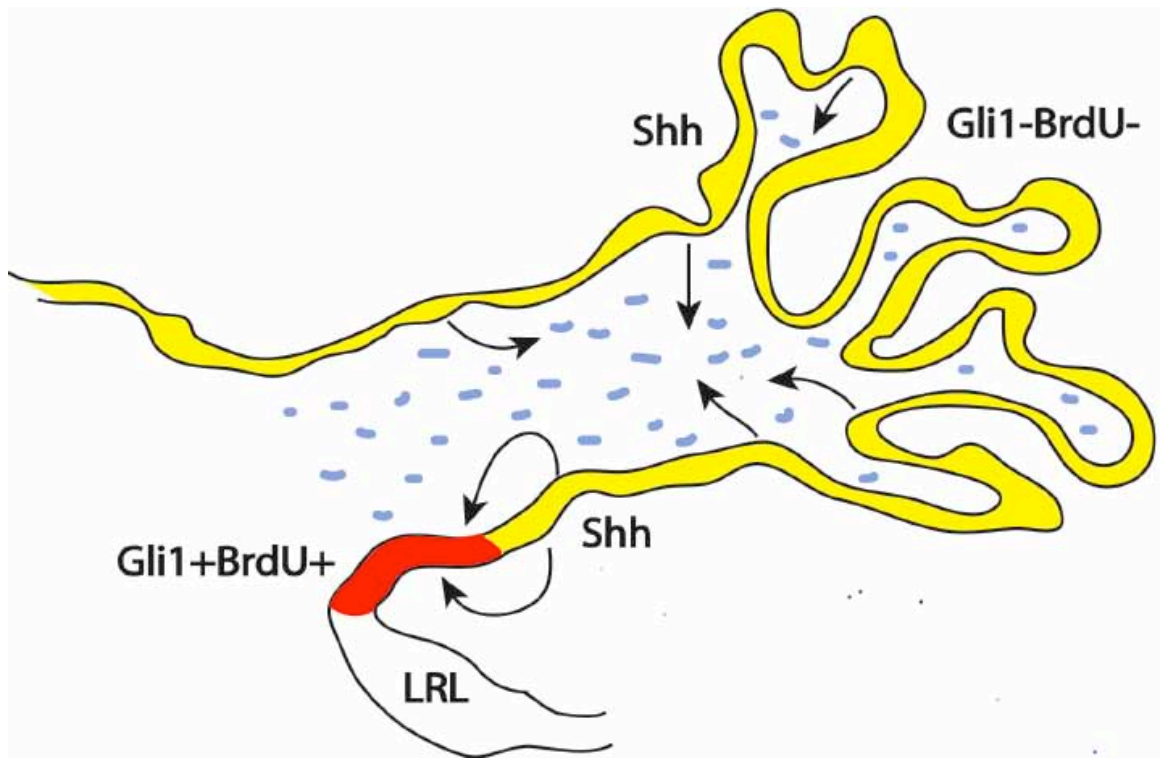
functions specifically to promote proliferation of this hChPe progenitor domain to ensure sufficient production of nascent hChPe cells that gradually get incorporated into the medial, differentiated hChPe. Therefore, we propose that Shh signaling defines a novel Lmx1a+ hChPe progenitor domain and Shh pathway activation is essential for regulating the proliferation of these progenitor cells critical to hChP biogenesis from ~E12.5 through late stages of development.

The finding that Shh signaling promotes the proliferation of epithelial progenitor cells destined to the hChPe which is itself a primary source of the Shh ligand reveals an interesting biological phenomenon in which the Shh target and producing cells are part of the same tissue, the ependymal epithelium. We show that Shh produced in the hChPe not only signals to the mesenchyme, a classic example of epithelial-mesenchymal interaction, but also to its own progenitor domain, thus a unique example of two distinct target fields within one organ. In several endoderm-derived organs displaying epithelial-mesenchymal interactions, it is thought that Shh produced by the epithelium exclusively signals to the mesenchyme which in turn generates another mitogenic signal to promote epithelial proliferation. Although the hChP mesenchyme could also contribute to hChPe growth, our finding reveals a tissue autonomous role of hChPe with regard to Shh production and signaling in driving the growth and expansion of a conspicuously large hindbrain choroid plexus (Fig. 23).

CHAPTER V

TRANSVENTRICULAR DELIVARY OF SONIC HEDGEHOG IS ESSENTIAL TO

CEREBELLAR VENTRICULAR ZONE DEVELOPMENT

Introduction

The cerebellum plays important roles in sensory perception and motor coordination. These functions are critically dependent on diverse neurons and glia originating from two distinct germinal neuroepithelia: RL and VZ. The cerebellum emerges from dorsal rhombomere 1 of the hindbrain as bilateral symmetrical bulges into the fourth ventricle (Altman and Bayer, 1997). As development proceeds, the two primitive cerebellar hemispheres meet in the midline to first form the superior and then inferior vermis. By the end of embryogenesis, the cerebellum acquires a well-defined three-dimensional cytoarchitecture which comprises an outer cortical structure, an inner core of white matter and clusters of deep cerebellar nuclei (DCN) (Altman and Bayer, 1997).

As in the cerebrum, neurons of the cerebellum are either inhibitory or excitatory depending on the expression of neurotransmitter GABA or glutamate, respectively (Carletti and Rossi, 2008). The principal excitatory neurons residing in the cerebellar granule layer are granule cells. During development, granule precursor cells generated from the RL migrate tangentially to the external granule layer (Wingate and Hatten, 1999) where they proliferate in response to Purkinje-derived Shh during late

embryogenesis and the early postnatal period (Wechsler-Reya and Scott, 1999a) (Dahmane and Ruiz i Altaba, 1999) (Wallace, 1999b). Aberrant activation of the Shh pathway in *Patched1* heterozygous mice results in medulloblastoma (MB), a malignant cerebellar tumor, which is thought to stem from massive deregulated granule neuron precursor proliferation (Goodrich et al., 1997). Similarly, mutations in *PATCHED1* significantly increase the occurrence of sporadic MB in humans (Raffel et al., 1997).

In contrast to glutamatergic neurons, the GABAergic neurons are generated from the VZ and consist of at least five different neuronal subtypes, including Purkinje cells and GABAergic interneurons (Pierce, 1975), (Miale and Sidman, 1961), (Morales and Hatten, 2006) Birthdating studies have revealed that neurons of the cerebellar VZ are generated in three sequential but overlapping waves (1, 9, (Miale and Sidman, 1961), (Morales and Hatten, 2006). The first-born are small DCN neurons (E10 to E12 in mice), which eventually settle in the white matter beneath internal granule neurons. A large proportion of the DCN neurons are RL-derived (Machold and Fishell, 2005) (Wang et al., 2005) while a recent study suggested that a subset of early-born DCN neurons likely belong to the class of GABAergic nucleo-olivary projection neurons (Leto et al., 2006). Purkinje cell progenitors are second to be generated from the VZ and they become postmitotic from E11 to E13 (Morales and Hatten, 2006). Purkinje cells then migrate dorsally along guiding radial glial processes to their final destination beneath the external granule layer. A third population of neurons, which consist of inhibitory interneurons of DCN, stellate, basket, Lugaro and Golgi cells, are generated during late embryonic (from E14) and postnatal development in an inside-out sequence, from DCN to granular (Golgi and Lugaro cells) and molecular layer (basket and stellate cells). In addition to GABAergic

116

neurons, astrocytes including Bergmann glia and oligodendrocytes are also derived from the VZ (Altman and Bayer, 1997). Mature Bergmann glia cells are situated in the Purkinje layer and provide support, nutrition and guidance cues for radial migration of postmitotic granule neurons from the EGL to the internal granule layer. By fate mapping studies, radial glial cells are recognized as VZ multipotent progenitors that give rise to all the aforementioned cerebellar cell types (Anthony et al., 2004) (Mori et al., 2006). Although the cellular origin and final fate of many cerebellar neurons are known, the signaling pathways that maintain the proliferative capacity of resident progenitors in the ventricular germinal neuroepithelia remain elusive.

The role of Shh signaling in regulating adult forebrain sub-ventricular zone neural stem cells has been studied extensively (Machold et al., 2003) (Palma et al., 2005) (Balordi and Fishell, 2007b) (Balordi and Fishell, 2007a). While these studies focused primarily on the role of Shh signaling in postnatal and adult stages, its definitive function during embryonic forebrain radial glia cell development has not been demonstrated (reviewed in (Ever and Gaiano, 2005). Moreover, prototypic midline signaling centers such as prechordal plate and floor plate that are continuous with embryonic neural epithelium and normally associated with neural progenitor specifications/maintenance are absent during cerebellum VZ development. Here, we reveal an essential and previously unappreciated function of Shh signaling in embryonic cerebellar development, providing the first evidence that Shh signaling regulates proliferation and expansion of cerebellar radial glia and neural progenitors derived from the VZ. We further determined that the cerebellum itself is not a source of Shh that targets the early cerebellar VZ and strongly implicate a transventricular route for delivery of Shh ligand to the cerebellar VZ. As

117

current pathological studies associated with deregulation of Shh signaling are mainly focused on external granule neurons, our findings may provide additional insights into the diverse cellular origin of cerebellar diseases.

Experimental Procedures

Mice

$Shh^{Cre/+}$ mice have been described previously (Li et al., 2006). $Ptch^{lacZ/+}$ (Goodrich et al., 1997), *R26R (Soriano, 1999), Nestin-cre* (Graus-Porta et al., 2001), $Shh^{f/f}$ *(Lewis et al., 2001), Wnt1-cre (Jiang et al., 2000), SmoM2 (Jeong et al., 2004)* and $Smo^{f/f}$ (Jeong et al., 2004) *mT/mG* (Muzumdar et al., 2007) mice were obtained from the Jackson Laboratory. $Gdf7^{cre/+}$ line was a gift of Dr. Tom Jessell and Dr. Jane Dodd.

Immunohistochemistry

All immunohistochemistry analyses were performed on tissue sections collected from OCT- or paraffin-embedded embryos. The primary antibodies were goat anti-Shh (Santa Cruz Biotechnology, 1:1000), mouse anti-Lhx1/5 (DSHB, 1:10), mouse anti-Cyclin D1 (BD Pharmingen, 1:100), rabbit anti-Sox9 (gift of Dr. Michael Wegner, 1:2000), rabbit anti-Sox2 (Chemicon, 1:1000), rabbit anti-Pax2 (ZYMED, 1:500), rabbit anti-Ptf1a (gift of Dr. Chris Wright, 1:1000), mouse anti-Mash1 (gift of Dr. Jane Johnson, 1:40), rabbit anti-BLBP (Chemicon, 1:500), mouse anti-beta galactosidase (Promega, 1:500), rabbit anti-Cleaved Caspase3 (Cell signaling, 1:100), mouse anti-acetylated Tubulin (Sigma, 1:500) and rabbit anti-Arl13b (gift of Tamara Caspary, 1:1000).

Cell counting and statistics

Defined areas selected for cerebellar cell counting are shown in Fig. 24. Boxed region indicates unit area defined by *ImageJ*. For cell countings from stainings that determine the proliferative capacity of cerebellar regions, we selected an 800x80 region (about 10 to 12 cells from the ventricular surface, which parallels the Ki67+ layer) along the medial VZ in E13.5 and E14.5 cerebella, as almost all proliferative activities occur in the VZ at this stage. For E16.5 and E18.5 embryos, we arbitrarily selected a broader 1000x100 region for vermis VZ (vVZ) and lateral VZ (lVZ) region to assess the proliferative effect of Shh signaling, as indicated by BrdU and CyclinD1 stainings. For stainings that determine GABAergic progenitors at E16.5, we selected the 1000x800 region for both vermal and lateral cerebellum, as reduced GABAergic cell types are considered to be a cumulative result of defective VZ radial glial proliferation.

The numbers of labeled cells vary greatly depending on markers, we therefore further normalized all mutant cell counts to those of the wildtype, presenting a % comparison for clarity. Three independent stainings were performed for each marker and at least 10 sections in each region were counted to generate a statistical comparison. To assess differences among groups, statistical analyses were performed using a one-way analysis of variance (ANOVA) with Microsoft Excel and significance accepted at $p<0.05$. Results are presented as mean $\pm$ standard deviation (sd).

X-gal staining and transcript detection

X-gal staining for ß-galactosidase was performed according to standard protocol. The following cDNAs were used as templates for synthesizing digoxygenin-labeled

Figure 24. Representative regions selected for cell countings and statistical analyses.

Boxed region indicates unit area defined by *ImageJ*. For cell countings from stainings that determine the proliferative capacity of cerebellar regions, we selected an 800x80 region (about 10 to 12 cells from the ventricular surface, which parallels the Ki67+ layer) along the medial VZ in E13.5 and E14.5 cerebella, as almost all proliferative activities occur in the VZ at this stage. For E16.5 and E18.5 embryos, we arbitrarily selected a broader 1000x100 region for vermis VZ (vVZ) and lateral VZ (lVZ) region to assess the proliferative effect of Shh signaling, as indicated by BrdU and CyclinD1 stainings. For stainings that determine GABAergic progenitors at E16.5, we selected the 1000x800 region for both vermal and lateral cerebellum, as reduced GABAergic cell types are considered to be a cumulative result of defective VZ radial glial proliferation.

For cell countings on E13.5/E14.5 WT and mutant embryo cerebellar VZ
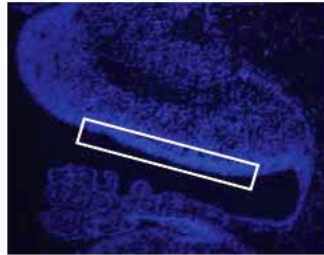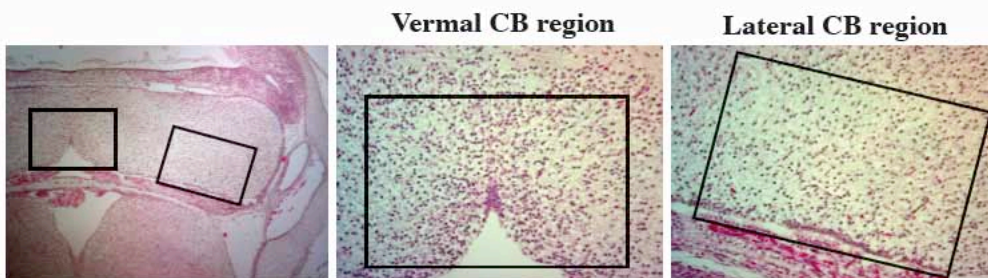

For cell countings from BrdU and CyclinD1 stainings on E16.5 WT and mutant cerebella

| **Vermal VZ region** | **Lateral VZ region** |
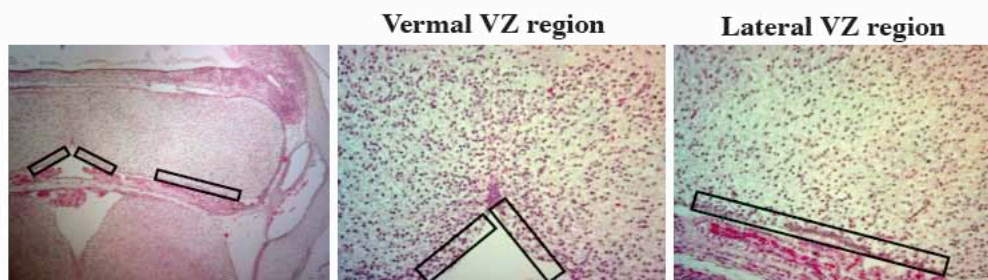
For cell countings from Pax2, Lhx1/5 stainings on E16.5 WT and mutant cerebella

| **Vermal CB region** | **Lateral CB region** |

riboprobes: *Shh, Patched1, Gli1, Msx1, Ngn2.*

Real-time RT-PCR

Whole cerebella were dissected from E12.5-E16.5 wildtype embryos. Total RNA was extracted using RNAeasy Mini kit (Qiagen) and treated with DNAse I to remove genomic DNA. 2μg of RNA was reverse transcribed to cDNA using Promega AMV-RT reverse transcriptase. All DNA and RNA concentrations were measured by Gene Spec I. Real-time detection and quantification of cerebellar cDNA were performed with the iCycler instrument (Bio-Rad). qPCR was performed in a 50μl reaction mixture containing 1x SYBR^4 Green DNA polymerase mixture (Stratagene), 0.4μM of each pair of primers (see Table 1), and 1μl of cDNA template. 40 cycles of amplification was performed according to manufacturer's instructions. Fluorescence data were collected at annealing stages and real-time analysis performed with iCycler™ iQ Optical System Software V3.0a. Serial dilutions of cDNAs were used for construction of the standard curve. Ct values were determined with automatically set baseline and manually adjusted fluorescence threshold. Gene expressions of *Shh*, *Gli1* and *Ihh* were normalized with that of *GAPDH*. All experiments were repeated three times and statistical values were calculated using Microsoft Excel. The PCR primers used are as follows: *GAPDH,* Forward, TTCACCACCATGGAGAAGGC, Reverse, GGCATGGACTGTGGTCATGA; *Shh,* Forward, TCTGTGATGAACCAGTGGCC, Reverse, GCCACGGAGTTCTCTGCTTT; *Gli1,* Forward, CTGGAGAACCTTAGGCTGGA, Reverse, CGGCTGACTGTGTAAGCAGA; Ihh, Forward, CCCCAACTACAATCCCGACATC, Reverse, CGCCAGCAGTCCATACTTATTTCG.

Retrieval of embryonic CSF and Shh ELISA

Wildtype embryos from CD1 females, at E12.5-15.5, were dissected in sterile ice-cold PBS and then placed on Kimwipe with hindbrain ventricle facing upwards. CSF was aspirated using a mouth-operated micropipette placed inside the hindbrain ventricle. As CSF is generated from the choroid plexus of lateral, third and fourth ventricles and all brain ventricles are connected, it is not possible to isolate CSF selectively in the fourth ventricle. Therefore, we determined the presence of Shh protein in the context of the entire CSF. We typically retrieved 2 to 4 ul of CSF per embryo depending on the age. CSF was subjected to centrifugation for 10 min at 16,000g and then transferred to a pre-cooled tube prior to storage at −80C. About 150 ul CSF was pooled for each stage followed by ELISA. Shh concentration in CSF was measured according to manufacturer's instructions (DuoSet$^{®}$ ELISA Development System, R&D Systems). ELISA was performed on two-fold dilution of CSF at a starting concentration of 1:1.83 (reagent diluent: CSF) for E12.5 and E15.5 and at 1:1.14 and 1:1.27 for E13.5 and E14.5 respectively. The colorimetric optical density was measured at 450nm (FLUOstar Omega, BMG Labtech). We also included purified Shh protein (ShhNp, starting at 0.063 nM) and NIH3T3 cell-conditioned media (negative control) in the analysis. NIH3T3 cells do not express Shh endogenously. As shown in Figure 5, Shh protein is present in the CSF at a concentration range of 100-300 pg/ml. The local concentration surrounding the hChP and cerebellar VZ could be much higher.
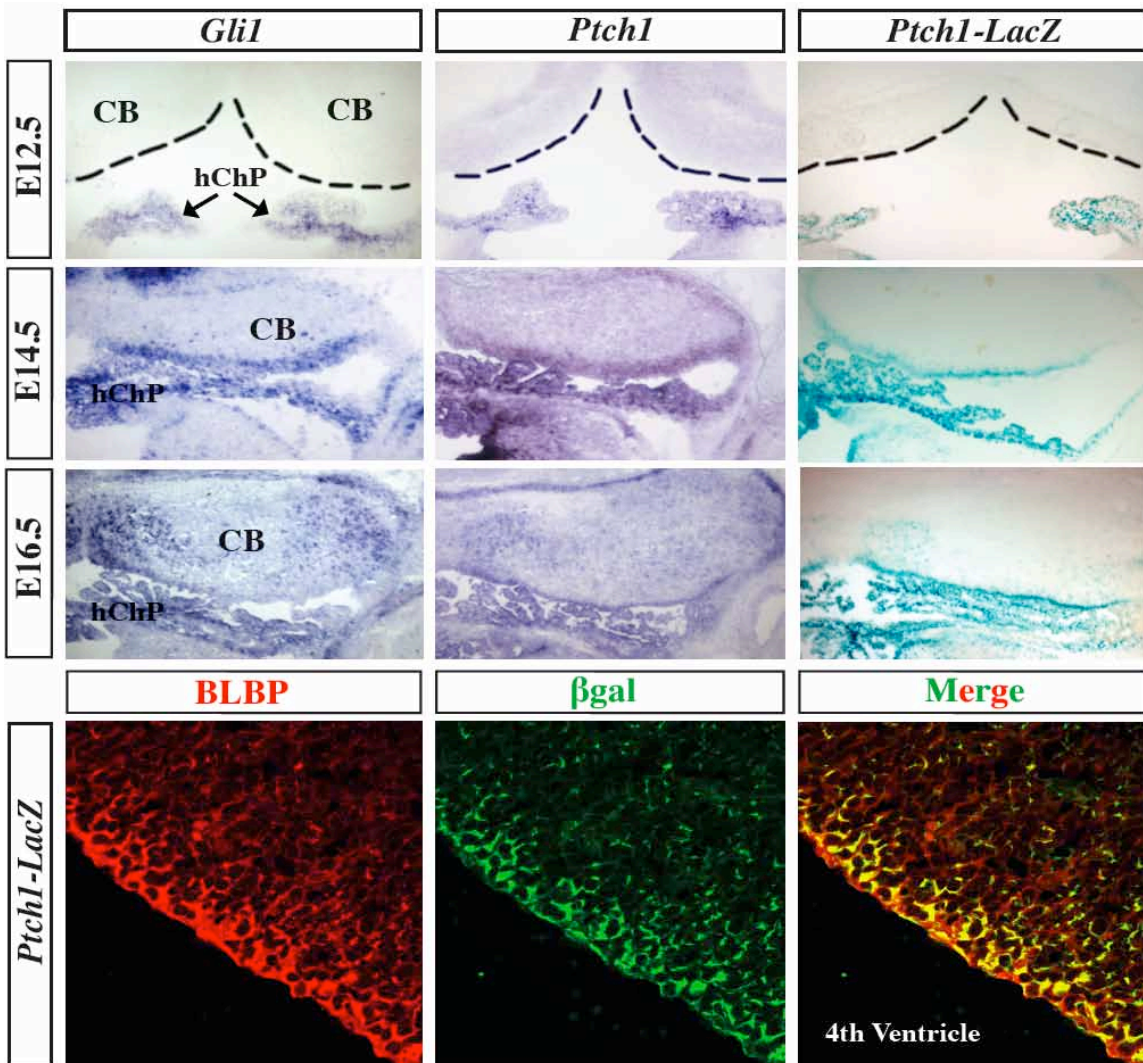
RESULTS

Cerebellar ventricular zone progenitors display Shh signaling

We have recently reported that the developing hindbrain choroid plexus epithelium (hChPe) robustly expresses Shh and the Shh signaling pathway targets a discrete epithelial tissue situated in between the hChP and lower rhombic lip (Huang et al., 2009). This distinct epithelial domain functions as the hChPe progenitor domain by directly contributing to the differentiated hChP epithelium, a proliferative process depending on active Shh signaling activity (Huang et al., 2009). To our surprise, during our examination of the expression of *Gli1* and *Ptch1* by RNA *in situ* hybridization for Shh pathway activation encompassing both the hChP and adjacent cerebellum, we also detected Shh signaling pathway activity in the cerebellar VZ along the medial-lateral axis at E14.5 (Fig. 25A). We observed similar expression pattern in sections from *Ptch1-LacZ* mice containing a LacZ reporter knock-in at the endogenous *Ptch1* locus (Fig. 25A). Shh signaling continued to be detected at E16.5 (Fig. 25A) in the cerebellar medial VZ and vermal region. While *Gli1* expression was relatively higher in the medial VZ, *Ptch1* and Ptch1-lacZ staining appeared to span the VZ medial-lateral axis. Shh signaling activity was not detectable in the cerebellum at E12.5, while evident in the developing hChP at all stages presented (Fig. 25A) (Huang et al., 2009). As radial glial cells are localized to the apical surface of the brain ventricular zone and recognized as the major source of neural progenitors in the cerebellum (Anthony et al., 2004), we examined whether Shh signaling is activated in these cells. Indeed, we observed co-localization of brain lipid binding protein (BLBP), a radial glial cell marker, and *Ptch1-lacZ* expression in E13.5 cerebellar

Figure 25. Shh signaling in the embryonic cerebellum

Gli1, *Ptch1* mRNA expression and *Ptch1-lacZ* expression in developing cerebellum. As shown by *Gli1*, *Ptch1* mRNA and *Ptch1-lacZ* signal, cerebellar VZ displays Shh signaling activity by E14.5. At E16.5, Shh signaling continues to be apparent along cerebellar VZ with higher expression in the medial portion. Note that at this stage, there are many positive cells beyond VZ within the cerebellar tissue. ß-gal+ cells overlap with BLBP+ cells in E13.5 $Ptch1^{LacZ/+}$ embryos, suggesting that Shh signaling directly targets radial glial progenitors.

	Gli1	*Ptch1*	*Ptch1-LacZ*
E12.5	CB CB hChP		
E14.5	CB hChP		
E16.5	CB hChrP		

|	**BLBP**	**βgal**	**Merge**
Ptch1-LacZ			4th Ventricle

VZ (Fig. 25B).

Shh signaling regulates cerebellar ventricular zone progenitor proliferation and GABAergic neuronal progenitor expansion

Next, we set out to determine the role of Shh pathway activation in the cerebellar VZ at E16.5, prior to the stages in which purkinje neurons apparently express Shh. We first analyzed the cerebellar phenotype of *Nestin-cre;Smo$^{f/-}$* mutants, in which Shh signaling is conditionally ablated in all neural cells throughout the developing CNS after E11.5 (Graus-Porta et al., 2001), Fig. 26A). At E16.5, *Nestin-cre;Smo$^{f/-}$* cerebellar VZ was remarkably thin, particularly in the medial region, and VZ cells were loosely arranged along the medial-lateral axis. We found significant reduction in VZ proliferation, by labeling one-hour pulsed BrdU incorporation, in *Nestin-cre;Smo$^{f/-}$* cerebella compared with WT ($14\pm1.9\%$ vs $100\pm3.4\%$ in vermis region, $p<0.001$; $22\pm4\%$ vs $100\pm7.2\%$ in lateral VZ, $p<0.001$, N=3, Fig. 25B and 25C). Cyclin D1 expression was prominent in E16.5 WT VZ cells and numerous migrating cells beyond the VZ, but its expression was dramatically down-regulated in *Nestin-cre;Smo$^{f/-}$* cerebella ($12\pm2.5\%$ vs $100\pm8.8\%$ in vermis region, $p<0.001$; $14\pm3.7\%$ vs $100\pm6.1\%$ in lateral VZ, $p<0.001$, N=3, Fig. 26B and 26C). Thus, CyclinD1 may also be the essential downstream mediator of Shh signaling in the VZ, as in the EGL (Kenney et al., 2003). Expression of Pax2, a paired box transcription factor, has been shown to identify GABAergic interneuron

127

Figure 26. *Nestin-cre; Smo$^{f/-}$* or *Nestin-cre; SmoM2* **mutants exhibit, respectively, reduced or augmented VZ progenitor proliferation and GABAergic interneuron expansion**

A. *Nestin-cre* activity is detected in almost all neural cells throughout the cerebellum, as indicated by whole-mount and sectioned view of X-gal staining in E13.5 *Nestin-cre;R26R* embryo, however, *Nestin-cre; SmoM2* mutants preferentially display enhanced Shh signaling in the cerebellar VZ. B. BrdU proliferation, CyclinD1, Pax2 and Lhx1/5 immunohistochemical analyses on WT, *Nestin-cre; Smo$^{f/-}$* and *Nestin-cre; SmoM2* mutants. Red boxes represent higher magnifications of medial and lateral cerebellar regions in adjacent panels. C. Quantifications of marker stainings in WT, *Nestin-cre; Smo$^{f/-}$* and *Nestin-cre; SmoM2* mutants.
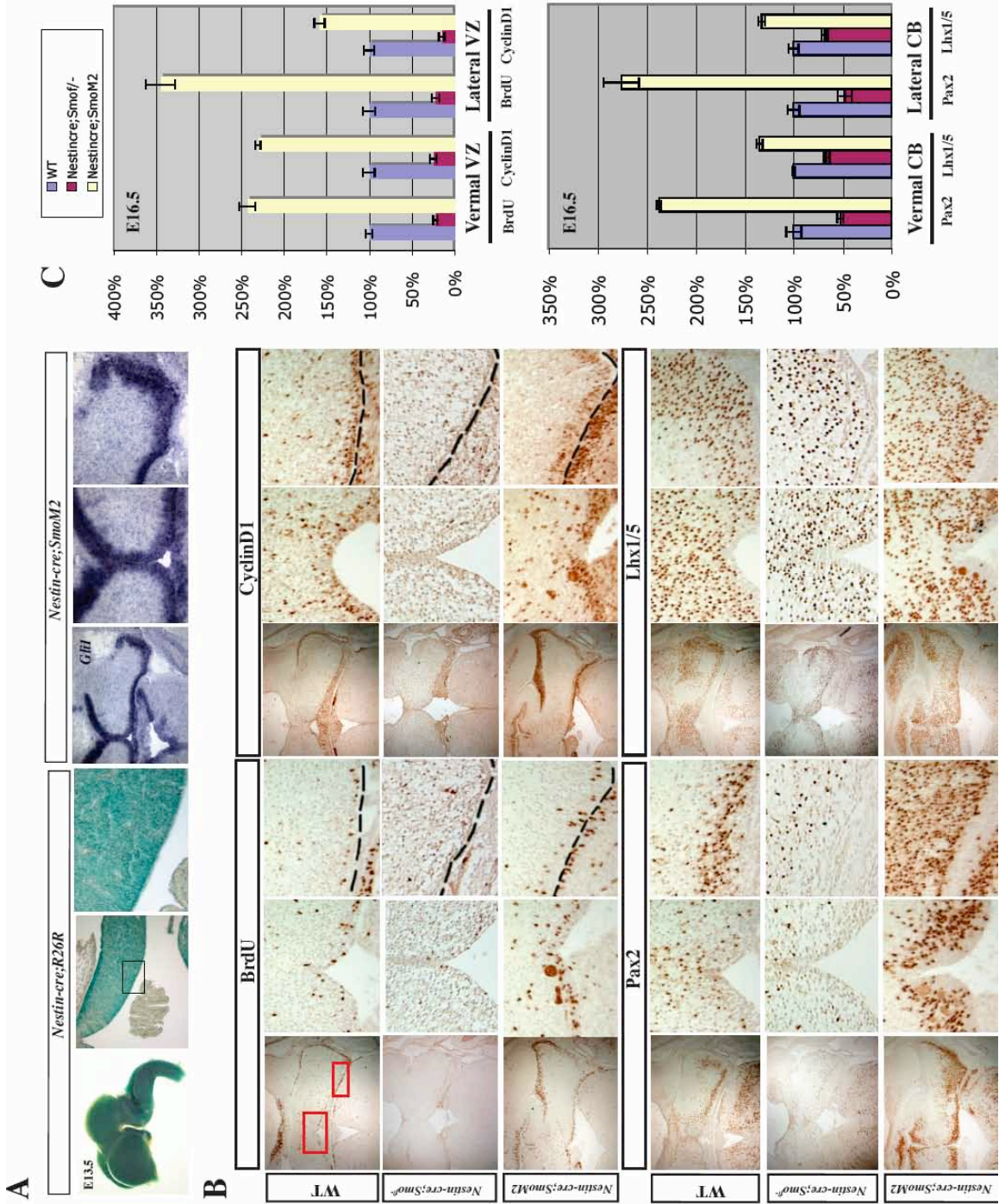
progenitors in the cerebellar cortex (including Golgi, basket and stellate cells) and in the DCN (Maricich and Herrup, 1999). Significantly reduced Pax2+ cell number was found in *Nestin-cre;Smo*$^{f/-}$ compared with WT (52$\pm$3.8% vs 100$\pm$7.5% in vermal region, p<0.001; 48$\pm$4.9% vs 100$\pm$6% in lateral VZ, p<0.001, N=3, Fig. 26B and 26C), demonstrating a dramatic reduction of GABAergic interneuron population. Similarly, the expression of homeodomain protein Lhx1/5, which marks the immature Purkinje cell (PC) (Morales and Hatten, 2006) and Pax2+ GABAergic interneurons (data not shown), were also significantly reduced in *Nestin-cre;Smo*$^{f/-}$ mutants (66$\pm$2.9% vs 100$\pm$1.6% in vermal region, p<0.001; 68$\pm$2.9% vs 100$\pm$5% in lateral VZ, p<0.001, N=3, Fig. 26B and 26C). Together, we conclude that lack of sufficient Shh signaling in the embryonic cerebellar VZ leads to significant reduction in VZ proliferation and GABAergic interneuron progenitor cell expansion.

To further support the critical role of Shh in promoting embryonic cerebellar VZ proliferation, we crossed the *Nestin-cre* driver strain with *SmoM2* conditional mutant which harbors a constitutively activated form of *Smo* (Jeong et al., 2004) to generate mice with ectopic Shh signaling. At E14.5, we observed largely enhanced *Gli1* expression in *Nestin-cre; SmoM2* cerebella (Fig. 26A). Interestingly, ectopic Shh signaling was largely confined to the VZ where Shh signaling normally occurs, despite widespread *Nestin-cre;R26R* reporter expression in almost all neural cells (Fig. 26A). This is consistent with previous studies that enhanced Shh pathway activation preferentially occurs in tissues normally responsive to Hh signaling (Mao et al., 2006). *Nestin-cre; SmoM2* VZ displayed

augmented proliferation and enhanced BrdU incorporation compared with WT ($231\pm8\%$ vs $100\pm3.4\%$ in the vermal region, p<0.001; $345\pm17.5\%$ vs $100\pm7.2\%$ in lateral VZ, p<0.001, N=3, Fig. 26B and 26C). CyclinD1 was robustly expressed in a larger percentage of cells in *Nestin-cre; SmoM2* compared to WT ($221\pm3.5\%$ vs $100\pm8.8\%$ in the vermal region, p<0.001; $158\pm6\%$ vs $100\pm6.1\%$ in lateral VZ, p<0.001, N=3, Fig. 26B and 26C). In agreement, a larger number of GABAergic neuronal progenitors was present in the ventral cerebellum of *Nestin-cre; SmoM2* compared with WT such as Pax2+ ($237\pm2.2\%$ vs $100\pm7.4\%$, in vermal region, p<0.001; $276\pm18.1\%$ vs $100\pm6\%$ in lateral VZ, p<0.001, N=3, Fig. 26B and 26C) and Lhx1/5+ ($135\pm3\%$ vs $100\pm1.6\%$ in vermal region, p<0.001; $133\pm3.5\%$ vs $100\pm5\%$ in lateral VZ, p<0.001, N=3, Fig. 26B and 26C). Our observation that cerebellar VZ neural progenitor population is expanded in the *Nestin-cre; SmoM2* mutants is consistent with the recently reported phenotype in another gain-of-function mutant, in which *Patched1* was conditionally removed from the neural stem cells (Yang et al., 2008). Together, we provide compelling evidence for the essential role of Shh signaling in driving proliferation of the cerebellar VZ progenitors and expansion of the GABAergic-lineage cells.

Cerebellar radial glial cell proliferation is defective in mutants deficient in Shh signaling

In line with our observation that Shh signaling directly targets radial glial progenitors in the cerebellar VZ, we detected strong reduction in radial glial cell proliferation in the E14.5 *Nestin-cre;Smo$^{f/-}$* mutants ($43.2\pm4.9\%$ vs $100\pm3.9\%$ for BLBP+ cells, p<0.001; $51.3\pm6.2\%$ vs $100\pm6.2\%$ for Sox2+ cells, p<0.001, N=5, Fig. 27A
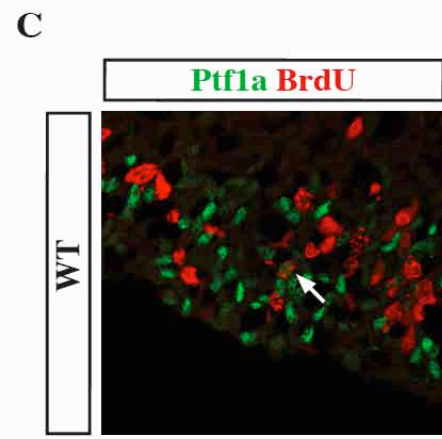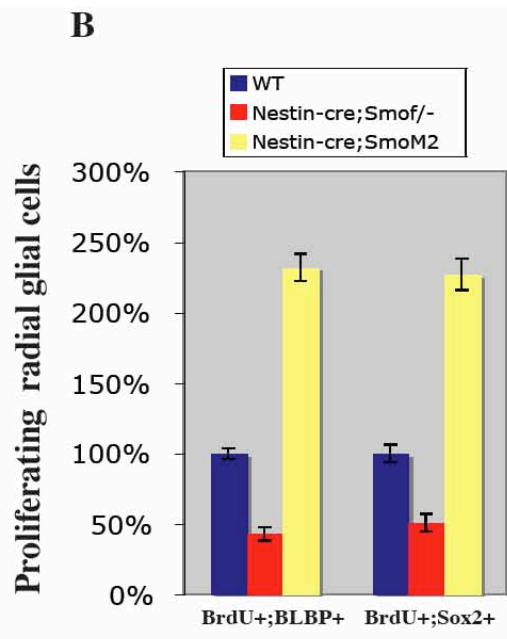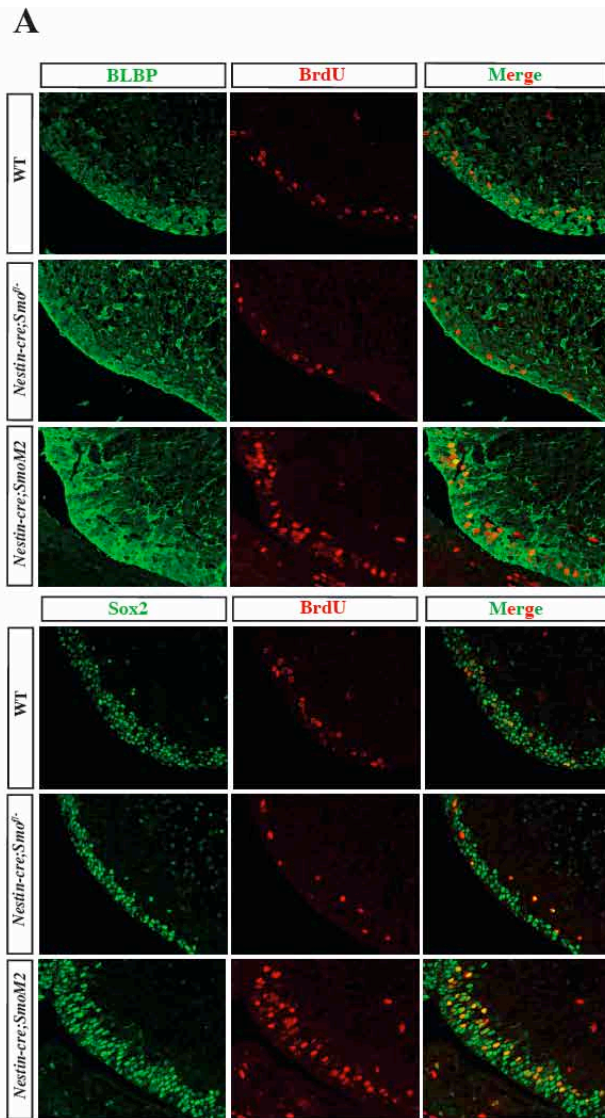
and 27B), while *Nestin-cre; SmoM2* mutants displayed enhanced radial glial proliferation (232.2±9.5% vs 100±8.2% for BLBP+ cells, p<0.001; 227.4±11.4% vs 100±7.3% for Sox2+ cells, p<0.001, N=5, Fig. 27A and 27B). Interestingly, the majority of proliferating cells in WT as indicated by one-hour BrdU pulse are radial glial cells (94.4%, n=284/301) (Fig. 27). Previous studies have shown that Ptf1a-expressing VZ progenitors give rise to mature Purkinje neurons and GABAergic interneurons (Hoshino et al., 2005; Pascual et al., 2007). Surprisingly, we found that Ptf1a-expressing VZ progenitors are largely non-mitotic (Fig. 27C). Taken together, these data demonstrate that cerebellar VZ neurogenesis and progenitor expansion is fulfilled by proliferation of the radial glial cells, but not committed Ptf1a-expressing progenitor cells, and this process is essentially regulated by Shh signaling.

The cerebellum does not express Shh endogenously prior to E15.5

Previous studies showed that *Shh* expression in the cerebellum begins at E17.5 in the Purkinje cell layer but not in the ventral VZ (Dahmane and Ruiz i Altaba, 1999) (Corrales et al., 2004) (Lewis et al., 2004). Our study revealing early Shh signaling in the cerebellar VZ prompted us to re-examine *Shh* expression in the developing cerebellum. We found that *Shh* transcript began to be detectable in the cerebellum at E16.5, particularly in the putative Purkinje cell domain beneath the EGL (arrows in Fig. 28A). We also performed genetic fate-mapping in E13.5-18.5 embryos by mating $Shh^{cre/+}$ mice with *mT/mG* reporter, in which membrane-tethered GFP indelibly marks cells expressing, or once

132

Figure 27. **Radial glia cell proliferation is defective in *Nestin-cre; Smo$^{f/-}$* and *Nestin-cre; SmoM2* mutants**

A *Nestin-cre; Smo$^{f/-}$* or *Nestin-cre; SmoM2* mutants exhibit impaired or augmented BrdU incorporation in BLBP+ or Sox2+ radial glial cells, respectively. B. Quantification of proliferating radial glial cell number in WT, *Nestin-cre; Smo$^{f/-}$* and *Nestin-cre; SmoM2* mutants. C. Ptf1a-expressing cells are essentially not mitotic indicated by largely non-overlapping staining after one-hour BrdU pulse in E14.5 WT embryos. Arrow indicates one Ptf1a-expressing cell with weak, punctate BrdU signal that is rarely observed.

A

	BLBP	BrdU	Merge
WT			
Nestin-cre;Smo^f/-			
Nestin-cre;SmoM2			

	Sox2	BrdU	Merge
WT			
Nestin-cre;Smo^f/-			
Nestin-cre;SmoM2			

B

Legend: WT, Nestin-cre;Smof/-, Nestin-cre;SmoM2

Y-axis: Proliferating radial glial cells — 0%, 50%, 100%, 150%, 200%, 250%, 300%

X-axis: BrdU+;BLBP+, BrdU+;Sox2+
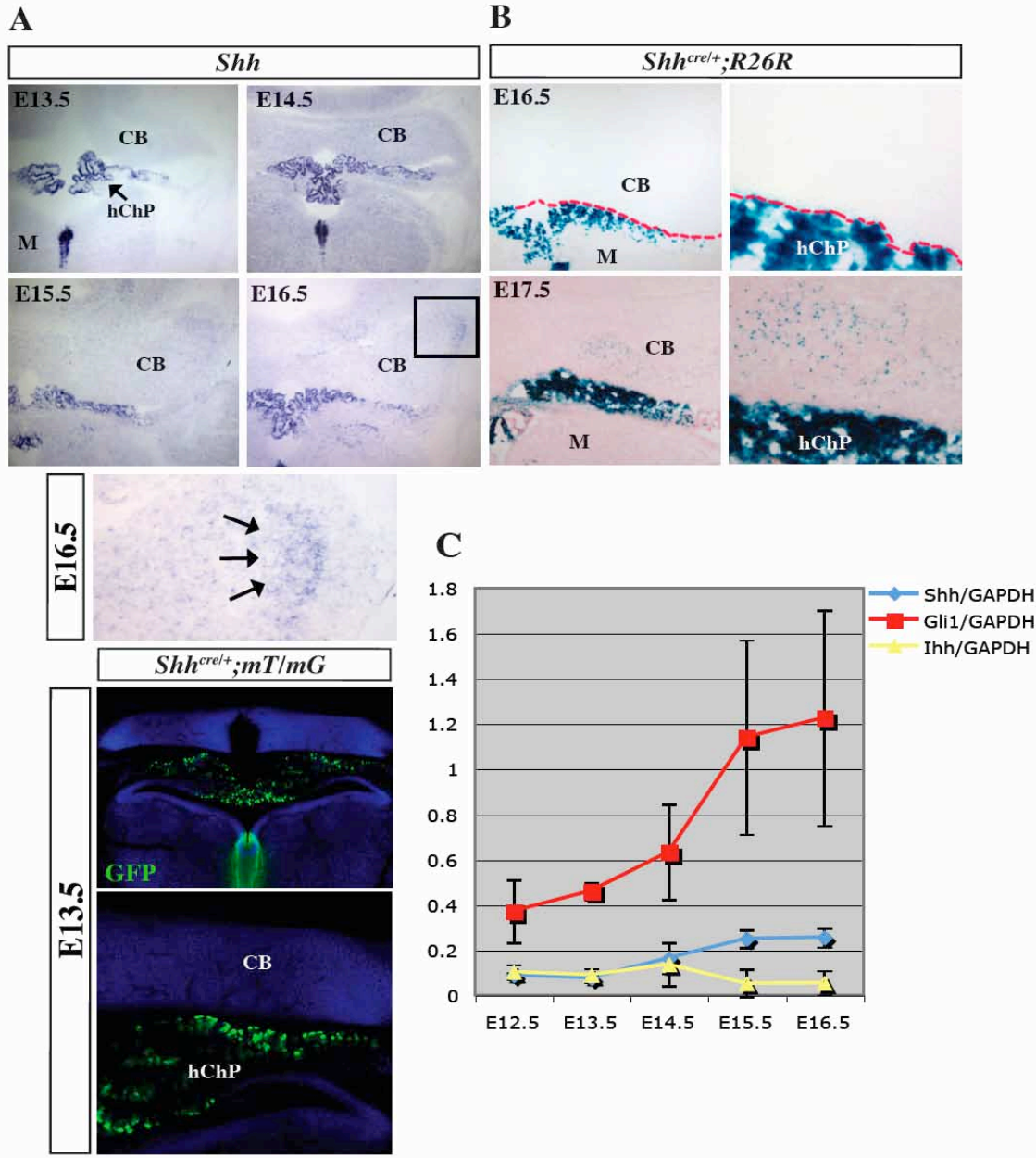
C

Ptf1a BrdU

WT

expressed Shh. We did not observe any GFP signal within the E13.5 cerebellum, a stage when Shh pathway activity in the cerebellar VZ was evident (Fig. 25B). As the rostral cerebellum adjoins the developing midbrain midline tissue which strongly expresses Shh, we asked whether this adjacent neural source of Shh could signal to the cerebellum, potentially by sending neuronal processes into the cerebellar tissue. However, we found that these neuronal processes do not extend anywhere close to the dorsal cerebellum (data not shown). In addition, we mated $Shh^{cre/+}$ mice with $R26R$ reporter and again only detected significant $lacZ$-positive cells in the cerebellum at E17.5 (Fig. 28B) which is in agreement with $in\ situ$ analysis considering that Cre recombinase begins to be functional ~12-24 hours after its promoter activation. We further performed quantitative real-time RT-PCR using dissected whole cerebella at E12.5-E17.5, using $Indian\ hedgehog$ (Ihh) as a negative control. We found that cerebellar Shh expression was only significantly different from that of Ihh starting from E15.5 (Fig. 28C). In contrast, significant $Gli1$ expression, which increased with developmental time, was detected at all stages analyzed starting from E12.5 (Fig. 28C). Together, these findings suggest that the cerebellum is unlikely the source of Shh that regulates early VZ proliferation and strongly argue for a transventricular route in delivering Shh ligand to the cerebellar VZ. We detected prominent Shh transcript in the developing hChPe starting at E12.5 (Fig. 28A), and that the hChPe mainly consisted of Shh-lineage cells (Fig. 28B).

Shh protein is present in the circulating embryonic cerebrospinal fluid

Cerebrospinal fluid (CSF), primarily generated from the CPs, is a source of chemicals

Figure 28. **Shh expression is not detected in the cerebellum prior to E15.5**

A. *Shh* mRNA expression in developing cerebellum; a faint signal could be detected at E16.5, in the putative Purkinje domain beneath EGL as indicated by arrows. B. Indelible marking and fate-mapping of *Shh*-expressing cells in the developing cerebellum. Note lack of any GFP signal in the E13.5 *Shh$^{cre/+}$; mT/mG* mice. *Shh$^{cre/+}$; R26R* mice begin to show positive staining within the cerebellar tissue starting at E17.5. C. Quantitative real-time RT-PCR analysis of *Shh*, *Gli1* and *Ihh* expression in the developing cerebellum. Of note, *Shh* expression significantly differ from that of *Ihh* control starting at E15.5, while a significant level of *Gli1* expression is already detected as early as E12.5.

A

Shh

E13.5 CB hChP M

E14.5 CB

E15.5 CB

E16.5 CB

E16.5

Shh^{cre/+};mT/mG

GFP

E13.5 CB hChP

B

Shh^{cre/+};R26R

E16.5 CB M hChP

E17.5 CB M hChP

C

Shh/GAPDH
Gli1/GAPDH
Ihh/GAPDH

137

and polypeptides with neuroprotective, surveillance and repair functions (Redzic et al., 2005; Segal, 2000). Since the cerebellar VZ is exposed to circulating CSF filling the fourth brain ventricle, we reason that Shh might be present in the CSF and affects cerebellar VZ development. In line with this notion, by ELISA assay, we detected Shh protein at a concentration range of 100-300 pg/ml in the pooled CSF retrieved from hindbrain ventricles of E12.5-E15.5 WT embryos (1 or 2 ul CSF per embryo, see Methods) (Fig. 29A). One limitation is that it is not possible to retrieve only hindbrain CSF, therefore, we performed ELISA on pooled CSF circulating in all brain ventricles and we always observed collapsed forebrain, midbrain and hindbrain ventricles after retrieval of the CSF. Thus, the measured Shh concentration may be significantly lower than the local concentration close to the cerebellar VZ. We did not observe an age-dependent increase in Shh protein in the CSF, perhaps due to the increase in CSF volume of the older embryos thereby diluting the overall protein concentration. Increasing evidence suggest that primary cilia function as the essential sensor of Shh ligand and regulator for transducing pathway activity (Caspary et al., 2007) (Haycraft et al., 2005) (Rohatgi et al., 2007). In agreement, we detected widespread presence of primary cilia in proliferating VZ radial glial progenitors (Fig. 29B).

Wnt1-cre; Shh$^{f/-}$ mutants display similar cerebellar VZ defects

Throughout the developing hindbrain system, we observed two prominent regions that express *Shh*, the ventral midline of the medulla and the hChP epithelium (hChPe) (Fig. 28) (Huang et al., 2009). We found that the medulla is unlikely the source of Shh ligand in activating Shh signaling in the cerebellar VZ, as targeted deletion of Shh using

Figure 29. Shh protein is present in embryonic cerebrospinal fluid

A. Embryonic CSF harbors Shh protein as assayed by ELISA. B. Primary cilia are present in proliferative radial glial VZ cells.

A

CSF retrieval from hindbrain ventricle

B

Arl13b	BrdU	Merge

Lateral VZ

4th Ventricle

Acetylated tubulin Sox2 Topro3

Vermal VZ

4th Ventricle
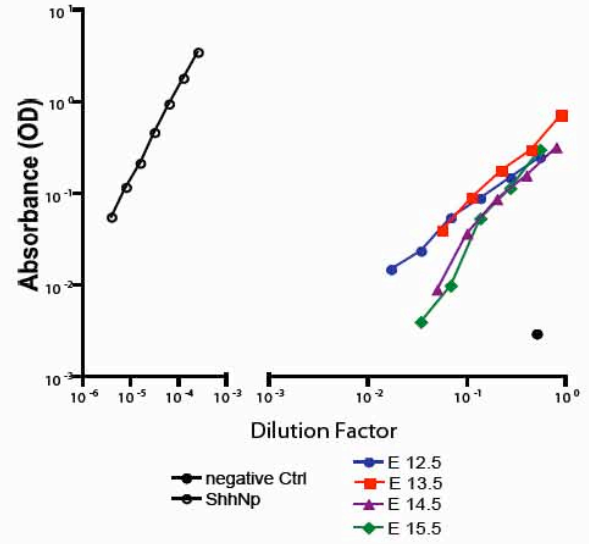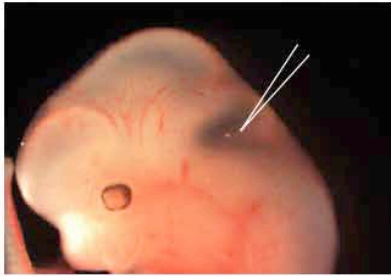
Wnt1-Cre leads to strong defects in VZ proliferation and GABAergic neuronal expansion without affecting Shh expression in the hindbrain medulla (Fig. 30A). The cerebellar VZ defects in *Wnt1-cre; Shh$^{f/-}$* mutants can be observed starting at E13.5 (Fig. 30B and 30C) and beca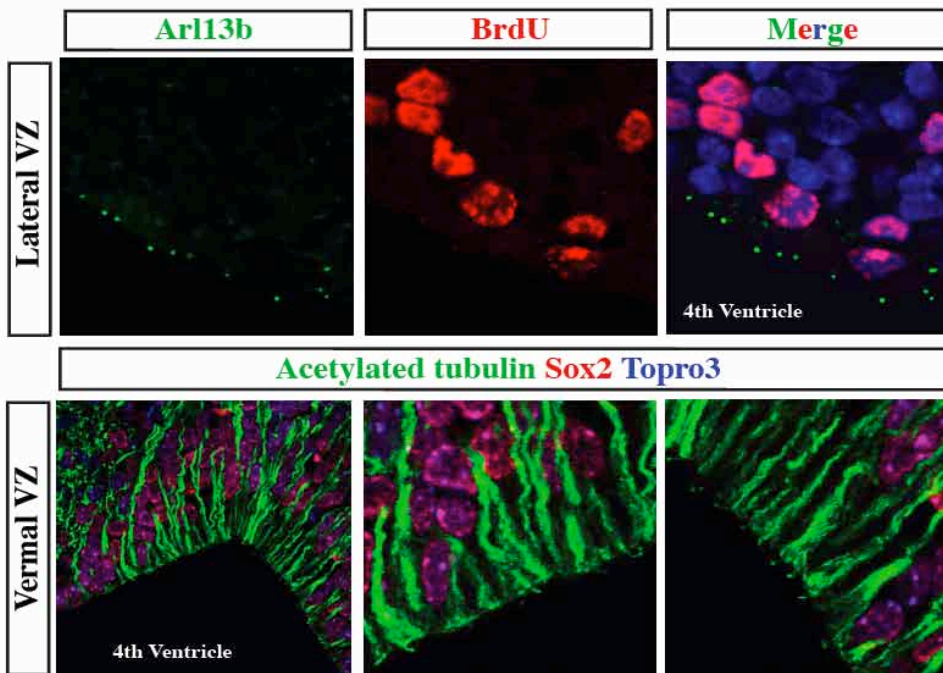me progressively more severe at E16.5 (data not shown). Consistent with our observation that Shh signaling is activated in the radial glial population, expression of BLBP+ and Sox2+ cells are all reduced in *Wnt1-cre; Shh$^{f/-}$* mutants (Fig. 30B). The expression of Ngn2 and Mash1 marks cerebellar VZ GABAergic progenitor cells (Zordan et al., 2008) *(Grimaldi et al., 2009)* and their expression are also largely reduced in the *Wnt1-cre; Shh$^{f/-}$* mutants (data not shown).

Discussion

We provide genetic evidence that activation of Shh signaling is necessary to regulate VZ progenitor proliferation and GABAergic progenitor expansion. We show that the source of Shh ligand to activate signaling in the early cerebellar VZ is not the cerebellum, therefore, implicating a transventricular system as a means to deliver Shh signal to the VZ.

It has been shown that Shh promotes GABAergic neuronal lineage restriction of forebrain stem cells, in part, by activation of the basic helix–loop–helix transcription factors, Olig2 and Mash1 (Yung et al., 2002). In addition, recombinant Shh protein similarly increased the number of tyrosine hydroxylase (TH)-positive GABAergic neurons in the midbrain (Volpicelli et al., 2004). Therefore, the action of Shh on RL-derived glutamatergic granule neurons in the cerebellum is in contrast with its well-established role in specifying and promoting proliferation of GABAergic interneurons

Figure 30. Genetic ablation of Shh results in marked cerebellar VZ phenotype

A. *Wnt1-cre* deleter strain drives Cre activity in hChPe, effectively ablating Shh expression selectively in hChPe but not the ventral midline of hindbrain medulla. B. E13.5 *Wnt1-Cre; Shh$^{f/-}$* mutant cerebellar VZ shows severely impaired proliferative capacity, GABAergic and radial glia population expansion compared with WT. BrdU, Ki67 and CyclinD1 stainings indicate proliferative activity. Ptf1a marks GABAergic progenitors. BLBP+ and Sox2+ cells represent radial glial population. Differentiating GABAergic progenitor cells, marked by Lhx1/5, ectopically occupy the *Wnt1-Cre; Shh$^{f/-}$* mutant cerebellar VZ at E13.5 which is never observed in WT. C. Statistical comparisons between WT and *Wnt1-Cre; Shh$^{f/-}$* mutant cerebella for BrdU+ ($41.5 \pm 10\%$ vs $100 \pm 12.6\%$, $p < 0.001$, N=5), Ki67+ ($37.9 \pm 3.1\%$ vs $100 \pm 6\%$, $p < 0.001$, N=5), CyclinD1+ ($35.2 \pm 4.2\%$ vs $100 \pm 9\%$, $p < 0.001$, N=5), Sox2+ ($71.3 \pm 2.9\%$ vs $100 \pm 9.1\%$, $p < 0.005$, N=5) and Ptf1a+ ($64 \pm 4.6\%$ vs $100 \pm 9.2\%$, $p < 0.001$, N=5) cells.

A

Wnt1-cre;R26R | **Shh**
CB / CB | CB / CB
M | M

Shh
Wnt1-cre;Shh^f/-
hChP | M

C

E13.5

WT
Wnt1cre;Shhf/-

120%
100%
80%
60%
40%
20%
0%

BrdU Ki67 CyclinD1 Sox2 Ptf1a

B

WT	Wnt1-cre;Shh^f/-	WT	Wnt1-cre;Shh^f/-
BrdU		Ki67	
BLBP		Sox2	
Ptf1a		Lhx1/5	

E13.5

143
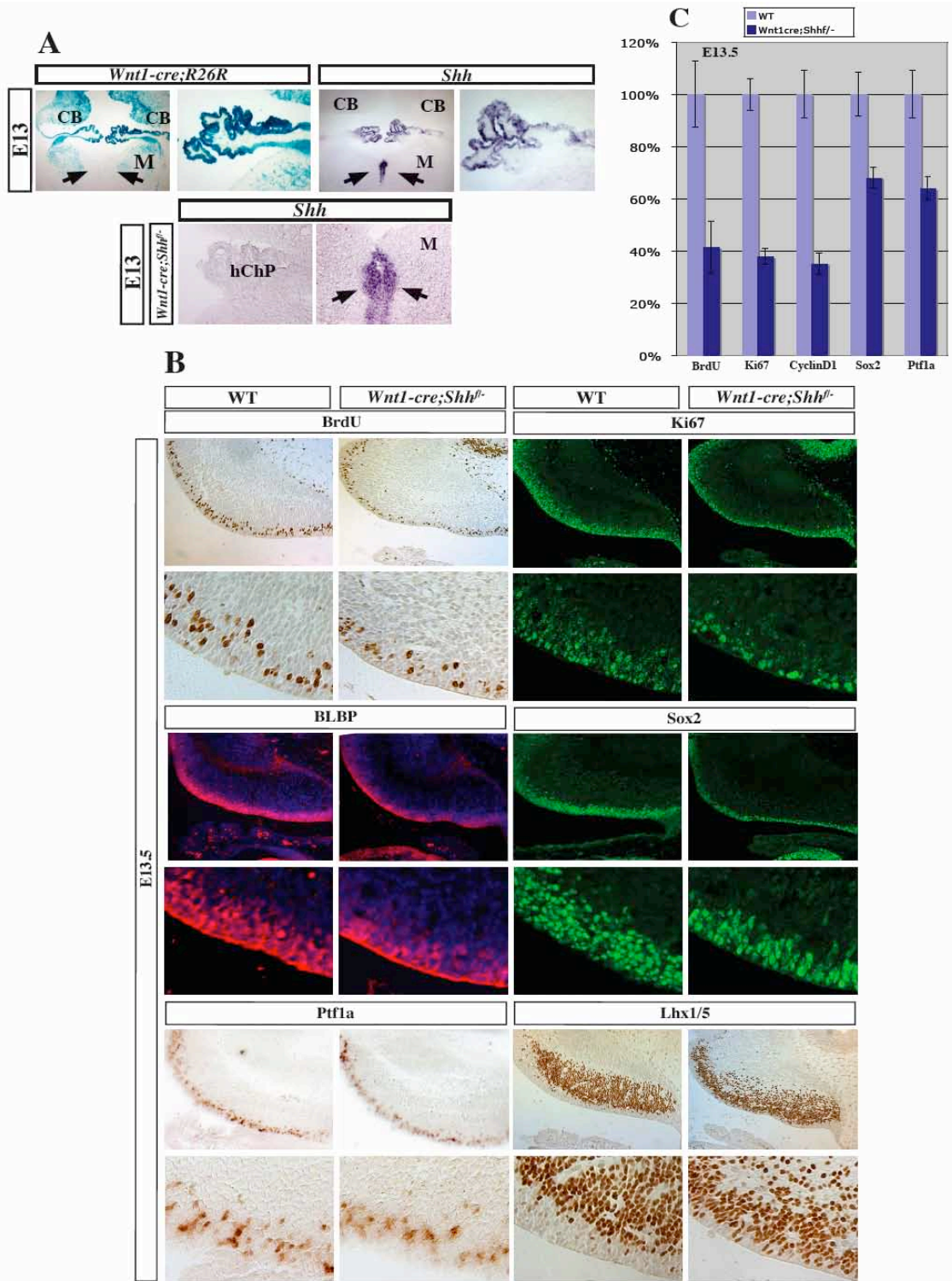
in other regions of the CNS. It is not known if a parallel situation exists in which Shh signaling plays a similar role in the developing cerebellar VZ which gives rise to GABAergic interneurons. In this study, we demonstrate that Shh signaling is essential to early embryonic cerebellar VZ proliferation, and defective Shh signaling in VZ severely impairs the generation of VZ-borne radial glial and neural progenitor cells. We identify Shh as the key signal in regulating cerebellar VZ radial glial cell proliferation and GABAergic interneuron population expansion, implicating VZ progenitors as a potential source for the cellular origin of cerebellar disorders associated with Shh dysregulation. This new finding is significant as current developmental or disease-related studies pertaining to Shh function in the cerebellum have been largely focused on granule neuron precursor cells at very late embryonic to postnatal stages since it is thought that Shh signaling plays a physiologically relevant role from E17.5 onward in mice.

Our data indicated that Shh is present in the embryonic CSF during critical stages of cerebellar VZ development. The CSF is generated from ChPe situated in different sites of the brain ventricles (Redzic et al., 2005; Segal, 2000). Notably, hChPe is in close apposition with the wall of cerebellar VZ throughout the development (see Fig. 28) and it is the only ChPe that expresses Shh. The observation that the medulla, the only other non-cerebellar source of Shh within the developing hindbrain system, is not required for the expansion for VZ progenitors, we argue that hChPe contributes to the cerebellar development. This is further supported by the fact that hChPe is capable of eliciting Shh pathway activation when cultured with a Shh reporter cell line and this effect can be blocked by Shh blocking antibody or by a Smo antagonist (Fig. 31). However, *Wnt1-Cre* is capable of removing Shh in other regions of the CNS including the ventral midbrain,

144

suggesting that other neural tissues may also capable of secreting Shh into CSF. However, we have determined that hChPe is a major source of the Shh promoting VZ development, as removal of *Shh* using *Gdf7-Cre*, a choroid plexus epithelium-specific Cre, led to a significant reduction of VZ proliferation (Fig. 32).

Extensive effort has been made to understand the molecular basis of genetic disorders involving cerebellar defects such as the neurodevelopmental Joubert syndrome (JS) and Bardet-Biedl syndrome (BBS), both of which are characterized by aplasia or severe hypoplasia of the cerebellar vermis (Louie and Gleeson, 2005) (Baskin et al., 2002). Recent progress in genetic mapping of human patients suggested a strong link to mutations in protein components of the primary cilia such as the intraflagellar transport (IFT) proteins (Chizhikov et al., 2007) (Spassky et al., 2008). The correlation between defective ciliogenesis and the etiology of cerebellar genetic disorders is particularly interesting, as many core components of the Shh pathway, such as membrane proteins Smoothened and Patched1 and Gli transcription factors are localized to, and function in, cilia during Shh signal transduction (Caspary et al., 2007) (Haycraft et al., 2005) (Rohatgi et al., 2007). Recent studies by conditional knockout of ciliary proteins, IFT88 and Kif3a, in the CNS showed granule neuron proliferation defects. This defect may be central to the cerebellar pathology observed in human cilia-related disorders, potentially stemming from a defective response to Shh signaling as a result of lack of normal cilia function in EGL cells (Chizhikov et al., 2007) (Spassky et al., 2008). In light of our finding that Shh is required to stimulate VZ radial glial proliferation, and the fact that abundant primary cilia were detected along the developing cerebellar VZ (Fig. 28), it would be important to fully assess the cerebellar defects of conditional cilia mutants and to establish a requirement of the primary cilia in VZ radial glia progenitor proliferation in response

Figure 31. hChP secretes Shh to elicit pathway activity *in vitro*

hChP-secreted Shh elicits signaling activity when co-cultured with Shh-LIGHT2 cells; induction can be ablated by adding Shh blocking antibody 5E1 or cyclopamine.

Light2 cells

| 8X Gli binding sites | Luciferase |

co-culture with hindbrain choroid plexuses

Relative Luciferase Units

Legend:
- Light2 cells only
- Light2 cells + hCPs
- Light2 cells + hCPs + 10ug/ml 5E1
- Light2 cells + hCPs + 4ug/ml cyclopamine
- Light2 cells + 125pM SAG

0   1   2   3   4   5   6
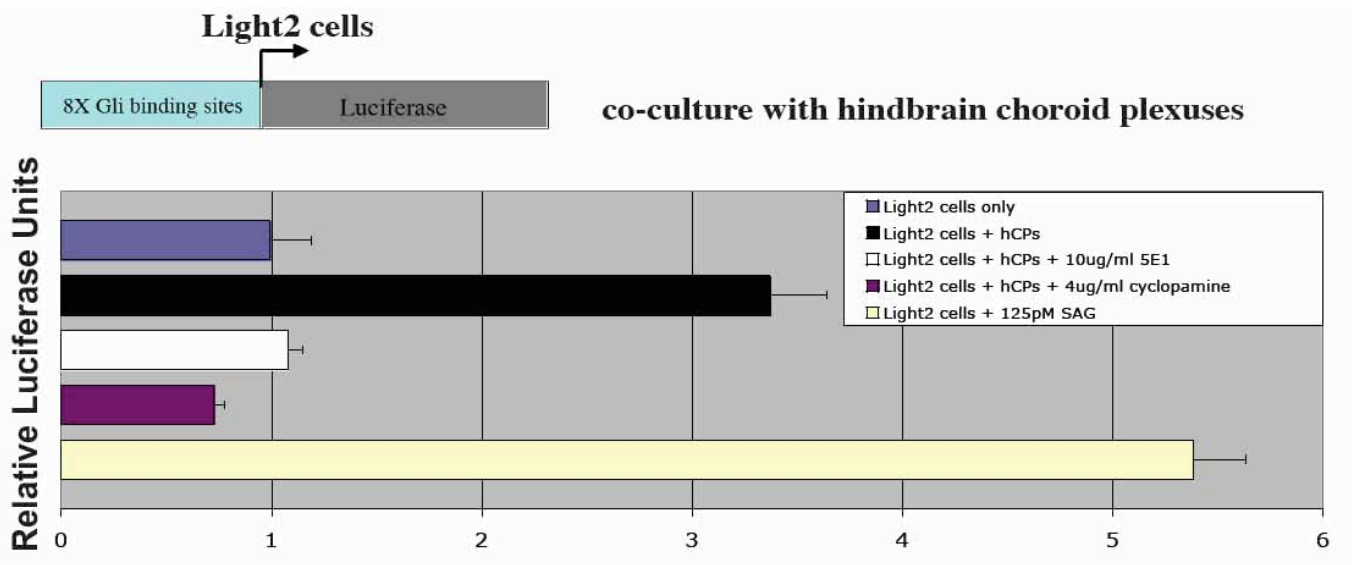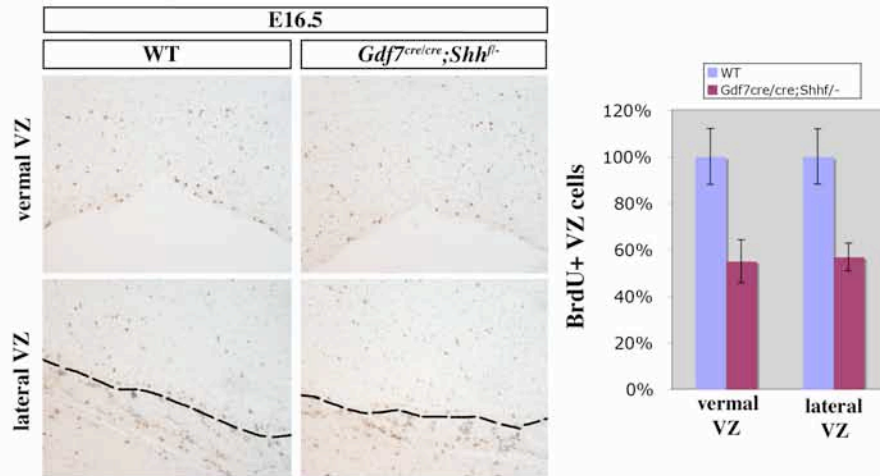
Figure 32. *Gdf7$^{cre/cre}$; Shh$^{f/-}$* **mutants show significant proliferative phenotype in the cerebellar VZ**

Gdf7$^{cre/cre}$; Shh$^{f/-}$ mutants display greatly impaired VZ progenitor proliferation in both the vermal and lateral regions.

E16.5

| WT | Gdf7$^{cre/cre}$;Shh$^{f/-}$ |

vermal VZ

lateral VZ

BrdU+ VZ cells

- WT
- Gdf7cre/cre;Shhf/-

vermal VZ   lateral VZ

149

to Shh signal.

Emerging lines of evidence suggest that there are two subtypes of MB with distinct oncogenic location and molecular characteristics; MBs are detected in most afflicted children in the vermal cerebellar region showing no MATH1 expression and in many adult patients, in the cerebellar hemispheres with high level of MATH1 expression (Salsano et al., 2004). In addition, while a subset of human MB samples displayed up-regulation of MATH1, others selectively exhibit expression of NGN1, a VZ-specific transcription factor, with no MATH1 expression (Salsano et al., 2007). It is therefore likely that current animal models of MB only mimic one subtype of MB that is generated from transformed EGL as the mice develop into adulthood. Recent findings demonstrated MATH1-positive granule progenitor lineage in the rhombic lip and EGL as the cellular origin for MB (Schuller et al., 2008) (Yang et al., 2008). However, these recent studies also emphasized commitment to the granule cell lineage as a prerequisite for MB, thus, the cellular origin of MATH1-negative pediatric tumors in the vermis remains enigmatic. As our study demonstrated an essential role of Shh signaling in the regulation of embryonic cerebellar VZ proliferation, it remains possible that aberrant Shh signaling at embryonic or perinatal stages could promote vermal MB oncogenesis originating from the cerebellar VZ. Future clinical investigation is warranted to assess whether indeed Shh signaling is hyperactive in the cerebellar VZ of the child MB patient.

In this study, we also provide evidence suggesting that the potential source of Shh ligand to activate signaling in the embryonic cerebellar VZ is likely not from endogenous cerebellar cells, but rather the hChP, which protrudes over the outer hindbrain and closely apposes the external surface of the developing cerebellum. The ChPs are heavily

vascularized structures ensheathed by a monolayer of ependymal-derived epithelial cells, which serve as a major interface forming the blood-brain barrier and act as a site for the production of CSF which circulates throughout the CNS ventricular system (Sturrock, 1979) (Redzic et al., 2005). Studies of ChP functions in adult mice suggested that they secrete numerous chemicals and polypeptides with neuroprotective, surveillance and repair functions (Emerich et al., 2005). Although several studies have documented that embryonic ChPs synthesize various growth and trophic signaling factors, such as IGF II, GDNF, transforming growth factor (TGF), GDF7, Bmp7 and Shh (Emerich et al., 2005) (Lee et al., 2000a) (Krizhanovsky and Ben-Arie, 2006) (Bitgood and McMahon, 1995), the physiologically relevant functions of these factors have not been further explored. Two previous reports, using *in vitro* studies, suggested that hChP-derived Bmp7 and retinoic acid may maintain RL-derived cells in undifferentiated states (Krizhanovsky and Ben-Arie, 2006) and promote cerebellar neurite outgrowth (Yamamoto et al., 1996), respectively. Here we provide the first *in vivo* genetic evidence demonstrating that the hindbrain ChP may function as a growth-promoting secretory organ involved in paracrine signaling to regulate the development of nearby brain structures such as the embryonic cerebellum.

CHAPTER VI

HINDBRAIN ROOF PLATE CELLS ARE MULTIPOTENT AND SUSCEPTIBLE TO

ONCOGENIC TRANSFORMATION BY DEREGULATED SONIC HEDGEHOG

SIGNALING

Introduction

The roof plate is a transient embryonic dorsal midline epithelial tissue spanning the

entire developing central nervous system (CNS). It consists of a distinct strip of most

dorsal-lateral neuroectodermal cells , which express many secreted signaling molecules

such as Bmp6, Bmp7, Gdf7 (Bmp12) and Wnt1 (Lee et al., 1998), (Lee et al., 2000a),

(Chizhikov and Millen, 2004), collectively functioning as an essential organizing center

regulating development of neighboring tissues. These roof plate-derived inductive

signals are important for directing differentiation of dorsal neuronal cell types (Lee et al.,

1998), (Lee et al., 2000a), (Chizhikov and Millen, 2004), (Chizhikov et al., 2006). It has

been shown that the LIM-homeodomain transcription factor Lmx1a is a central regulator

for roof plate development, as loss of Lmx1a resulted in absence of roof plate cells during

early embryogenesis (Chizhikov and Millen, 2004), (Millonig et al., 2000). While

regulating the development of neighboring tissues by secreted growth factors, the roof

plate itself has capacity to generate different cell types. However, distinct populations of

progenitors expressing various growth factors differ in their differentiating potential

along the rostral-caudal axis of the neural tube, highlighting the heterogeneity of the roof

plate (Awatramani et al., 2003), (Currle et al., 2005), (Hunter and Dymecki, 2007). For example, in the spinal cord region, Gdf7-expressing roof plate progenitors can generate different neurons and glia cells (Lo et al., 2005). However, the differentiation potential of the roof plate in the hindbrain appears to be different as several previous fate-mapping studies showed that it contributes to non-neural choroid plexus epithelial cells (Currle et al., 2005), (Landsberg et al., 2005), (Hunter and Dymecki, 2007)

Medulloblastoma, the most common pediatric CNS tumor, is characterized by its rapid progression and tendency to spread along the entire brain-spinal axis with dismal clinical outcome. Medulloblastoma is a neuroepithelial tumor of the cerebellum, accounting for 20% and 40% of intracranial and posterior fossa tumors in children, respectively (Rossi et al., 2008). It is now well established that Shh signaling stimulates proliferation of cerebellar granule neuron precursors (CGNPs) during cerebellar development (Wechsler-Reya and Scott, 1999a) (Dahmane and Ruiz i Altaba, 1999) (Wallace, 1999b). Numerous studies using mouse models in which Shh pathway is constitutively activated have linked Shh signaling with medulloblastoma and CGNPs as the cellular origin (Fan and Eberhart, 2008) (Yoon et al., 2009) (O'Dorisio et al., 2008) (Corcoran et al., 2008) (Corcoran et al., 2008; Fan and Eberhart, 2008; Gilbertson and Ellison, 2008; O'Dorisio et al., 2008; Yoon et al., 2009). Significantly, mutations in SHH pathway components have been detected in ~25% of sporadic human medulloblastoma cases, and patients with germline inactivation of *PTCH1* gene, frequently identified in Gorlin syndrome, are predisposed to a variety of familial cancer types including medulloblastoma (Johnson et al., 1996) (Hahn et al., 1996) (Gailani et al., 1996) (Wicking et al., 1997) (Hasenpusch-Theil et al., 1998) (Dong et al., 2000). However, the

153

diverse clinical presentations of medulloblastoma subtypes in human patients (nodular, desmoplastic, classical and large cell/anaplastic), and the fact that medulloblastoma is found in a subset of human patients with no ectopic expression of CGNP marker (Salsano et al., 2007), suggest that the cellular and molecular origins of medulloblastoma are more complex and far from being completely deciphered. Therefore, it is essential to determine whether there is an alternative medulloblastoma tumor cell-of-origin based on which cell-type specific therapeutic modality can be developed.

Choroid plexuses (ChPs) are non-neural, vascularized secretory organs involved in the regulation of brain homeostasis and function as the blood-cerebrospinal fluid (CSF) barrier (Redzic et al., 2005; Segal, 2000). Among the four brain ChPs, the hindbrain choroid plexus (hChP) develops in close apposition to the cerebellum. In our recent study aiming to understand the biogenesis of hChP, we have identified a discrete population of hChP epithelial (hChPe) progenitor cells that are descendents of the *Gdf7*-expressing roof plate. Shh signaling is active in these hChPe progenitor cells to promote their proliferation (Huang et al., 2009). Strikingly, by generating *Gdf7$^{Cre/+}$; SmoM2* mice with selective over-activation of the Shh pathway in *Gdf7*-lineage cells, we observed profound phenotypes in both the hChP and cerebellum. Here we focus on the Gdf7-lineage cells during cerebellar development and show that the *Gdf7*-expressing roof plate cells first give rise to a discrete population of cerebellar vermal radial glia cells and later to multiple cerebellar neuronal and glial cell types, highlighting their multi-potency. Importantly, ectopic Shh signaling in the *Gdf7*-lineage cells invariably leads to formation of medulloblastoma with CGNP features, indicating that focal activation of the Shh signaling pathway in hindbrain roof plate cells is sufficient to promote cerebellar

154

tumorigenesis, confirming that becoming CGNP is a cellular prerequisite for cerebellar tumorigenesis, and demonstrating that medulloblastoma can stem from a very small number of CGNPs.

Experimental procedures

Mice

The generation of *Gdf7$^{Cre/+}$* mice was described previously (Lee et al., 2000a). *SmoM2* (Jeong et al., 2004)*, ROSA26-LacZ* (Soriano, 1999) and *ROSA26-eYFP* mice (Srinivas et al., 2001), non-obese diabetes/severe combined immuno-deficient mice (*NOD.CB17-Prkdcscid/J*) mice were obtained from the Jackson Laboratory. *Gdf7$^{Cre/+}$; SmoM2* mice were identified by their smaller size, bulging cranium and confirmed by genotyping. Fate-mapping studies were performed on *Gdf7$^{Cre/+}$; ROSA26-LacZ* and *Gdf7$^{Cre/+}$; ROSA26-eYFP* mice. At least three animals from control and mutants were used for each morphological/molecular analysis shown in each figure.

Histological analyses, immunohistochemistry and immunocytochemistry

Standard hematoxylin and eosin stainings were performed to compare the histological features of control and mutant mice. All immunohistochemistry analyses were performed on sections collected from OCT- or paraffin-embedded tissues. Twenty minutes of antigen retrieval at 95C^{o} with citrate buffer (Ph=6.0) was performed for all stainings on paraffin sections. The primary antibodies used were rabbit anti-GFP, (Molecular Probe, 1:500), chicken anti-GFP, (Aves Labs, 1:200), rabbit anti-Sox2,

(Millipore, 1:400), rabbit anti-BLBP, (Millipore, 1:1000), rabbit anti-Pax6, (Covance, 1:500), mouse anti-NeuN, (Millipore, 1:200), mouse anti-Nestin, (Developmental Studies Hybridoma Bank, 1:50), mouse anti-Calbindin, (Swant, 1:500), mouse anti-Parvalbumin, (Sigma, 1:200), rabbit anti-Math1 (gift of Jane Johnson, 1:400), rabbit anti-Ki67 (NeoMarkers, 1:400), rabbit anti-GFAP (Neuromics, 1:500), mouse anti-GFAP (Neuromics, 1:200), mouse anti-Cyclin D2 (NeoMarkers, 1:500), rabbit-anti-phospho-Rb (Ser807/811) (Cell Signaling, 1:300), mouse-anti-p27Kip1 (Transduction Laboratories, 1:1000). Immunocytochemical stainings were performed on established lines of $Gdf7^{Cre/+}$; *SmoM2* tumor cells grown for 48 hours on gelatinized glass coverslips. The primary antibodies were rabbit anti-GFP, (Molecular Probe, 1:2000), mouse anti-Nestin, (Developmental Studies Hybridoma Bank, 1:500), mouse anti-Sox2, (Millipore, 1:500) mouse anti-Tuj1, (Sigma, 1:1000), mouse anti-NeuN, (Millipore, 1:1000), mouse anti-GFAP, (Neuromics, 1:1000), mouse anti-CNPase, (Sigma, 1:1000). All fluorescent images were taken using Zeiss LSM 510 Confocal microscope. Independent stainings were performed on at least three animals for each marker and representative images are shown.

X-gal staining and transcript detection

X-gal staining for ß-galactosidase was performed according to standard protocol. Section *in situ* hybridizations were performed on 20 micron frozen sections as previously described (Litingtung and Chiang, 2000). The following cDNAs were used as templates for synthesizing digoxygenin-labeled riboprobes: *Gdf7* (Tom Jessell, Columbia

University)*, Gli1* (C.C. Hui, University of Toronto)*, Patched1* (Matthew Scott, Stanford University)*, Nmyc* (Mary E. Palko, NCI)*, Math1* (ATCC, I.M.A.G.E.No. 6530849)*.

Medulloblastoma cell culture and orthotopic grafting

Medulloblastoma tissue dissociation and tumor cell culture were performed essentially according to a previous study (Ward et al., 2009). Specifically, the cerebella bearing tumor tissues in $Gdf7^{Cre/+}$; $SmoM2$ mice over 14 days old were dissected in sterile, ice-cold PBS, minced with 50% Accutase in PBS for 5 minutes followed by repetitive pipeting with Pipetman P1000 for 3 minutes, then cell pellets were collected after brief centrifugation. Pelleted cells were then resuspended in neural stem cell culture medium and plated in gelatinized 60mm tissue culture dish. The stem cell culture medium is composed of Neurobasal medium with glutamine, plus 25 ng/ml human EGF and 25ng/ml basic FGF. The unattached cells were removed by changing medium on the following day after initial seeding. Culture medium was then changed every four days and growth factors were supplemented fresh every other day.

Orthotopic tumor cell grafting was performed as described with minor modifications (Sarangi et al., 2009). $10x^5$ cultured tumor cells were transplanted into the right cerebellar hemisphere of NOD/SCID mice according a protocol approved by the Vanderbilt Institutional Animal Care and Use Committee. Mice were anesthetized with ketamine and xylazine and placed on a stereotactic apparatus. An incision was made in the scalp to reveal the posterior skull. A small hole was drilled 2 mm lateral and 2mm below to the lambda suture. 4 ul of tumor cells were implanted using a Hamilton syringe. Mice were maintained in sterile housing conditions and those displaying typical medulloblastoma

symptoms were sacrificed for further studies.

Results and discussions

Targeted activation of Shh signaling pathway in Gdf7-lineage leads to rapid cerebellar hyperplasia

We recently reported that the hChPe robustly expresses Shh and the Shh signaling defines a discrete hChPe progenitor domain close to the lower rhombic lip (Huang et al., 2009). In line with the regulation of Shh signaling in hChP biogenesis, we observed enlarged hChP in the gain-of-function $Gdf7^{Cre/+}$; *SmoM2* mutant mice (Huang et al., 2009). Notably, all $Gdf7^{Cre/+}$; *SmoM2* mice died within three weeks after birth (Fig. 32A) and those that survived close to three weeks often displayed bulging cranium particularly at the hindbrian region and impaired motor coordination, indicative of cerebellar defects (Fig. 32A, data not shown). Notably, the dissected $Gdf7^{Cre/+}$; *SmoM2* cerebella often lacked visible foliations that are normally seen in the control mice, suggestive of filled spaces between cerebellar lobules (Fig. 32A). We then examined the histological features of the $Gdf7^{Cre/+}$; *SmoM2* mice in sections encompassing the whole hindbrain system. While we did not find apparent histological differences in control and $Gdf7^{Cre/+}$; *SmoM2* cerebella prior to P10, many focal hyperplasia were obvious in the $Gdf7^{Cre/+}$; *SmoM2* mice after P14 (Fig. 32B), a stage when the EGL cells have completed their inward migration to form the mature IGL in control mice (Fuccillo et al., 2006), (Sillitoe and Joyner, 2007). Stringkly, the ectopic cellular clusters highly resembled preneoplastic lesions reported in other mouse models of medulloblastoma (Oliver et al., 2005). The
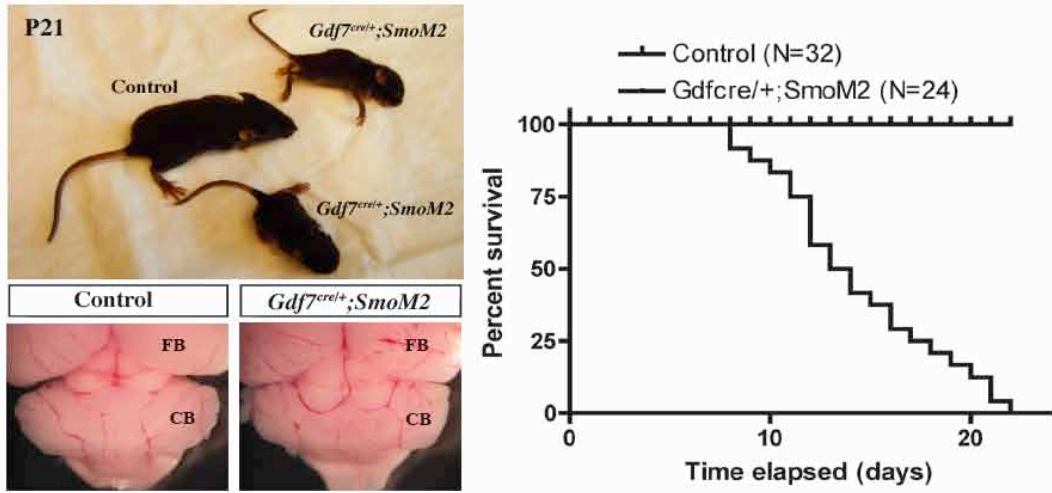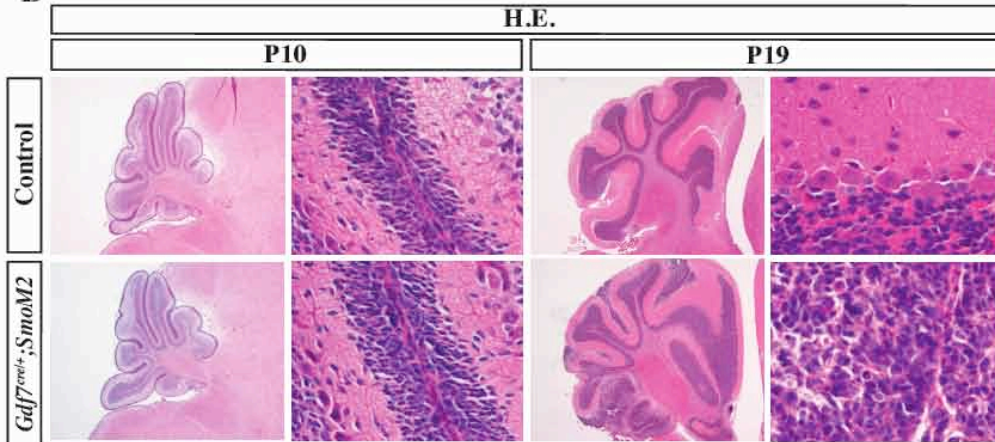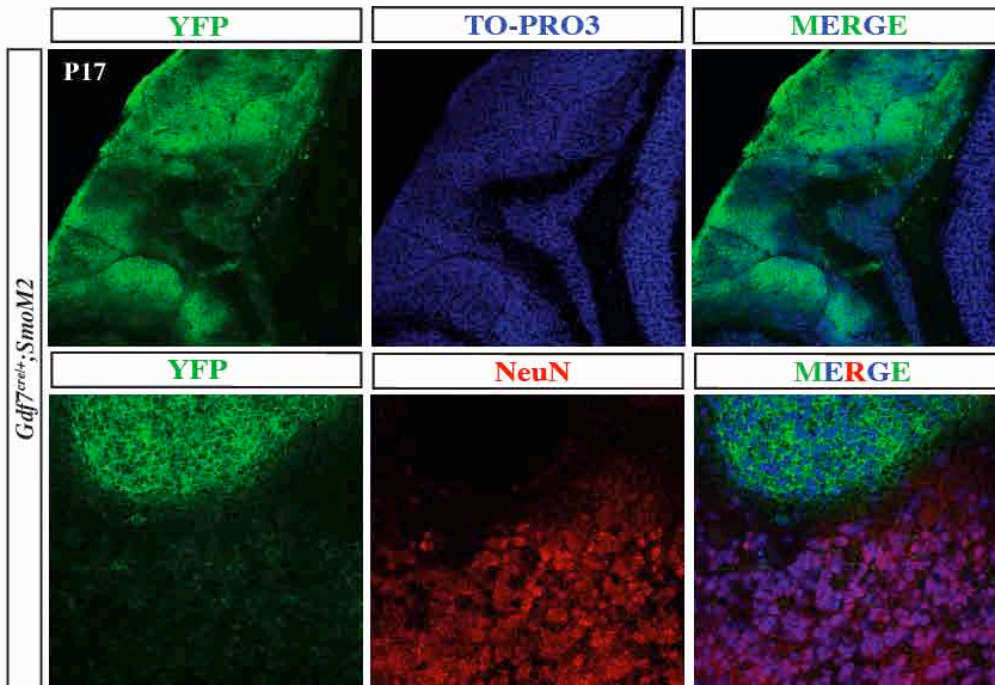
ectopic foci in *Gdf7^{Cre/+}; SmoM2* mice consisted of densely packed cells with high nuclear-to-cytoplasm ratio and nuclear polymorphism (Fig. 32B). As the cell membrane-localized SmoM2 protein is fused with a YFP reporter protein (Jeong et al., 2004), we determined that these ectopic cellular clusters were all indeed YFP positive covering most of the cerebellar surface in *Gdf7^{Cre/+}; SmoM2* mice (Fig. 32C), demonstraing that these cells are derived from Gdf7-expressing progenitor cells. Importantly, YFP-positive cells did not express differentiated neuronal marker such as NeuN (Fig. 32C). These data suggest that targeted Shh signaling within the Gdf7-lineage can rapidly lead to cerebellar focal hyperplasia that highly resembles aberrant cerebellar granule neuron precursors undergoing neoplastic transformation.

Gdf7^{Cre/+}; SmoM2 derived medulloblastomas display cerebellar granule neuron precursor fate and similar molecular pheotypes to those of *Patched1^{LacZ/+}* mice

Consistent with the fact that constitutively active SmoM2 was expressed within the Gdf7-lineage cells and the ectopic cellular clusters are marked by SmoM2-YFP, we detected high level of Shh signaling, as evidenced by robust expression of pathway target genes *Gli1* and *Ptch1*, in the focal hyperplastic cerebellar tissue of the *Gdf7^{Cre/+}; SmoM2* mice (Fig. 33A), whereas normally moderate Shh signaling was only seen in the putative Bergmann glial cells in the control cerebella (Fig. 33A). Emerging evidence suggests that Nmyc is an essential oncogenic mediator for Shh-dependent medulloblastoma formation (Kenney et al., 2003), (Kenney et al., 2004), (Hatton et al., 2006), (Thomas et al., 2009). More importantly, a recent study demonstrated that Nmyc promotes the

Figure 33. Shh pathway activation in Gdf7-lineage cells leads to cerebellar hyperplasia

Gdf7^{Cre/+}; SmoM2 gain-of-function mutant mice exhibit early post-natal lethality and cerebellar defects. (A) *Gdf7^{Cre/+}; SmoM2* mutant pups, which cannot survive over three weeks, are runted and display impaired motor function. The lack of externally apparent cerebellar lobules is shown. (B) *Gdf7^{Cre/+}; SmoM2* mutants over 14 days old develop ectopic foci of densely packed cells within the molecular layer of their cerebella. Higher magnification view of these foci reveals no discernible layer organization and resemblance to pre-neoplastic lesions. (C) The ectopic foci consist of cells of the Gdf7-lineage as indicated by their expression of SmoM2-YFP.

A

P21
Control
Gdf7^{cre/+};SmoM2
Gdf7^{cre/+};SmoM2

Control
FB
CB

Gdf7^{cre/+};SmoM2
FB
CB

Control (N=32)
Gdfcre/+;SmoM2 (N=24)

Percent survival
100
75
50
25
0

Time elapsed (days)
0   10   20

B

H.E.

	P10		P19	

Control

Gdf7^{cre/+};SmoM2

C

YFP TO-PRO3 MERGE

P17

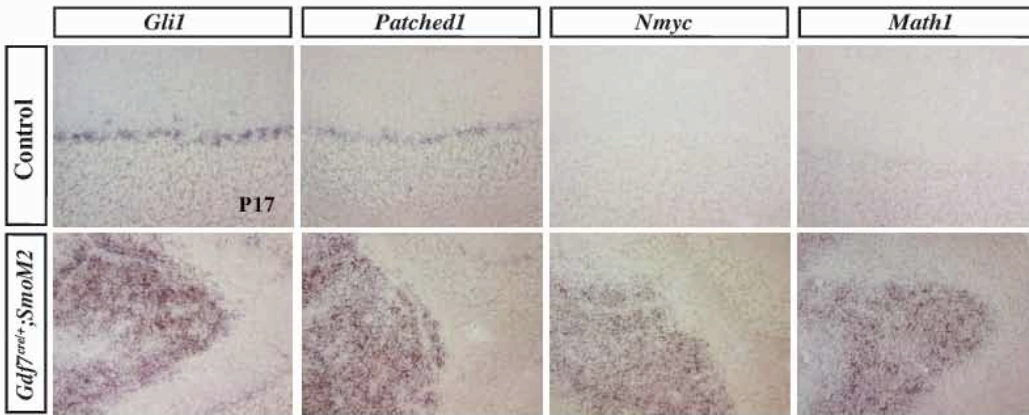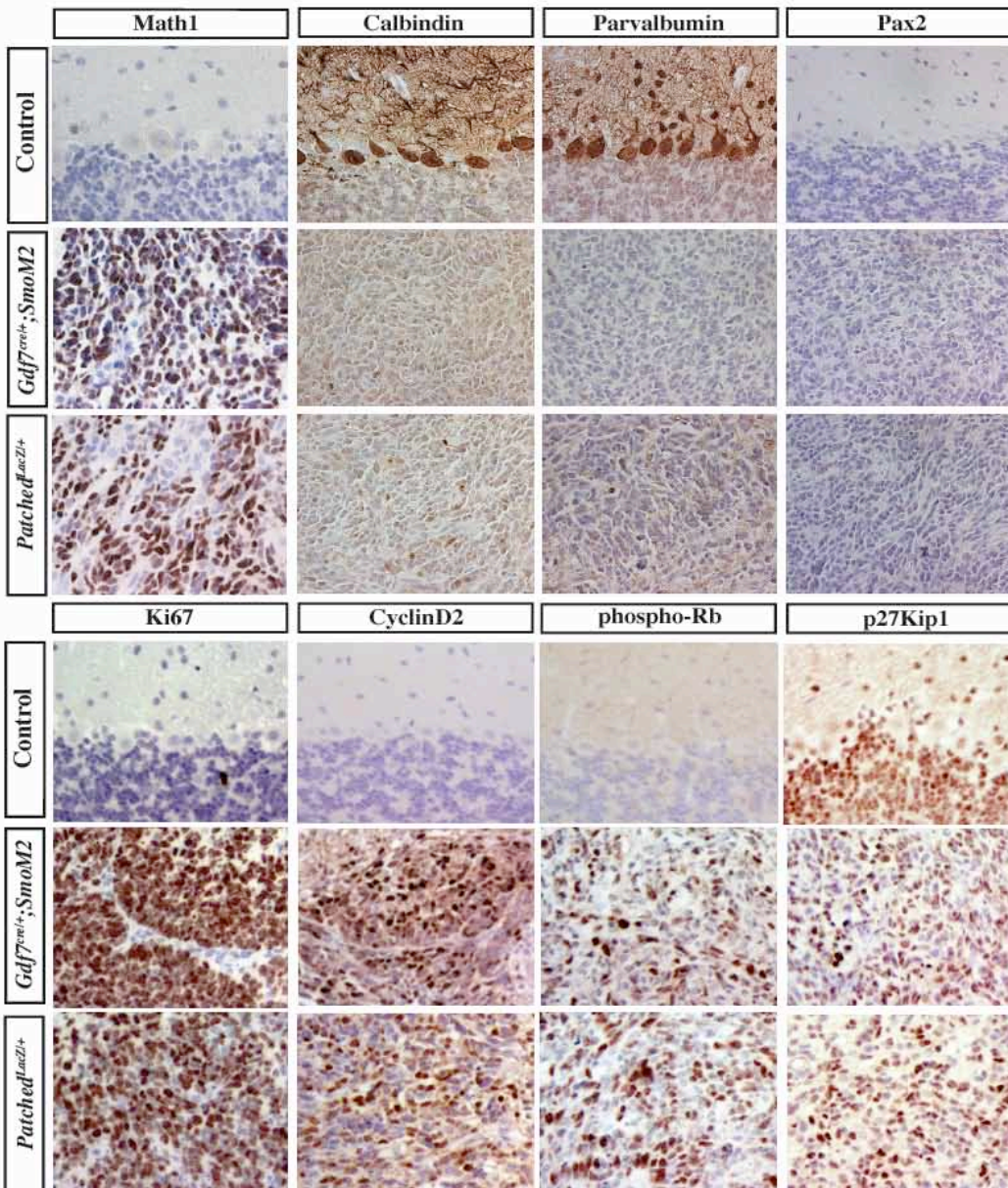Gdf7^{cre/+};SmoM2

YFP NeuN MERGE

161

progression from preneoplastic lesions to medulloblastoma (Kessler et al., 2009). While *Nmyc* expression is not detectable in the cerebella of control mice older than 2 weeks, its expression is robust in the ecotpic tissue foci of the *Gdf7^{Cre/+}; SmoM2* mice (Fig. 33A), suggesting that these cells were undergoing oncogenic transformation. Previous studies have shown that acquisition of CGNP fate is a prerequisite to medullollastoma formation (Schuller et al., 2008), (Yang et al., 2008). We also detected strong expression of *Math1* transcript and protein which mark cells of the CGNP fate (Fig. 33A and 33B), while the tumor tissues of both *Gdf7^{Cre/+}; SmoM2* and *Patched1^{LacZ/+}* mice were not significantly composed of Calbindin-positive Purkinje neurons, parvalbumin-positive GABAergic interneurons or Pax2-positive GABAergic interneuron progenitors (Fig. 33B). Similar to the full-blown medulloblastoma of the *Patched1^{LacZ/+}* mice, the aberrant *Gdf7^{Cre/+}; SmoM2* cerebellar tissues express neural progenitor markers Nestin and are highly proliferative as indicated by strong expression of Ki67, CyclinD2 phosphorylated Rb and lack of differention marker p27Kip1 (Fig. 33B). Taken together, these data demonstrate that indeed the *Gdf7^{Cre/+}; SmoM2* mice develop medulloblastomas which consist of cells of CGNP fate and exhibit similar molecular pheotypes to those of the *Patched1^{LacZ/+}* mice.

A subset of Gdf7-lineage roof plate cells are transformed into cancer stem-like cells

A recent report has shown that a subset of medulloblastoma cells arising from *Patched1^{LacZ/+}* mice are cancer stem cells and these cells are capable of initiating and propagating tumors (Ward et al., 2009). In order to ask whether the ectopic tissue foci

Figure 34. *Gdf7^{Cre/+}; SmoM2* **mice develop medulloblastoma with CGNP features**

(A) The aberrant tissue foci of *Gdf7^{Cre/+}; SmoM2* mice cerebella display high level of Shh signaling and *Nmyc* and *Math1* expression. (B) *Gdf7^{Cre/+}; SmoM2* mice indeed develop medulloblastoma consisting of cells of the CGNP fate. Tumors developed in *Gdf7^{Cre/+}; SmoM2* mice and adult *Patched1^{LacZ/+}; SmoM2* mice are very similar.

A

	Gli1	*Patched1*	*Nmyc*	*Math1*
Control		P17		
Gdf7^cre/+;SmoM2				

B

	Math1	Calbindin	Parvalbumin	Pax2
Control				
Gdf7^cre/+;SmoM2				
Patched^LacZ/+				

	Ki67	CyclinD2	phospho-Rb	p27Kip1
Control				
Gdf7^cre/+;SmoM2				
Patched^LacZ/+				

developed in the $Gdf7^{Cre/+}$; *SmoM2* mice indeed contained fully-transformed tumor cells, we sought to determine the presence of potential cancer stem cells. Consistently, we were able to detect the presence of Nestin+ and GFAP+ cells in $Gdf7^{Cre/+}$; *SmoM2* tumor foci, suggestive of tumor stem cells (Fig. 34A). We then dissected the cerebella of the control and $Gdf7^{Cre/+}$; *SmoM2* mice that were older than 14 days, dissociated them and cultured the cells in neural stem cell medium. We did not observe an appreciable colony formed by the disscoiated control cerebellar cells under this culture condition (Fig. 34B). In line with the malignant nature of these cells, we observed numerous highly proliferative colonies established in days from every analyzed mutant cerebellum. These cells robustly expressed many neural stem cell markers such as Nestin, Sox2 and GFAP, can undergo serial passages (N>20) and were clonogenic (Fig. 34B). While the cultured $Gdf7^{Cre/+}$; *SmoM2* cerebellar tumor cells are mostly small, bipolar cells with high nucleus-to-cytoplasm ratio, these cells dramatically altered their morphology, extending multiple cellular processes, became more flattened and withdrew from the cell cycle upon switching to regular cell culture medium supplemented with 10% fetal bovine serum (Fig. 34B, data not shown). More importantly, the YFP-marked tumor cells differentiated into Tuj1+ or NeuN+ neurons, GFAP+ astrocytes or CNPase+ oligodendrocytes, highlighting their multi-potency (Fig. 34B). Furthermore, these cells were capable of propagating secondary medulloblastoma when orthotopically grafted into host mice (Fig. 34C). Importantly, these tumor initiating cells are of the Gdf7-lineage as evidenced by their strong expression of YFP (Fig. 34C). These data suggest that, the $Gdf7^{Cre/+}$; *SmoM2* cerebella indeed contain fully-transformed tumor cells, and a subset of Gdf7-lineage roof plate cells are transformed into cancer stem-like cells in the presence of constitutively
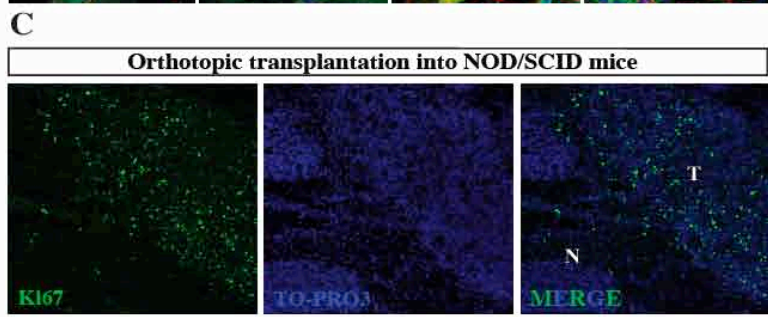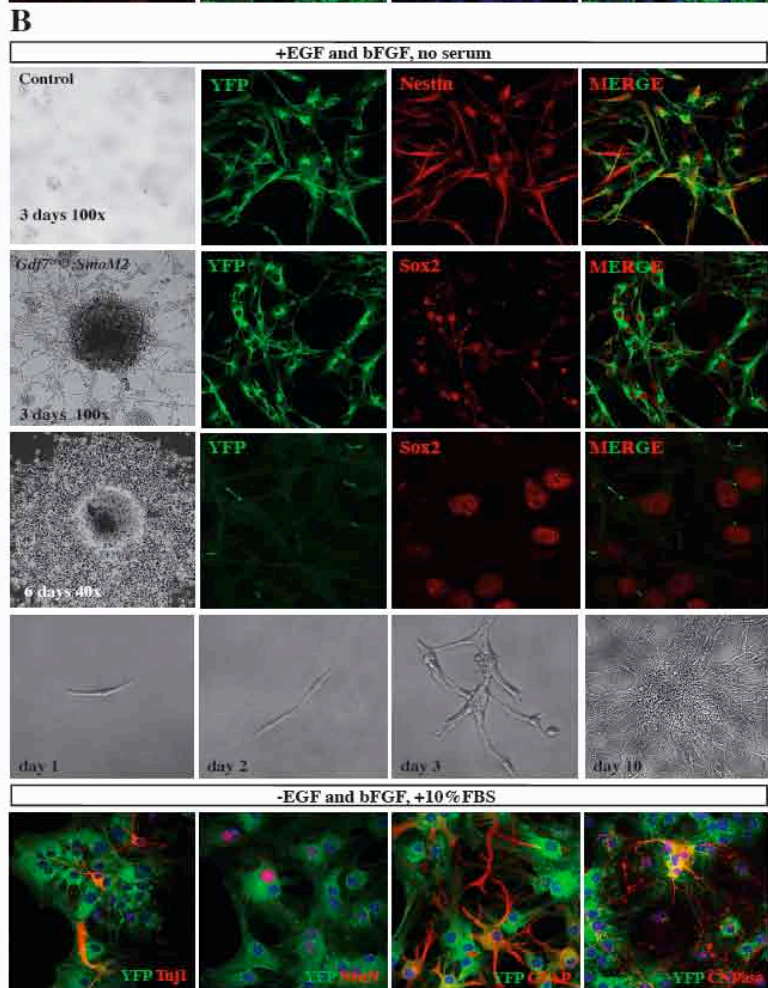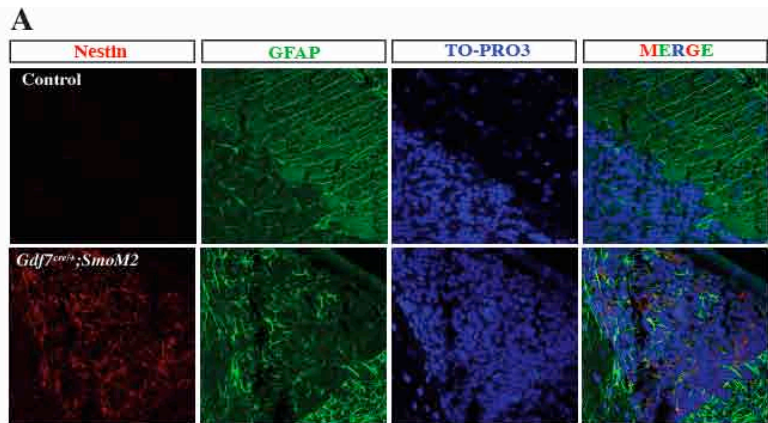
165

active Shh signaling.

Distinct Gdf7-expressing cerebellar vermal ventricular zone cells are radial glias that extensively contribute to different mature cerebellar cell types

The unexpected finding that the *Gdf7$^{Cre/+}$; SmoM2* mice displayed extensive cerebellar oncogenic transformation prompted us to ask whether the Gdf7-lineage cells only diffenrentiate into mature hChPe cells as previously recognized, or contribute to other cerebellar cell types including the cerebellar granule neurons that are susceptible to oncogenic transformation by aberrant Shh signaling. We then performed detailed fate-mapping of the Gdf-7 lineage in *Gdf7$^{Cre/+}$; ROSA26-eYFP* and *Gdf7$^{Cre/+}$; ROSA26-eYFP* mice, in which enhanced YFP indelibly marks cells that are, or once were, expressing Gdf7. As expected, the Gdf7-lineage cells distributed to the dorsal midline along the whole brain-spinal axis (Fig. 35A). In this hindbrain region, Gdf7-lineage cells emanate from the lateral side towards the medial portion of the roof plate, a migratory pattern similar to reported *Ttr*-expressing primitive hChPe cells (Fig. 35A) (Hunter and Dymecki, 2007). Surpisingly, we also noted a previously unrecognized streak of Gdf7-lineage cells present in the midline vermal cerebellar tissue where the two hemispheres meet (Fig. 35A). This observation is consistent with the fact that we detected restricted *Gdf7*-expressing cells of the cerebellar midline tissue (Fig. 35A). Interestingly, the identical tissue domain highly expressed *Msx1*, a Bmp signaling target gene, indicative of autocrine signaling. We then set to determine the identity of these Gdf7-expressing cells. Since there is no good Gdf7 antibody available, we performed cell

Figure 35. Subset of Gdf7-lineage cells are oncogenically transformed into cancer stem-like cells

(A) Many cells co-expressing neural stem cell markers can be identified within the tumor tissue of the *Gdf7$^{Cre/+}$; SmoM2* mice. (B) Tumor cell lines can be invariably established from each *Gdf7$^{Cre/+}$; SmoM2* cerebellum dissociated. These cells highly express multiple neural stem cell markers, can undergo serial passages, display clonogenic capacity and are multipotent. Here one representative colony is shown cultured for 3 days and 6 days. (C) The cells of established *Gdf7$^{Cre/+}$; SmoM2* tumor cell lines are tumorigenic as evidenced by their capacity to initiate secondary tumor after grafting into immuno-compromised recipients.

A

Nestin	GFAP	TO-PRO3	MERGE

Control

Gdf7cre/+;SmoM2

B

+EGF and bFGF, no serum

Control	YFP	Nestin	MERGE

3 days 100x

Gdf7cre/+;SmoM2
3 days 100x — YFP — Sox2 — MERGE

6 days 40x — YFP — Sox2 — MERGE

day 1 — day 2 — day 3 — day 10

-EGF and bFGF, +10%FBS

YFP Tuj1 — YFP Map2 — YFP GFAP — YFP CnPase

C

Orthotopic transplantation into NOD/SCID mice

Ki67 — TO-PRO3 — MERGE

T

N

marker staining in the *Gdf7*$^{Cre/+}$*; ROSA26-eYFP* mice. Radial glia cells have been shown to be multipotent neural stem cells during embryogenesis (Anthony et al., 2004). We observed that all the Gdf-lineage cells localized to the vermal ventriular zone expressed radial glial cell markers BLBP and Sox2 (Fig. 35A), while Gdf7-lineage cells localized in the hChPe and distal rhombic lip were negative for BLBP and Sox2 (Fig. 35A). These data suggested that the Gdf7-expressing cerebellar vermal cells are a distinct sub-population of multi-potent embryonic radial glia cells. Consistent with the fact that CGNPs are differentiated from radial glia cells, we usually observed few YFP-marked Gdf7-lineage cells that appear to be migrating away from the cerebellar midline vermal ventricular region towards the peripheral forming external granule layer (Fig. 35A). Importantly, these migratory cells begin to express CGNP marker Pax6 and no longer express Gdf7 or radial glial markers (Fig. 35A). Interestingly, using Pax6 expression level we were able to clearly demarcate the three different progenitor tissue domains of the developing cerebellum: Gdf7 non-expressing radial glia cells expressed low but detectable Pax6, Gdf7-expressing vermal radial glia cells do not express Pax6, CGNPs of the developing external granule neuron layer strongly expressed Pax6. The difference in developmental potentials between lateral BLBP+;Sox2+;Pax6^{low};Gdf7- and vermal BLBP+;Sox2+;Pax6-;Gdf7+ radial glia cells remain to be determined. We did not observe Gdf7-lineage cells expressing Pax6 in the distal rhombic lip region (Fig. 35A), suggesting that the Gdf7-expressing cells outside of the cerebellum likely do not give rise to CGNPs. As radial glia cells are rapidly proliferating during embryonic stages, we asked whether Gdf7 can act as a proliferative signal. The lack of apparent Gdf7 and Msx1 expression in the Math1+ tumor tissue (Fig. 35B) of the *Gdf7*$^{Cre/+}$*; SmoM2* mice argues

against that possibility.

We then analyzed the fate of Gdf7-lineage cells at postnatal stages. All the mature hChPe cells, but not the hChP mesenchyme, highly expressed YFP (Fig. 35C), indicating that they are derived from Gdf-7 lineage roof plate progenitor cells. Consistent with our observation of a subset of Gdf7-expressing vermal radial glia cells, we also detected apparent YFP signal in the EGL, and other tissue layers of the P7 cerebellum (Fig. 35C, data not shown). In line with their widespread distribution in P7 cerebellum, we found that the Gdf7-lineage cells contributed extensively to various mature cerebellar cell types. In adult $Gdf7^{Cre/+}$; $Rosa-eYFP$ cerebellum, YFP-marked cells co-expressed granule neuron marker NeuN (~3%), Purkinje neuron marker Calbindin (<0.1%), GABAergic interneuron marker Parvalbumin (<0.1%), white matter astrocyte cell marker GFAP (<0.1%). A subset of Bergmann glia cells, identified by their typical morphology and localization to the Purkinje layer, can also be seen with robust YFP signal (<0.1%) (Fig. 35C). It is interesting to note that while GDF7-lineage cells indeed are multipotent, the granule neurons are the predominent cellular derivatives. A similar situation has been reported that Gdf7-expressing roof plate cells of the spinal cord region preferentially become sensory neurons, a process suggested to be mediated by the function of Gdf7 itself (Lo et al., 2005). Future studies are warranted to determine whether Gdf7 can elicit discrete Bmp signaling in a autocrine manner, as revealed by Msx1 expression within the cerebellar vermal ventricular zone, and whether this Bmp signaling imposes a biased granule neuron fate on the radial glia progenitors. Taken together, our data demonstrate that the previouslly reported unipotent Gdf7-expressing roof plate cells in the hindbrain region are in fact multipotent, contributing to many types of mature GABAergic and
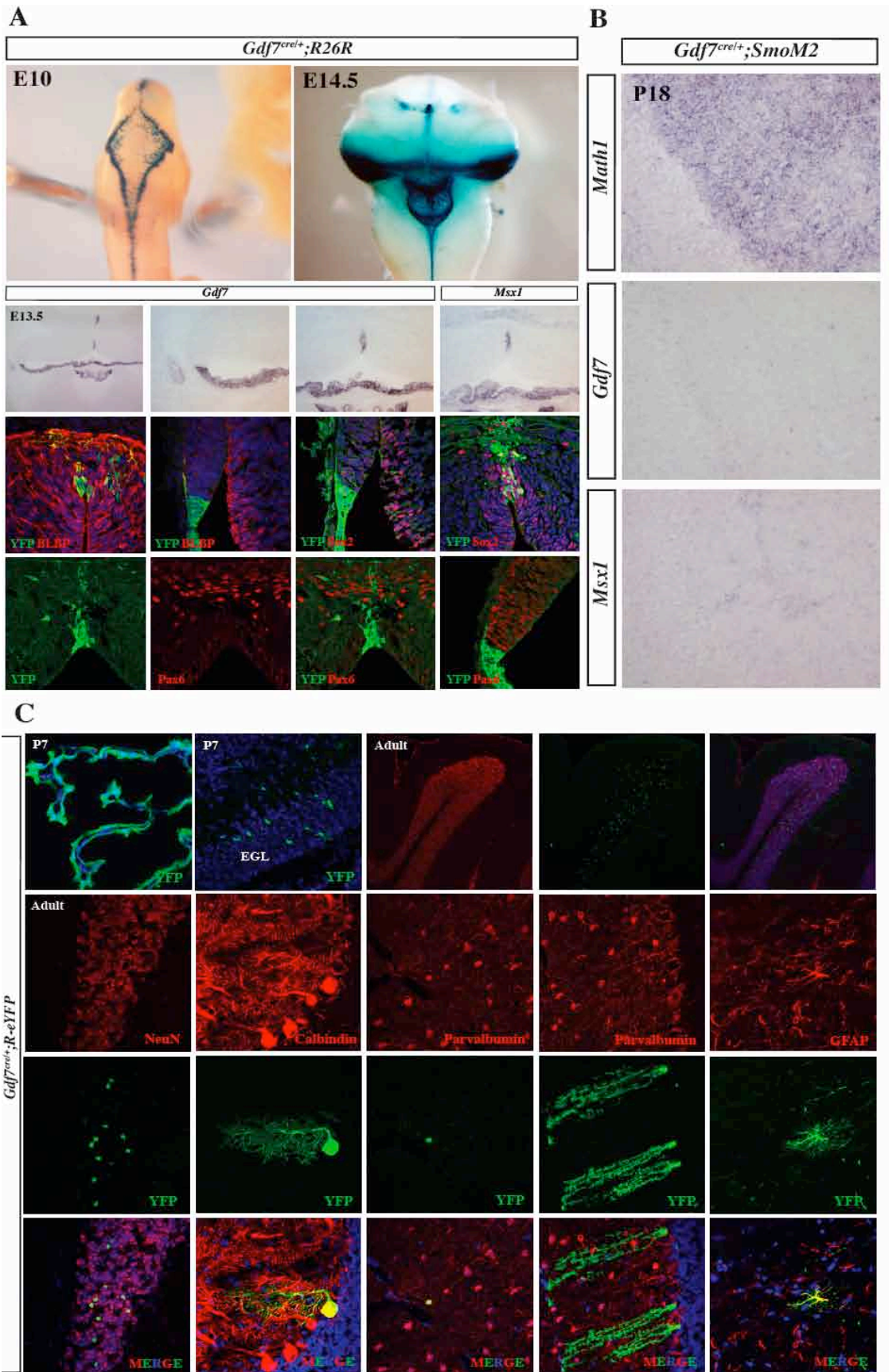
glutamatergic neuronal cells as well as glial cells. Despite Gdf7-expressing progenitors are able to give rise to all these different cell types, our observation that the *Gdf7$^{Cre/+}$; SmoM2* mice developed medulloblastoma, all of which displaying features of CGNPs, confirms that becoming CGNPs is a necessary step during cerebellar tumorigenesis.

Figure 36. Roof plate cells give rise to a distinct population of cerebellar vermal radial glia cells

(A) A distinct population of cerebellar vermal ventricular zone radial glia cells express Gdf7 and Msx1, fate-mapping of Gdf7-lineage consistently demonstrate their presence. (B) The *Math1+ Gdf7$^{Cre/+}$; SmoM2* tumor tissue does not express *Gdf7* or *Msx1*. (C) Fate-mapping studies in *Gdf7$^{Cre/+}$; ROSA-eYFP* mice show that the Gdf7-lineage cells distribute to all the mature cerebellar tissue layers and contribute to granule neurons, Purkinje neurons, GABAergic interneurons, Bergmann glias, white matter astrocytes, as well as non-neural hindbrain choroid plexus epithelial cells.

CHAPTER VII

FUTURE DIRECTIONS

As introduced in Chapter V, the excitatory or glutamatergic neurons including cerebellar granule neurons, large DCN neurons as well as unipolar brush cells are generated from Math1-expressing RL progenitors (Machold and Fishell, 2005) (Wang et al., 2005) (Fink et al., 2006). CGNPs generated from the RL migrate tangentially and occupy their transitory location to form the external granule layer (EGL). On the other hand, the inhibitory or GABAergic neurons are generated from the VZ by a single population of Ptf1a-expressing multipotent progenitors (Altman and Bayer, 1997; Laine and Axelrad, 2002), (Hoshino et al., 2005; Pascual et al., 2007). Since our study (described in Chapter V) demonstrated that Shh signaling is required for the expansion of radial glia cells, progenitors of Ptf1a-expressing cells, in the cerebellum, it opens the possibility that deregulated Shh signaling in the Ptf1a-lineage may also cause medulloblastoma. Indeed, we have obtained exciting preliminary results showing that constitutive Shh pathway activation in the GABAergic-lineage leads to medulloblastoma formation. In this section of " Future Directions", I will describe these preliminary data, and propose additional experiments aiming at looking into the mechanism of oncogenic transformation. I hope that by continuing this project one would provide important insights into an alternative genetic basis and cellular origin of medulloblastoma.

***Ptf1a$^{cre/+}$; SmoM2* mice rapidly develop medulloblastoma at high incidence**

In order to determine whether VZ-derived lineage-restricted GABAergic progenitors could be oncogenically transformed in the presence of constitutively activated Shh signaling, we took advantage of the *Ptf1a$^{cre/+}$* driver line, which expresses Cre recombinase under the control of endogenous *Ptf1a* promoter (Pascual et al., 2007) and can activate R26R-lacZ reporter gene expression specifically in all GABAergic lineages (Hoshino et al., 2005; Pascual et al., 2007). To activate Shh signaling in the Ptf1a-lineage, we mated the *Ptf1a$^{cre/+}$* driver line to *SmoM2* mouse line (Jeong et al., 2004). While *Ptf1a$^{cre/+}$; SmoM2* pups are born with no discernable phenotype compared to control littermates (data not shown), many *Ptf1a$^{cre/+}$; SmoM2* adult mice became runted, displayed hydrocephalus and typical neurological signs of medulloblastoma, including posterior paralysis and failure to regain upright position when overturned. While the cerebella of controls displayed well-defined hemisphere and vermal structures, the cerebella of *Ptf1a$^{cre/+}$; SmoM2* mice were often enlarged, amorphous with a smooth surface and conspicuous blood vessels. Indeed, hemotoxylin-eosin stained sections of *Ptf1a$^{cre/+}$; SmoM2* cerebella showed absence of any tissue layer (molecular, Purkinje or internal granule neuron layers) compared with controls (Fig. 36). Instead *Ptf1a$^{cre/+}$; SmoM2* medulloblastoma tissue consisted of uniform and densely packed cells with large, irregular nuclei and scant cytoplasm, which closely parallel the histological features of classic medulloblastoma in humans (Gilbertson and Ellison, 2008). Importantly, *Ptf1a$^{cre/+}$; SmoM2* medulloblastoma is highly proliferative and also displays increased apoptosis (Fig. 36), histopathological features that are also found in human patients. More than 50% of *Ptf1a$^{cre/+}$; SmoM2* mice developed tumors and eventually succumbed to terminal medulloblastoma within 12 months (Fig. 36).

175

Figure 37. *Ptf1a^{cre/+}; SmoM2* mice rapidly develop medulloblastoma

Adult *Ptf1a^{cre/+};SmoM2* mice are often runted with severe neurological symptoms. Their tumor-bearing cerebella are amorphous, enlarged with no distinguishable tissue layers. The *Ptf1a^{cre/+};SmoM2* mice medulloblastoma is highly proliferative and apoptotic, as shown by prominent Ki67 and cleaved-caspase 3 staining signals, respectively. Apparent ectopic blood vessels surrounded by CD34+ endothelial cells are present in the tumor tissue. Note that most of the *Ptf1a^{cre/+};SmoM2* mice develop and succumb to medulloblastoma within 12 months after birth. V, vermis; H, hemisphere; M, molecular layer; P, Purkinje neuron; G, granule neuron layer.
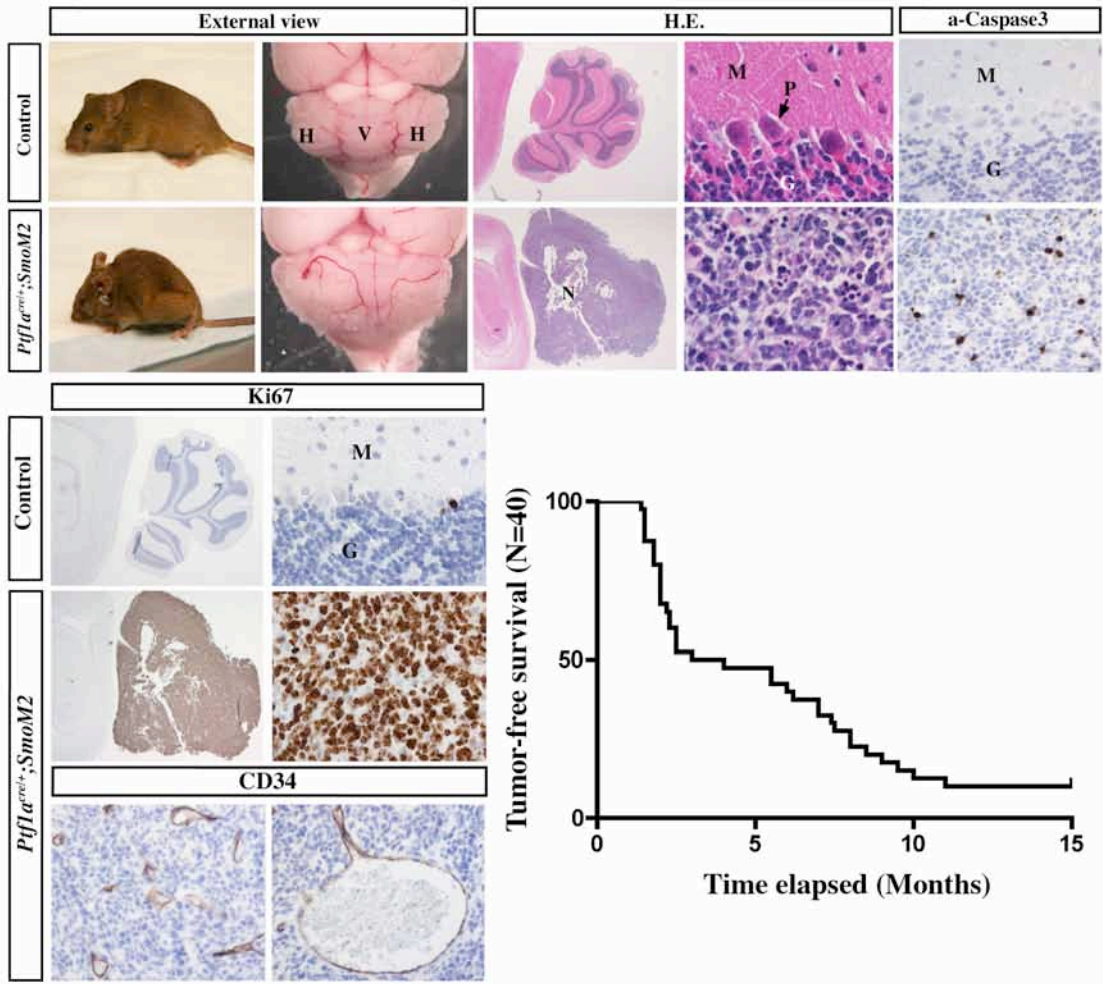
Medulloblastoma in *Ptf1a^cre/+^; SmoM2* mice displays high level of ectopic Shh signaling

As Ptf1a-lineage cells express constitutively active SmoM2, we determined whether the tumor tissue in *Ptf1a^cre/+^; SmoM2* mice maintains high level Shh pathway activity. Indeed, we found that *Ptf1a^cre/+^; SmoM2* medulloblastoma tissue displays high level of Shh signaling as indicated by abundant expression of *Ptch1 and Gli1* transcripts by *in situ* staining analyses, while in the controls, moderate level of Shh signaling can only be detected in the putative Bergmann glia cells (Fig. 37) (Corrales et al., 2004). Consistently, Shh target genes, *Hhip1* (Chuang et al., 2003), *Sfrp1* (Lee et al., 2003) and proto-oncogene *Nmyc* (Kenney et al., 2003) (Hatton et al., 2006) were largely up-regulated in tumor samples indicated by RT-PCR using RNAs from cerebella of controls and tumor-bearing *Ptf1a^cre/+^; SmoM2* mice (Fig. 37). We did not detect apparent expression of Shh in the *Ptf1a^cre/+^; SmoM2* mice tumor tissue, although its expression is detected in Purkinje cells of the normal cerebellum (Fig. 37), in line with the fact that the pathway was activated at the Smo receptor level, bypassing the requirement of ligand.

Medulloblastomas in *Ptf1a^cre/+^; SmoM2* mice adopt a CGNP fate and exhibit similar molecular phenotypes as tumors in traditional *Ptch^LacZ/+^* heterozygous mice

Previous studies suggested that Ptf1a-expressing progenitors give rise to GABAergic lineage cells (Hoshino et al., 2005) (Pascual et al., 2007). Therefore, it is essential to determine whether medulloblastoma developed in *Ptf1a^cre/+^; SmoM2* mice are composed of GABAergic cells, a situation differing from the established hypothesis that only CGNPs are capable of undergoing oncogenic transformation. Or an unknown non-

cell autonomous mechanism activating Shh pathway in GABAergic progenitors triggers tumorigenesis in the adjacent CGNPs. Interestingly, molecular maker analyses showed that the tumors developed in *Ptf1a*^*cre/+*^*; SmoM2* mice are very similar to those developed in *Gdf7*^*Cre/+*^*; SmoM2* mice and *Patched1*^*LacZ/+*^ mice, in that the most abundant cells are Math1+ CGNPs while no Ptf1a+ cells are present (Fig. 38). In addition, large-scale gene expression profiling by Affymetrix Exon Array demonstrated high similarity between the tumor tissues derived from *Ptf1a*^*cre/+*^*; SmoM2* mice and *Patched1*^*LacZ/+*^ mice (Fig. 38). Next, we asked whether these CGNPs are derived from Ptf1a-lineage. In other words, we probed whether ectopic Shh pathway activation promoted Ptf1a-expressing progenitor cells to switch their fate into Math1-expressing CGNPs. We performed genetic fate-mapping studies to indelibly mark VZ-derived Ptf1a-lineage cells by determining YFP expression in *Ptf1a*^*cre/+*^*; SmoM2* mice as the SmoM2-YFP protein will only be present in the Ptf1a-lineage cells. As shown in Fig. 39, the tumor tissue in *Ptf1a*^*cre/+*^*; SmoM2* cerebellum highly expressed eYFP, and sectional view demonstrated robust SmoM2-eYFP expression on the tumor cell membrane, indicating that the tumor indeed consists of GABAergic lineage cells. In summary, we have acquired preliminary results showing that medulloblastoma can arise from Ptf1a-lineage GABAergic progeny cells, a largely unexpected observation since all previous studies reached at the conclusion that only normal CGNPs can be target of oncogenic transformation. Our task then is to understand the underlying mechanism for this unusual tumorigenic process.

Figure 38. Medulloblastoma developed in *Ptf1a^{cre/+}; SmoM2* mice exhibit high-level of Shh pathway activity

Ptf1a^{cre/+}; SmoM2 medulloblastoma displays high level of Shh signaling pathway activity, indicated by robust expression of *Gli1* and *Patched1*. The Shh pathway components and other target gene expressions are also prominent, including those of *Gli2, Nmyc, Hhip1* and *Sfrp1*. Interestingly, *Gli3* is not detectable in the tumor. Note that the Shh ligand is not ectopically expressed in the *Ptf1a^{cre/+}; SmoM2* mutants. Red boxes are magnified as shown in the right adjacent panels. N, normal cerebellar tissue; T, tumor tissue; M, molecular layer; G, granule layer.
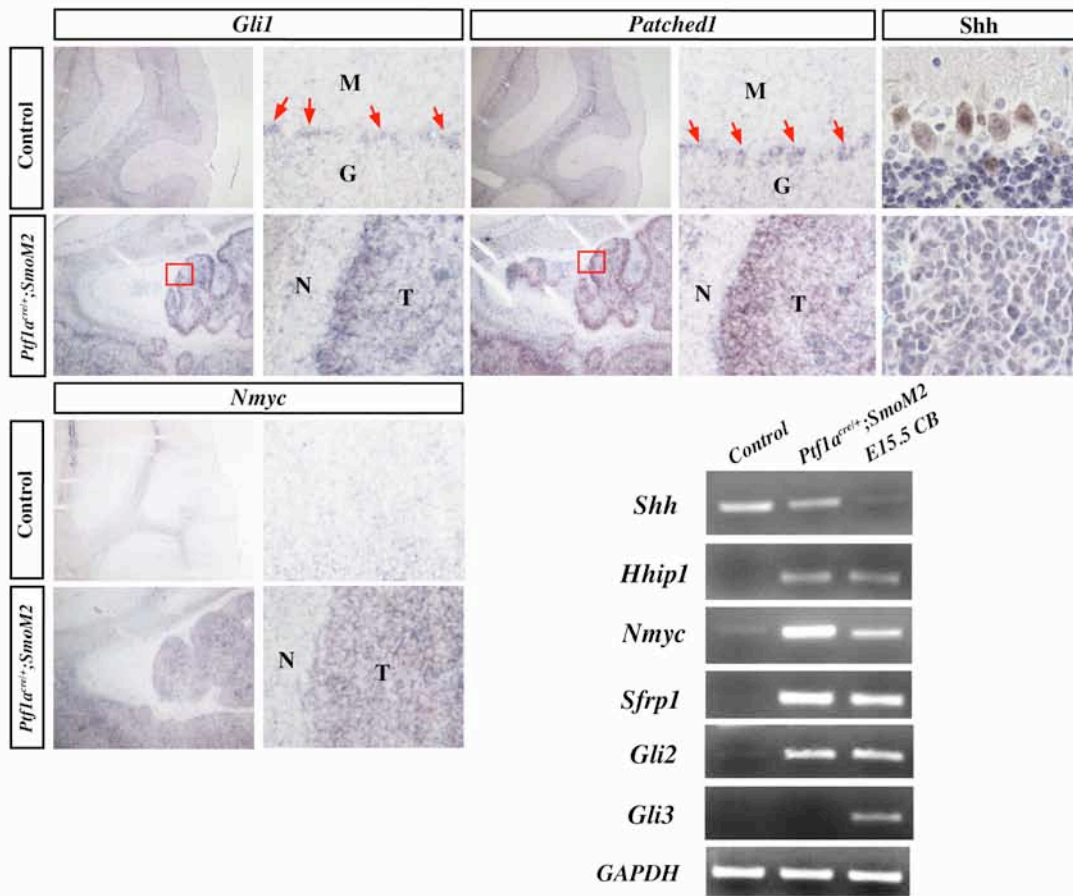
Figure 39. Medulloblastoma cells of *Ptf1a$^{cre/+}$; SmoM2* mice adopt CGNP fate and display highly similar gene expression profiles to those of *Ptch1$^{LacZ/+}$* mice

Ptf1a$^{cre/+}$; SmoM2 medulloblastoma consists of Nestin+, BLBP+, GFAP+ neural progenitor cells, and Math1+ CGNPs, with no appreciable amounts of Calbindin+ Purkinje neurons, Pax2+ interneuron progenitors or Ptf1a+ GABAergic progenitors. Medulloblastoma developed in *Ptf1a$^{cre/+}$; SmoM2* and *Ptch1$^{LacZ/+}$* mice are highly similar both in cell type marker expressions and large-scale gene expression profiles.
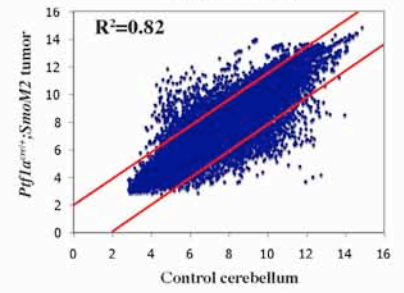
Figure 40. Medulloblastoma in *Ptf1a^{cre/+}; SmoM2* mice derives from GABAergic Ptf1a-lineage cells

Ptf1a^{cre/+}; SmoM2 medulloblastoma tissue expresses strong membranous SmoM2-YFP in both whole-mount and sectional views. N, normal cerebellar tissue; T, tumor tissue.

Ptf1a^{cre/+}*;SmoM2*

Possible mechanisms for tumorigenesis in *Ptf1a^{cre/+}; SmoM2* mice

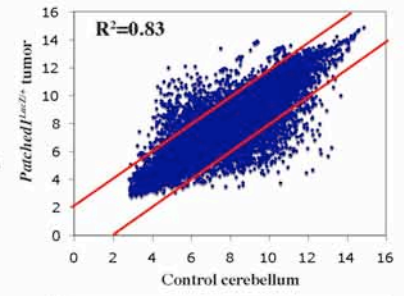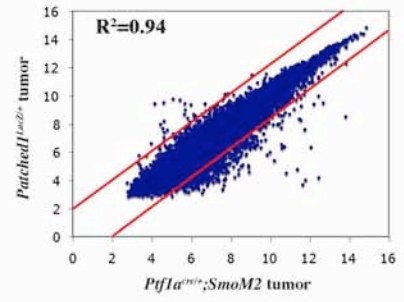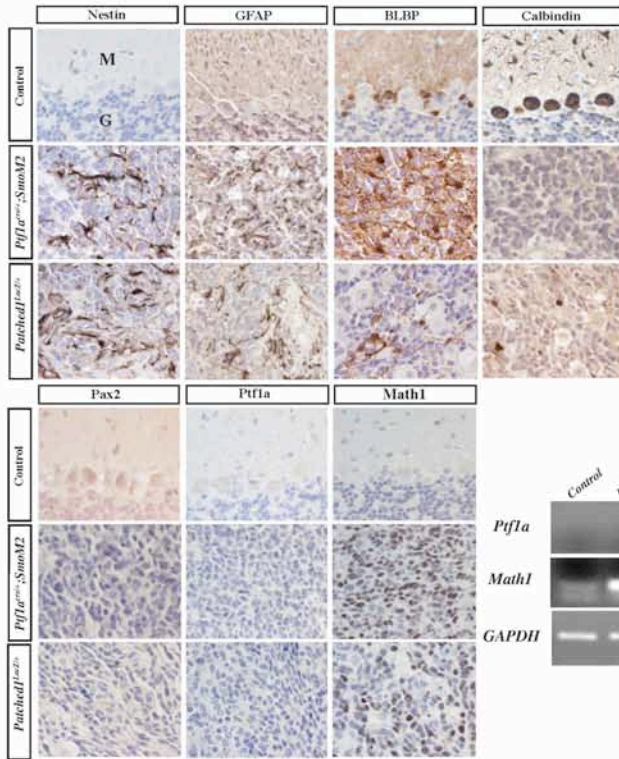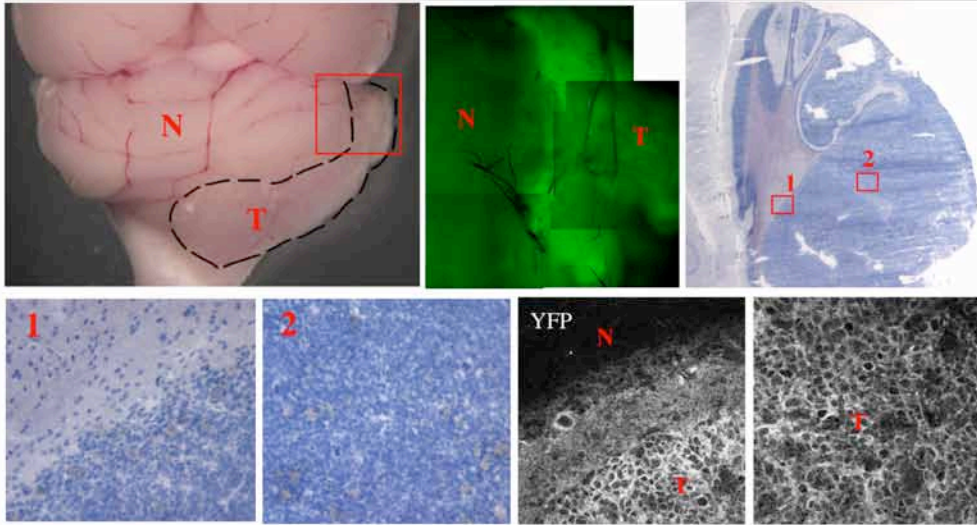Our studies show that Ptf1a-lineage GABAergic cells can be oncogenically transformed by constitutively active Shh signaling and we propose three possible mechanisms. First, the heterozygosity of Ptf1a allele renders some VZ progenitor cells incapable of maintaining their fate as GABAergic progenitors and stochastically become Math1+ CGNPs. Consistent with this notion, we have found that Ptf1a-lineage cells contribute to a small population of Pax6+ CGNPs in P0 embyos (Fig. 41). However, this unexpected observation could also be due to ectopic Shh pathway activation. A definitive conclusion awaits the generation of a transgenic Ptf1a-cre line, which does not reduce the endogenous level of Ptf1a protein, for fate-mapping its lineage. Second, the Ptf1a-expressing ventricular zone progenitors may be multipotent and can give rise to a discrete population of CGNPs in physiologically relevant context, rather than being only the GABAergic progenitors as reported (Hoshino et al., 2005) (Pascual et al., 2007). It is our experience that one can easily misinterpret a fate-mapping data if the immunostaining experiments were not performed optimally. Therefore, to test this possibility, we need to perform straightforward and extensive fate-mapping experiments, with high resolution and fidelity, on *Ptf1a^{cre/+}; ROSA-eYFP* mice cerebella. We can also determine whether there are subsets of Ptf1a+ cells expressing radial glia cell markers such as Sox2 and BLBP. If indeed some Ptf1a+ cells are multipotent progenitors that can give rise to CGNPs, we can conclude for a novel and additional progeny cell type for the Ptf1a+ progenitors. Alternatively, if we find no evidence supporting the first proposed possibility, we will attempt to determine the validity of the third possible explanation, which is that ectopic Shh signaling induces a fate-switch of Ptf1a+ cells to Math1+

Figure 41. Subset of Ptf1a-lineage cells become CGNPs at P0 in *Ptf1a$^{cre/+}$; R-eYFP* embryos
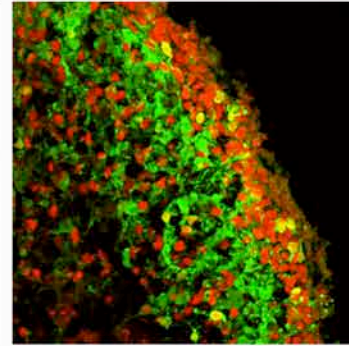
A small population of Pax6+ CGNPs are of Ptf1a-lineage as evidenced by co-expression of YFP and Pax6 in the P0 *Ptf1a$^{cre/+}$; R-eYFP* embryonic cerebellum.

Ptf1a^{cre/+};R-eYFP		
YFP	Pax6	MERGE
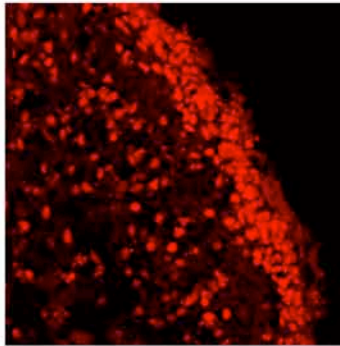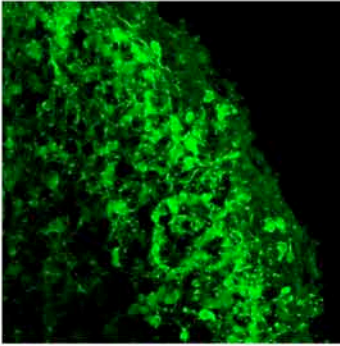
cells. Previous study showed that the VZ progenitors became Math1+ progenitors when Ptf1a function is ablated (Pascual et al., 2007). One can then imagine that if the ectopic Shh pathway activation somehow renders Ptf1a non-functional, fate-switching is possible. Hes1, a basic helix-loop-helix transcription factor, has been suggested to bind the promoter region of Ptf1a and assumes a transcriptional repressive role (Fukuda et al., 2006). Interestingly, Shh signaling has been shown to induce Hes1 expression in the developing retinal tissue in a cell-autonomous manner (Wall et al., 2009). We propose that high-level Shh signaling in Ptf1a+ cells inhibits Ptf1a transcription by inducing Hes1 expression. One can test this possibility by many experiments, including those testing for ectopic Hes1 expression and reduced Ptf1a expression in the VZ progenitors. Ultimately, one needs to generate *Ptf1a^{cre/+}; SmoM2; Hes1^{f/-}* mice and determine whether medulloblastoma initiation or maintenance is impaired.

BIBLIOGRAPHY

Agarwala, S., Sanders, T. A. and Ragsdale, C. W. (2001). Sonic hedgehog control of size and shape in midbrain pattern formation. *Science* **291**, 2147-50.

Ahn, S. and Joyner, A. L. (2004). Dynamic changes in the response of cells to positive hedgehog signaling during mouse limb patterning. *Cell* **118**, 505-16.

Altman, J. and Bayer, S. (1997). Development of the cerebellar system in relation to its evolution, structures and functions. *New York: CRC Press.*

Anthony, T. E., Klein, C., Fishell, G. and Heintz, N. (2004). Radial glia serve as neuronal progenitors in all regions of the central nervous system. *Neuron* **41**, 881-90.

Aoto, K., Nishimura, T., Eto, K. and Motoyama, J. (2002). Mouse GLI3 regulates Fgf8 expression and apoptosis in the developing neural tube, face, and limb bud. *Dev Biol* **251**, 320-32.

Assemat, E., Chatelet, F., Chandellier, J., Commo, F., Cases, O., Verroust, P. and Kozyraki, R. (2005). Overlapping expression patterns of the multiligand endocytic receptors cubilin and megalin in the CNS, sensory organs and developing epithelia of the rodent embryo. *Gene Expr Patterns* **6**, 69-78.

Awatramani, R., Soriano, P., Rodriguez, C., Mai, J. J. and Dymecki, S. M. (2003). Cryptic boundaries in roof plate and choroid plexus identified by intersectional gene activation. *Nat Genet* **35**, 70-5.

Bachler, M. and Neubuser, A. (2001). Expression of members of the Fgf family and their receptors during midfacial development. *Mech Dev* **100**, 313-6.

Backman, M., Machon, O., Mygland, L., van den Bout, C. J., Zhong, W., Taketo, M. M. and Krauss, S. (2005). Effects of canonical Wnt signaling on dorso-ventral specification of the mouse telencephalon. *Dev Biol* **279**, 155-68.

Balordi, F. and Fishell, G. (2007a). Hedgehog signaling in the subventricular zone is required for both the maintenance of stem cells and the migration of newborn neurons. *J Neurosci* **27**, 5936-47.

Balordi, F. and Fishell, G. (2007b). Mosaic removal of hedgehog signaling in the adult SVZ reveals that the residual wild-type stem cells have a limited capacity for self-renewal. *J Neurosci* **27**, 14248-59.

Banizs, B., Pike, M. M., Millican, C. L., Ferguson, W. B., Komlosi, P., Sheetz, J., Bell, P. D., Schwiebert, E. M. and Yoder, B. K. (2005). Dysfunctional cilia lead to altered ependyma and choroid plexus function, and result in the formation of hydrocephalus. *Development* **132**, 5329-39.

Barkovich, A. J. and Quint, D. J. (1993). Middle interhemispheric fusion: an unusual variant of holoprosencephaly. *AJNR Am J Neuroradiol* **14**, 431-40.

Baskin, E., Kayiran, S. M., Oto, S., Alehan, F., Agildere, A. M. and Saatci, U. (2002). Cerebellar vermis hypoplasia in a patient with Bardet-Biedl syndrome. *J Child Neurol* **17**, 385-7.

Bill, B. R., Balciunas, D., McCarra, J. A., Young, E. D., Xiong, T., Spahn, A. M., Garcia-Lecea, M., Korzh, V., Ekker, S. C. and Schimmenti, L. A. (2008). Development and Notch signaling requirements of the zebrafish choroid plexus. *PLoS ONE* **3**, e3114.

Bitgood, M. J. and McMahon, A. P. (1995). Hedgehog and Bmp genes are coexpressed at many diverse sites of cell-cell interaction in the mouse embryo. *Dev Biol* **172**, 126-38.

Briscoe, J. and Ericson, J. (2001). Specification of neuronal fates in the ventral neural tube. *Curr Opin Neurobiol* **11**, 43-9.

Britto, J., Tannahill, D. and Keynes, R. (2002). A critical role for sonic hedgehog signaling in the early expansion of the developing brain. *Nat Neurosci* **5**, 103-10.

Brown, L. Y., Odent, S., David, V., Blayau, M., Dubourg, C., Apacik, C., Delgado, M. A., Hall, B. D., Reynolds, J. F., Sommer, A. et al. (2001). Holoprosencephaly due to mutations in ZIC2: alanine tract expansion mutations may be caused by parental somatic recombination. *Hum Mol Genet* **10**, 791-6.

Brown, S. A., Warburton, D., Brown, L. Y., Yu, C. Y., Roeder, E. R., Stengel-Rutkowski, S., Hennekam, R. C. and Muenke, M. (1998). Holoprosencephaly due to mutations in ZIC2, a homologue of Drosophila odd-paired. *Nat Genet* **20**, 180-3.

Callejo, A., Torroja, C., Quijada, L. and Guerrero, I. (2006). Hedgehog lipid modifications are required for Hedgehog stabilization in the extracellular matrix. *Development* **133**, 471-83.

Campbell, K. (2003). Dorsal-ventral patterning in the mammalian telencephalon. *Curr Opin Neurobiol* **13**, 50-6.

Carletti, B. and Rossi, F. (2008). Neurogenesis in the cerebellum. *Neuroscientist* **14**, 91-100.

Casarosa, S., Fode, C. and Guillemot, F. (1999). Mash1 regulates neurogenesis in the ventral telencephalon. *Development* **126**, 525-34.

Caspary, T., Garcia-Garcia, M. J., Huangfu, D., Eggenschwiler, J. T., Wyler, M. R., Rakeman, A. S., Alcorn, H. L. and Anderson, K. V. (2002). Mouse Dispatched homolog1 is required for long-range, but not juxtacrine, Hh signaling. *Curr Biol* **12**, 1628-32.

Caspary, T., Larkins, C. E. and Anderson, K. V. (2007). The graded response to Sonic Hedgehog depends on cilia architecture. *Dev Cell* **12**, 767-78.

Charron, F., Stein, E., Jeong, J., McMahon, A. P. and Tessier-Lavigne, M. (2003). The morphogen sonic hedgehog is an axonal chemoattractant that collaborates with netrin-1 in midline axon guidance. *Cell* **113**, 11-23.

Chen, M. H., Li, Y. J., Kawakami, T., Xu, S. M. and Chuang, P. T. (2004a). Palmitoylation is required for the production of a soluble multimeric Hedgehog protein complex and long-range signaling in vertebrates. *Genes Dev* **18**, 641-59.

Chen, W., Ren, X. R., Nelson, C. D., Barak, L. S., Chen, J. K., Beachy, P. A., de Sauvage, F. and Lefkowitz, R. J. (2004b). Activity-dependent internalization of smoothened mediated by beta-arrestin 2 and GRK2. *Science* **306**, 2257-60.

Cheng, X., Hsu, C. M., Currle, D. S., Hu, J. S., Barkovich, A. J. and Monuki, E. S. (2006). Central roles of the roof plate in telencephalic development and holoprosencephaly. *J Neurosci* **26**, 7640-9.

Chiang, C., Litingtung, Y., Lee, E., Young, K. E., Corden, J. L., Westphal, H. and Beachy, P. A. (1996). Cyclopia and defective axial patterning in mice lacking Sonic hedgehog gene function. *Nature* **383**, 407-13.

Chizhikov, V. V., Davenport, J., Zhang, Q., Shih, E. K., Cabello, O. A., Fuchs, J. L., Yoder, B. K. and Millen, K. J. (2007). Cilia proteins control cerebellar morphogenesis by promoting expansion of the granule progenitor pool. *J Neurosci* **27**, 9780-9.

Chizhikov, V. V., Lindgren, A. G., Currle, D. S., Rose, M. F., Monuki, E. S. and Millen, K. J. (2006). The roof plate regulates cerebellar cell-type specification and proliferation. *Development* **133**, 2793-804.

Chizhikov, V. V. and Millen, K. J. (2004). Control of roof plate formation by Lmx1a in the developing spinal cord. *Development* **131**, 2693-705.

Chuang, P. T., Kawcak, T. and McMahon, A. P. (2003). Feedback control of mammalian Hedgehog signaling by the Hedgehog-binding protein, Hip1, modulates Fgf signaling during branching morphogenesis of the lung. *Genes Dev* **17**, 342-7.

Chuang, P. T. and McMahon, A. P. (1999). Vertebrate Hedgehog signalling modulated by induction of a Hedgehog-binding protein. *Nature* **397**, 617-21.

Cohen, M. M., Jr. (2006). Holoprosencephaly: clinical, anatomic, and molecular dimensions. *Birth Defects Res A Clin Mol Teratol* **76**, 658-73.

Cooper, M. K., Porter, J. A., Young, K. E. and Beachy, P. A. (1998). Teratogen-mediated inhibition of target tissue response to Shh signaling. *Science* **280**, 1603-7.

Corbin, J. G., Gaiano, N., Machold, R. P., Langston, A. and Fishell, G. (2000). The Gsh2 homeodomain gene controls multiple aspects of telencephalic development. *Development* **127**, 5007-20.

Corcoran, R. B., Bachar Raveh, T., Barakat, M. T., Lee, E. Y. and Scott, M. P. (2008). Insulin-like growth factor 2 is required for progression to advanced medulloblastoma in patched1 heterozygous mice. *Cancer Res* **68**, 8788-95.

Corrales, J. D., Rocco, G. L., Blaess, S., Guo, Q. and Joyner, A. L. (2004). Spatial pattern of sonic hedgehog signaling through Gli genes during cerebellum development. *Development* **131**, 5581-90.

Crossley, P. H., Martinez, S., Ohkubo, Y. and Rubenstein, J. L. (2001). Coordinate expression of Fgf8, Otx2, Bmp4, and Shh in the rostral prosencephalon during development of the telencephalic and optic vesicles. *Neuroscience* **108**, 183-206.

Currle, D. S., Cheng, X., Hsu, C. M. and Monuki, E. S. (2005). Direct and indirect roles of CNS dorsal midline cells in choroid plexus epithelia formation. *Development* **132**, 3549-59.

Dahmane, N. and Ruiz i Altaba, A. (1999). Sonic hedgehog regulates the growth and patterning of the cerebellum. *Development* **126**, 3089-100.

Dahmane, N. and Ruiz-i-Altaba, A. (1999). Sonic hedgehog regulates the growth and patterning of the cerebellum. *Development*. **126**, 3089-100.

Dale, J. K., Vesque, C., Lints, T. J., Sampath, T. K., Furley, A., Dodd, J. and Placzek, M. (1997). Cooperation of BMP7 and SHH in the induction of forebrain ventral midline cells by prechordal mesoderm. *Cell* **90**, 257-69.

Danesin, C., Agius, E., Escalas, N., Ai, X., Emerson, C., Cochard, P. and Soula, C. (2006). Ventral Neural Progenitors Switch toward an Oligodendroglial Fate in Response to Increased Sonic Hedgehog (Shh) Activity: Involvement of Sulfatase 1 in Modulating Shh Signaling in the Ventral Spinal Cord. *J Neurosci* **26**, 5037-5048.

Dang, L., Fan, X., Chaudhry, A., Wang, M., Gaiano, N. and Eberhart, C. G. (2006). Notch3 signaling initiates choroid plexus tumor formation. *Oncogene* **25**, 487-91.

DasGupta, R. and Fuchs, E. (1999). Multiple roles for activated LEF/TCF transcription complexes during hair follicle development and differentiation. *Development* **126**, 4557-68.

Dawber, R. J., Hebbes, S., Herpers, B., Docquier, F. and van den Heuvel, M. (2005). Differential range and activity of various forms of the Hedgehog protein. *BMC Dev Biol* **5**, 21.

Dong, J., Gailani, M. R., Pomeroy, S. L., Reardon, D. and Bale, A. E. (2000). Identification of PATCHED mutations in medulloblastomas by direct sequencing. *Hum Mutat* **16**, 89-90.

Echelard, Y., Epstein, D. J., St-Jacques, B., Shen, L., Mohler, J., McMahon, J. A. and McMahon, A. P. (1993). Sonic hedgehog, a member of a family of putative signaling molecules, is implicated in the regulation of CNS polarity. *Cell* **75**, 1417-30.

Emerich, D. F., Skinner, S. J., Borlongan, C. V., Vasconcellos, A. V. and Thanos, C. G. (2005). The choroid plexus in the rise, fall and repair of the brain. *Bioessays* **27**, 262-74.

Engelking, L. J., Evers, B. M., Richardson, J. A., Goldstein, J. L., Brown, M. S. and Liang, G. (2006). Severe facial clefting in Insig-deficient mouse embryos caused by sterol accumulation and reversed by lovastatin. *J Clin Invest* **116**, 2356-65.

Ericson, J., Muhr, J., Placzek, M., Lints, T., Jessell, T. M. and Edlund, T. (1995). Sonic hedgehog induces the differentiation of ventral forebrain neurons: a common signal for ventral patterning within the neural tube. *Cell* **81**, 747-56.

Ericson, J., Rashbass, P., Schedl, A., Brenner-Morton, S., Kawakami, A., van Heyningen, V., Jessell, T. M. and Briscoe, J. (1997). Pax6 controls progenitor cell identity and neuronal fate in response to graded Shh signaling. *Cell* **90**, 169-80.

Evans, D. G., Ladusans, E. J., Rimmer, S., Burnell, L. D., Thakker, N. and Farndon, P. A. (1993). Complications of the naevoid basal cell carcinoma syndrome: results of a population based study. *J Med Genet* **30**, 460-4.

Ever, L. and Gaiano, N. (2005). Radial 'glial' progenitors: neurogenesis and signaling. *Curr Opin Neurobiol* **15**, 29-33.

Fan, X. and Eberhart, C. G. (2008). Medulloblastoma stem cells. *J Clin Oncol* **26**, 2821-7.

Feng, J., White, B., Tyurina, O. V., Guner, B., Larson, T., Lee, H. Y., Karlstrom, R. O. and Kohtz, J. D. (2004). Synergistic and antagonistic roles of the Sonic hedgehog N- and C-terminal lipids. *Development* **131**, 4357-70.

Feng, X. H. and Derynck, R. (2005). Specificity and versatility in tgf-beta signaling through Smads. *Annu Rev Cell Dev Biol* **21**, 659-93.

Fink, A. J., Englund, C., Daza, R. A., Pham, D., Lau, C., Nivison, M., Kowalczyk, T. and Hevner, R. F. (2006). Development of the deep cerebellar nuclei: transcription factors and cell migration from the rhombic lip. *J Neurosci* **26**, 3066-76.

Franz, T. (1994). Extra-toes (Xt) homozygous mutant mice demonstrate a role for the Gli-3 gene in the development of the forebrain. *Acta Anat (Basel)* **150**, 38-44.

Fuccillo, M., Joyner, A. L. and Fishell, G. (2006). Morphogen to mitogen: the multiple roles of hedgehog signalling in vertebrate neural development. *Nat Rev Neurosci* **7**, 772-83.

Fuccillo, M., Rallu, M., McMahon, A. P. and Fishell, G. (2004). Temporal requirement for hedgehog signaling in ventral telencephalic patterning. *Development* **131**, 5031-40.

Fukuda, A., Kawaguchi, Y., Furuyama, K., Kodama, S., Horiguchi, M., Kuhara, T., Koizumi, M., Boyer, D. F., Fujimoto, K., Doi, R. et al. (2006). Ectopic pancreas formation in Hes1 -knockout mice reveals plasticity of endodermal progenitors of the gut, bile duct, and pancreas. *J Clin Invest* **116**, 1484-93.

Furuta, Y., Piston, D. W. and Hogan, B. L. (1997). Bone morphogenetic proteins (BMPs) as regulators of dorsal forebrain development. *Development* **124**, 2203-12.

Gaiano, N., Kohtz, J. D., Turnbull, D. H. and Fishell, G. (1999). A method for rapid gain-of-function studies in the mouse embryonic nervous system. *Nat Neurosci* **2**, 812-9.

Gailani, M. R., Stahle-Backdahl, M., Leffell, D. J., Glynn, M., Zaphiropoulos, P. G., Pressman, C., Unden, A. B., Dean, M., Brash, D. E., Bale, A. E. et al. (1996). The role of the human homologue of Drosophila patched in sporadic basal cell carcinomas. *Nat Genet* **14**, 78-81.

Galceran, J., Miyashita-Lin, E. M., Devaney, E., Rubenstein, J. L. and Grosschedl, R. (2000). Hippocampus development and generation of dentate gyrus granule cells is regulated by LEF1. *Development* **127**, 469-82.

Gallet, A., Ruel, L., Staccini-Lavenant, L. and Therond, P. P. (2006). Cholesterol modification is necessary for controlled planar long-range activity of Hedgehog in Drosophila epithelia. *Development* **133**, 407-18.

Garcia-Lecea, M., Kondrychyn, I., Fong, S. H., Ye, Z. R. and Korzh, V. (2008). In vivo analysis of choroid plexus morphogenesis in zebrafish. *PLoS ONE* **3**, e3090.

Gato, A., Moro, J. A., Alonso, M. I., Bueno, D., De La Mano, A. and Martin, C. (2005). Embryonic cerebrospinal fluid regulates neuroepithelial survival, proliferation, and neurogenesis in chick embryos. *Anat Rec A Discov Mol Cell Evol Biol* **284**, 475-84.

Gilbertson, R. J. and Ellison, D. W. (2008). The origins of medulloblastoma subtypes. *Annu Rev Pathol* **3**, 341-65.

Gimeno, L., Brulet, P. and Martinez, S. (2003). Study of Fgf15 gene expression in developing mouse brain. *Gene Expr Patterns* **3**, 473-81.

Goodrich, L. V., Johnson, R. L., Milenkovic, L., McMahon, J. A. and Scott, M. P. (1996). Conservation of the hedgehog/patched signaling pathway from flies to mice: induction of a mouse patched gene by Hedgehog. *Genes Dev* **10**, 301-12.

Goodrich, L. V., Milenkovic, L., Higgins, K. M. and Scott, M. P. (1997). Altered neural cell fates and medulloblastoma in mouse patched mutants. *Science* **277**, 1109-13.

Gopal, P., Parker, J. R., Debski, R. and Parker, J. C., Jr. (2008). Choroid plexus carcinoma. *Arch Pathol Lab Med* **132**, 1350-4.

Graus-Porta, D., Blaess, S., Senften, M., Littlewood-Evans, A., Damsky, C., Huang, Z., Orban, P., Klein, R., Schittny, J. C. and Muller, U. (2001). Beta1-class integrins regulate the development of laminae and folia in the cerebral and cerebellar cortex. *Neuron* **31**, 367-79.

Grimaldi, P., Parras, C., Guillemot, F., Rossi, F. and Wassef, M. (2009). Origins and control of the differentiation of inhibitory interneurons and glia in the cerebellum. *Dev Biol* **328**, 422-33.

Grove, E. A. and Fukuchi-Shimogori, T. (2003). Generating the cerebral cortical area map. *Annu Rev Neurosci* **26**, 355-80.

Grove, E. A., Tole, S., Limon, J., Yip, L. and Ragsdale, C. W. (1998). The hem of the embryonic cerebral cortex is defined by the expression of multiple Wnt genes and is compromised in Gli3-deficient mice. *Development* **125**, 2315-25.

Gurdon, J. B. and Bourillot, P. Y. (2001). Morphogen gradient interpretation. *Nature* **413**, 797-803.

Gutin, G., Fernandes, M., Palazzolo, L., Paek, H., Yu, K., Ornitz, D. M., McConnell, S. K. and Hebert, J. M. (2006). FGF signalling generates ventral telencephalic cells independently of SHH. *Development* **133**, 2937-46.

Hahn, H., Wicking, C., Zaphiropoulous, P. G., Gailani, M. R., Shanley, S., Chidambaram, A., Vorechovsky, I., Holmberg, E., Unden, A. B., Gillies, S. et al. (1996). Mutations of the human homolog of Drosophila patched in the nevoid basal cell carcinoma syndrome. *Cell* **85**, 841-51.

Hasenpusch-Theil, K., Bataille, V., Laehdetie, J., Obermayr, F., Sampson, J. R. and Frischauf, A. M. (1998). Gorlin syndrome: identification of 4 novel germ-line mutations

of the human patched (PTCH) gene. Mutations in brief no. 137. Online. *Hum Mutat* **11**, 480.

Hatton, B. A., Knoepfler, P. S., Kenney, A. M., Rowitch, D. H., de Alboran, I. M., Olson, J. M. and Eisenman, R. N. (2006). N-myc is an essential downstream effector of Shh signaling during both normal and neoplastic cerebellar growth. *Cancer Res* **66**, 8655-61.

Hayashi, S., Lewis, P., Pevny, L. and McMahon, A. P. (2002). Efficient gene modulation in mouse epiblast using a Sox2Cre transgenic mouse strain. *Mech Dev* **119 Suppl 1**, S97-S101.

Haycraft, C. J., Banizs, B., Aydin-Son, Y., Zhang, Q., Michaud, E. J. and Yoder, B. K. (2005). Gli2 and Gli3 localize to cilia and require the intraflagellar transport protein polaris for processing and function. *PLoS Genet* **1**, e53.

Hayhurst, M. and McConnell, S. K. (2003). Mouse models of holoprosencephaly. *Curr Opin Neurol* **16**, 135-41.

Hebert, J. M., Hayhurst, M., Marks, M. E., Kulessa, H., Hogan, B. L. and McConnell, S. K. (2003). BMP ligands act redundantly to pattern the dorsal telencephalic midline. *Genesis* **35**, 214-9.

Hebert, J. M., Mishina, Y. and McConnell, S. K. (2002). BMP signaling is required locally to pattern the dorsal telencephalic midline. *Neuron* **35**, 1029-41.

Herz, J., Willnow, T. E. and Farese, R. V., Jr. (1997). Cholesterol, hedgehog and embryogenesis. *Nat Genet* **15**, 123-4.

Ho, K. S. and Scott, M. P. (2002). Sonic hedgehog in the nervous system: functions, modifications and mechanisms. *Curr Opin Neurobiol* **12**, 57-63.

Hogan, B., Beddington, R., Constantini, F. and Lacy, E. (1994). Manipulating the mouse embryo: A laboratory manual. New York: Cold Spring Harbor Laboratory Press.

Hollway, G. E., Maule, J., Gautier, P., Evans, T. M., Keenan, D. G., Lohs, C., Fischer, D., Wicking, C. and Currie, P. D. (2006). Scube2 mediates Hedgehog signalling in the zebrafish embryo. *Dev Biol* **294**, 104-18.

Horton, S., Meredith, A., Richardson, J. A. and Johnson, J. E. (1999). Correct coordination of neuronal differentiation events in ventral forebrain requires the bHLH factor MASH1. *Mol Cell Neurosci* **14**, 355-69.

Hoshino, M., Nakamura, S., Mori, K., Kawauchi, T., Terao, M., Nishimura, Y. V., Fukuda, A., Fuse, T., Matsuo, N., Sone, M. et al. (2005). Ptf1a, a bHLH transcriptional gene, defines GABAergic neuronal fates in cerebellum. *Neuron* **47**, 201-13.

Huang, X., Ketova, T., Fleming, J. T., Wang, H., Dey, S. K., Litingtung, Y. and Chiang, C. (2009). Sonic hedgehog signaling regulates a novel epithelial progenitor domain of the hindbrain choroid plexus. *Development* **136**, 2535-43.

Huang, X., Litingtung, Y. and Chiang, C. (2007a). Ectopic sonic hedgehog signaling impairs telencephalic dorsal midline development: implication for human holoprosencephaly. *Hum Mol Genet* **16**, 1454-68.

Huang, X., Litingtung, Y. and Chiang, C. (2007b). Region-specific requirement for cholesterol modification of sonic hedgehog in patterning the telencephalon and spinal cord. *Development* **134**, 2095-105.

Hunter, N. L. and Dymecki, S. M. (2007). Molecularly and temporally separable lineages form the hindbrain roof plate and contribute differentially to the choroid plexus. *Development* **134**, 3449-60.

Ingham, P. W. and McMahon, A. P. (2001). Hedgehog signaling in animal development: paradigms and principles. *Genes Dev* **15**, 3059-87.

Jeong, J., Mao, J., Tenzen, T., Kottmann, A. H. and McMahon, A. P. (2004). Hedgehog signaling in the neural crest cells regulates the patterning and growth of facial primordia. *Genes Dev* **18**, 937-51.

Jessell, T. M. (2000). Neuronal specification in the spinal cord: inductive signals and transcriptional codes. *Nat Rev Genet* **1**, 20-9.

Jiang, X., Rowitch, D. H., Soriano, P., McMahon, A. P. and Sucov, H. M. (2000). Fate of the mammalian cardiac neural crest. *Development* **127**, 1607-16.

Johnson, R. L., Rothman, A. L., Xie, J., Goodrich, L. V., Bare, J. W., Bonifas, J. M., Quinn, A. G., Myers, R. M., Cox, D. R., Epstein, E. H., Jr. et al. (1996). Human homolog of patched, a candidate gene for the basal cell nevus syndrome. *Science* **272**, 1668-71.

Jullien, J. and Gurdon, J. (2005). Morphogen gradient interpretation by a regulated trafficking step during ligand-receptor transduction. *Genes Dev* **19**, 2682-94.

Kawakami, T., Kawcak, T., Li, Y. J., Zhang, W., Hu, Y. and Chuang, P. T. (2002). Mouse dispatched mutants fail to distribute hedgehog proteins and are defective in hedgehog signaling. *Development* **129**, 5753-65.

Kenney, A. M., Cole, M. D. and Rowitch, D. H. (2003). Nmyc upregulation by sonic hedgehog signaling promotes proliferation in developing cerebellar granule neuron precursors. *Development* **130**, 15-28.

Kenney, A. M., Widlund, H. R. and Rowitch, D. H. (2004). Hedgehog and PI-3 kinase signaling converge on Nmyc1 to promote cell cycle progression in cerebellar neuronal precursors. *Development* **131**, 217-28.

Kessler, J. D., Hasegawa, H., Brun, S. N., Yang, Z. J., Dutton, J. W., Wang, F. and Wechsler-Reya, R. J. (2009). N-myc alters the fate of preneoplastic cells in a mouse model of medulloblastoma. *Genes Dev* **23**, 157-70.

Kinsman, S. L., Plawner, L. L. and Hahn, J. S. (2000). Holoprosencephaly: recent advances and new insights. *Curr Opin Neurol* **13**, 127-32.

Kohtz, J. D., Baker, D. P., Corte, G. and Fishell, G. (1998). Regionalization within the mammalian telencephalon is mediated by changes in responsiveness to Sonic Hedgehog. *Development* **125**, 5079-89.

Kohtz, J. D., Lee, H. Y., Gaiano, N., Segal, J., Ng, E., Larson, T., Baker, D. P., Garber, E. A., Williams, K. P. and Fishell, G. (2001). N-terminal fatty-acylation of sonic hedgehog enhances the induction of rodent ventral forebrain neurons. *Development* **128**, 2351-63.

Komada, M., Saitsu, H., Kinboshi, M., Miura, T., Shiota, K. and Ishibashi, M. (2008). Hedgehog signaling is involved in development of the neocortex. *Development* **135**, 2717-27.

Krizhanovsky, V. and Ben-Arie, N. (2006). A novel role for the choroid plexus in BMP-mediated inhibition of differentiation of cerebellar neural progenitors. *Mech Dev* **123**, 67-75.

Laine, J. and Axelrad, H. (2002). Extending the cerebellar Lugaro cell class. *Neuroscience* **115**, 363-74.

Landsberg, R. L., Awatramani, R. B., Hunter, N. L., Farago, A. F., DiPietrantonio, H. J., Rodriguez, C. I. and Dymecki, S. M. (2005). Hindbrain rhombic lip is comprised of discrete progenitor cell populations allocated by Pax6. *Neuron* **48**, 933-47.

Lazzaro, D., Price, M., de Felice, M. and Di Lauro, R. (1991). The transcription factor TTF-1 is expressed at the onset of thyroid and lung morphogenesis and in restricted regions of the foetal brain. *Development* **113**, 1093-104.

Lee, K. J., Dietrich, P. and Jessell, T. M. (2000a). Genetic ablation reveals that the roof plate is essential for dorsal interneuron specification. *Nature* **403**, 734-40.

Lee, K. J. and Jessell, T. M. (1999). The specification of dorsal cell fates in the vertebrate central nervous system. *Annu Rev Neurosci* **22**, 261-94.

Lee, K. J., Mendelsohn, M. and Jessell, T. M. (1998). Neuronal patterning by BMPs: a requirement for GDF7 in the generation of a discrete class of commissural interneurons in the mouse spinal cord. *Genes Dev* **12**, 3394-407.

Lee, S. M., Tole, S., Grove, E. and McMahon, A. P. (2000b). A local Wnt-3a signal is required for development of the mammalian hippocampus. *Development* **127**, 457-67.

Lee, Y., Miller, H. L., Jensen, P., Hernan, R., Connelly, M., Wetmore, C., Zindy, F., Roussel, M. F., Curran, T., Gilbertson, R. J. et al. (2003). A molecular fingerprint for medulloblastoma. *Cancer Res* **63**, 5428-37.

Leto, K., Carletti, B., Williams, I. M., Magrassi, L. and Rossi, F. (2006). Different types of cerebellar GABAergic interneurons originate from a common pool of multipotent progenitor cells. *J Neurosci* **26**, 11682-94.

Lewis, A. J., Simon, E. M., Barkovich, A. J., Clegg, N. J., Delgado, M. R., Levey, E. and Hahn, J. S. (2002). Middle interhemispheric variant of holoprosencephaly: a distinct cliniconeuroradiologic subtype. *Neurology* **59**, 1860-5.

Lewis, P. M., Dunn, M. P., McMahon, J. A., Logan, M., Martin, J. F., St-Jacques, B. and McMahon, A. P. (2001). Cholesterol modification of sonic hedgehog is required for long-range signaling activity and effective modulation of signaling by Ptc1. *Cell* **105**, 599-612.

Lewis, P. M., Gritli-Linde, A., Smeyne, R., Kottmann, A. and McMahon, A. P. (2004). Sonic hedgehog signaling is required for expansion of granule neuron precursors and patterning of the mouse cerebellum. *Dev Biol* **270**, 393-410.

Li, Y., Zhang, H., Choi, S. C., Litingtung, Y. and Chiang, C. (2004). Sonic hedgehog signaling regulates Gli3 processing, mesenchymal proliferation, and differentiation during mouse lung organogenesis. *Dev Biol* **270**, 214-31.

Li, Y., Zhang, H., Litingtung, Y. and Chiang, C. (2006). Cholesterol modification restricts the spread of Shh gradient in the limb bud. *Proc Natl Acad Sci U S A* **103**, 6548-53.

Litingtung, Y. and Chiang, C. (2000). Specification of ventral neuron types is mediated by an antagonistic interaction between Shh and Gli3. *Nat Neurosci* **3**, 979-85.

Litingtung, Y., Dahn, R. D., Li, Y., Fallon, J. F. and Chiang, C. (2002). Shh and Gli3 are dispensable for limb skeleton formation but regulate digit number and identity. *Nature* **418**, 979-83.

Litingtung, Y., Lei, L., Westphal, H. and Chiang, C. (1998). Sonic hedgehog is essential to foregut development. *Nat Genet* **20**, 58-61.

Lo, L., Dormand, E. L. and Anderson, D. J. (2005). Late-emigrating neural crest cells in the roof plate are restricted to a sensory fate by GDF7. *Proc Natl Acad Sci U S A* **102**, 7192-7.

Lo, L. C., Johnson, J. E., Wuenschell, C. W., Saito, T. and Anderson, D. J. (1991). Mammalian achaete-scute homolog 1 is transiently expressed by spatially restricted subsets of early neuroepithelial and neural crest cells. *Genes Dev* **5**, 1524-37.

Louie, C. M. and Gleeson, J. G. (2005). Genetic basis of Joubert syndrome and related disorders of cerebellar development. *Hum Mol Genet* **14 Spec No. 2**, R235-42.

Ma, Y., Erkner, A., Gong, R., Yao, S., Taipale, J., Basler, K. and Beachy, P. A. (2002). Hedgehog-mediated patterning of the mammalian embryo requires transporter-like function of dispatched. *Cell* **111**, 63-75.

Machold, R. and Fishell, G. (2005). Math1 is expressed in temporally discrete pools of cerebellar rhombic-lip neural progenitors. *Neuron* **48**, 17-24.

Machold, R., Hayashi, S., Rutlin, M., Muzumdar, M. D., Nery, S., Corbin, J. G., Gritli-Linde, A., Dellovade, T., Porter, J. A., Rubin, L. L. et al. (2003). Sonic hedgehog is required for progenitor cell maintenance in telencephalic stem cell niches. *Neuron* **39**, 937-50.

Mann, R. K. and Beachy, P. A. (2004). Novel lipid modifications of secreted protein signals. *Annu Rev Biochem* **73**, 891-923.

Mao, J., Ligon, K. L., Rakhlin, E. Y., Thayer, S. P., Bronson, R. T., Rowitch, D. and McMahon, A. P. (2006). A novel somatic mouse model to survey tumorigenic potential applied to the Hedgehog pathway. *Cancer Res* **66**, 10171-8.

Maricich, S. M. and Herrup, K. (1999). Pax-2 expression defines a subset of GABAergic interneurons and their precursors in the developing murine cerebellum. *J Neurobiol* **41**, 281-94.

Maruoka, Y., Ohbayashi, N., Hoshikawa, M., Itoh, N., Hogan, B. L. and Furuta, Y. (1998). Comparison of the expression of three highly related genes, Fgf8, Fgf17 and Fgf18, in the mouse embryo. *Mech Dev* **74**, 175-7.

McCarthy, R. A., Barth, J. L., Chintalapudi, M. R., Knaak, C. and Argraves, W. S. (2002). Megalin functions as an endocytic sonic hedgehog receptor. *J Biol Chem* **277**, 25660-7.

Miale, I. L. and Sidman, R. L. (1961). An autoradiographic analysis of histogenesis in the mouse cerebellum. *Exp Neurol* **4**, 277-96.

Millonig, J. H., Millen, K. J. and Hatten, M. E. (2000). The mouse Dreher gene Lmx1a controls formation of the roof plate in the vertebrate CNS. *Nature* **403**, 764-9.

Minowada, G., Jarvis, L. A., Chi, C. L., Neubuser, A., Sun, X., Hacohen, N., Krasnow, M. A. and Martin, G. R. (1999). Vertebrate Sprouty genes are induced by FGF signaling and can cause chondrodysplasia when overexpressed. *Development* **126**, 4465-75.

Monuki, E. S. and Walsh, C. A. (2001). Mechanisms of cerebral cortical patterning in mice and humans. *Nat Neurosci* **4 Suppl**, 1199-206.

Morales, D. and Hatten, M. E. (2006). Molecular markers of neuronal progenitors in the embryonic cerebellar anlage. *J Neurosci* **26**, 12226-36.

Morava, E., Bartsch, O., Czako, M., Frensel, A., Kalscheuer, V., Karteszi, J. and Kosztolanyi, G. (2003). Small inherited terminal duplication of 7q with hydrocephalus, cleft palate, joint contractures, and severe hypotonia. *Clin Dysmorphol* **12**, 123-7.

Mori, T., Tanaka, K., Buffo, A., Wurst, W., Kuhn, R. and Gotz, M. (2006). Inducible gene deletion in astroglia and radial glia--a valuable tool for functional and lineage analysis. *Glia* **54**, 21-34.

Motoyama, J., Takabatake, T., Takeshima, K. and Hui, C. (1998). Ptch2, a second mouse Patched gene is co-expressed with Sonic hedgehog. *Nat Genet* **18**, 104-6.

Muenke, M. and Beachy, P. A. (2000). Genetics of ventral forebrain development and holoprosencephaly. *Curr Opin Genet Dev* **10**, 262-9.

Muzumdar, M. D., Tasic, B., Miyamichi, K., Li, L. and Luo, L. (2007). A global double-fluorescent Cre reporter mouse. *Genesis* **45**, 593-605.

Nagai, T., Aruga, J., Minowa, O., Sugimoto, T., Ohno, Y., Noda, T. and Mikoshiba, K. (2000). Zic2 regulates the kinetics of neurulation. *Proc Natl Acad Sci U S A* **97**, 1618-23.

Nanni, L., Ming, J. E., Bocian, M., Steinhaus, K., Bianchi, D. W., Die-Smulders, C., Giannotti, A., Imaizumi, K., Jones, K. L., Campo, M. D. et al. (1999). The mutational spectrum of the sonic hedgehog gene in holoprosencephaly: SHH mutations cause a significant proportion of autosomal dominant holoprosencephaly. *Hum Mol Genet* **8**, 2479-88.

Naruse, I. and Keino, H. (1993). Induction of agenesis of the corpus callosum by the destruction of anlage of the olfactory bulb using fetal laser surgery exo utero in mice. *Brain Res Dev Brain Res* **71**, 69-74.

O'Dorisio, M. S., Khanna, G. and Bushnell, D. (2008). Combining anatomic and molecularly targeted imaging in the diagnosis and surveillance of embryonal tumors of the nervous and endocrine systems in children. *Cancer Metastasis Rev* **27**, 665-77.

Ohkubo, Y., Chiang, C. and Rubenstein, J. L. (2002). Coordinate regulation and synergistic actions of BMP4, SHH and FGF8 in the rostral prosencephalon regulate morphogenesis of the telencephalic and optic vesicles. *Neuroscience* **111**, 1-17.

Oliver, T. G., Read, T. A., Kessler, J. D., Mehmeti, A., Wells, J. F., Huynh, T. T., Lin, S. M. and Wechsler-Reya, R. J. (2005). Loss of patched and disruption of granule cell development in a pre-neoplastic stage of medulloblastoma. *Development* **132**, 2425-39.

Palma, V., Lim, D. A., Dahmane, N., Sanchez, P., Brionne, T. C., Herzberg, C. D., Gitton, Y., Carleton, A., Alvarez-Buylla, A. and Ruiz i Altaba, A. (2005). Sonic hedgehog controls stem cell behavior in the postnatal and adult brain. *Development* **132**, 335-44.

Parada, C., Martin, C., Alonso, M. I., Moro, J. A., Bueno, D. and Gato, A. (2005). Embryonic cerebrospinal fluid collaborates with the isthmic organizer to regulate mesencephalic gene expression. *J Neurosci Res* **82**, 333-45.

Pascual, M., Abasolo, I., Mingorance-Le Meur, A., Martinez, A., Del Rio, J. A., Wright, C. V., Real, F. X. and Soriano, E. (2007). Cerebellar GABAergic progenitors adopt an external granule cell-like phenotype in the absence of Ptf1a transcription factor expression. *Proc Natl Acad Sci U S A* **104**, 5193-8.

Pierce, E. T. (1975). Histogenesis of the deep cerebellar nuclei in the mouse: an autoradiographic study. *Brain Res* **95**, 503-18.

Pulitzer, S. B., Simon, E. M., Crombleholme, T. M. and Golden, J. A. (2004). Prenatal MR findings of the middle interhemispheric variant of holoprosencephaly. *AJNR Am J Neuroradiol* **25**, 1034-6.

Raffel, C., Jenkins, R. B., Frederick, L., Hebrink, D., Alderete, B., Fults, D. W. and James, C. D. (1997). Sporadic medulloblastomas contain PTCH mutations. *Cancer Res* **57**, 842-5.

Rallu, M., Machold, R., Gaiano, N., Corbin, J. G., McMahon, A. P. and Fishell, G. (2002). Dorsoventral patterning is established in the telencephalon of mutants lacking both Gli3 and Hedgehog signaling. *Development* **129**, 4963-74.

Redzic, Z. B., Preston, J. E., Duncan, J. A., Chodobski, A. and Szmydynger-Chodobska, J. (2005). The choroid plexus-cerebrospinal fluid system: from development to aging. *Curr Top Dev Biol* **71**, 1-52.

Rice, R., Spencer-Dene, B., Connor, E. C., Gritli-Linde, A., McMahon, A. P., Dickson, C., Thesleff, I. and Rice, D. P. (2004). Disruption of Fgf10/Fgfr2b-coordinated epithelial-mesenchymal interactions causes cleft palate. *J Clin Invest* **113**, 1692-700.

Rohatgi, R., Milenkovic, L. and Scott, M. P. (2007). Patched1 regulates hedgehog signaling at the primary cilium. *Science* **317**, 372-6.

Rossi, A., Caracciolo, V., Russo, G., Reiss, K. and Giordano, A. (2008). Medulloblastoma: from molecular pathology to therapy. *Clin Cancer Res* **14**, 971-6.

Saha, K. and Schaffer, D. V. (2006). Signal dynamics in Sonic hedgehog tissue patterning. *Development* **133**, 889-900.

Salsano, E., Croci, L., Maderna, E., Lupo, L., Pollo, B., Giordana, M. T., Consalez, G. G. and Finocchiaro, G. (2007). Expression of the neurogenic basic helix-loop-helix transcription factor NEUROG1 identifies a subgroup of medulloblastomas not expressing ATOH1. *Neuro Oncol* **9**, 298-307.

Salsano, E., Pollo, B., Eoli, M., Giordana, M. T. and Finocchiaro, G. (2004). Expression of MATH1, a marker of cerebellar granule cell progenitors, identifies different medulloblastoma sub-types. *Neurosci Lett* **370**, 180-5.

Sarangi, A., Valadez, J. G., Rush, S., Abel, T. W., Thompson, R. C. and Cooper, M. K. (2009). Targeted inhibition of the Hedgehog pathway in established malignant glioma xenografts enhances survival. *Oncogene* **28**, 3468-76.

Sawamoto, K., Wichterle, H., Gonzalez-Perez, O., Cholfin, J. A., Yamada, M., Spassky, N., Murcia, N. S., Garcia-Verdugo, J. M., Marin, O., Rubenstein, J. L. et al. (2006). New neurons follow the flow of cerebrospinal fluid in the adult brain. *Science* **311**, 629-32.

Schuller, U., Heine, V. M., Mao, J., Kho, A. T., Dillon, A. K., Han, Y. G., Huillard, E., Sun, T., Ligon, A. H., Qian, Y. et al. (2008). Acquisition of granule neuron precursor identity is a critical determinant of progenitor cell competence to form Shh-induced medulloblastoma. *Cancer Cell* **14**, 123-34.

Segal, M. B. (2000). The choroid plexuses and the barriers between the blood and the cerebrospinal fluid. *Cell Mol Neurobiol* **20**, 183-96.

Shimamura, K., Hartigan, D. J., Martinez, S., Puelles, L. and Rubenstein, J. L. R. (1995). Longitudinal organization of the anterior neural plate and neural tube. *Development* **121**, 3923-3933.

Shimamura, K. and Rubenstein, J. L. (1997a). Inductive interactions direct early regionalization of the mouse forebrain. *Development*. **124**, 2709-18.

Shimamura, K. and Rubenstein, J. L. (1997b). Inductive interactions direct early regionalization of the mouse forebrain. *Development* **124**, 2709-18.

Shimogori, T., Banuchi, V., Ng, H. Y., Strauss, J. B. and Grove, E. A. (2004). Embryonic signaling centers expressing BMP, WNT and FGF proteins interact to pattern the cerebral cortex. *Development* **131**, 5639-47.

Shinozaki, K., Yoshida, M., Nakamura, M., Aizawa, S. and Suda, Y. (2004). Emx1 and Emx2 cooperate in initial phase of archipallium development. *Mech Dev* **121**, 475-89.

Sillitoe, R. V. and Joyner, A. L. (2007). Morphology, molecular codes, and circuitry produce the three-dimensional complexity of the cerebellum. *Annu Rev Cell Dev Biol* **23**, 549-77.

Simon, E. M., Hevner, R. F., Pinter, J. D., Clegg, N. J., Delgado, M., Kinsman, S. L., Hahn, J. S. and Barkovich, A. J. (2002). The middle interhemispheric variant of holoprosencephaly. *AJNR Am J Neuroradiol* **23**, 151-6.

Soriano, P. (1999). Generalized lacZ expression with the ROSA26 Cre reporter strain. *Nat Genet* **21**, 70-1.

Spassky, N., Han, Y. G., Aguilar, A., Strehl, L., Besse, L., Laclef, C., Ros, M. R., Garcia-Verdugo, J. M. and Alvarez-Buylla, A. (2008). Primary cilia are required for cerebellar development and Shh-dependent expansion of progenitor pool. *Dev Biol* **317**, 246-59.

Srinivas, S., Watanabe, T., Lin, C. S., William, C. M., Tanabe, Y., Jessell, T. M. and Costantini, F. (2001). Cre reporter strains produced by targeted insertion of EYFP and ECFP into the ROSA26 locus. *BMC Dev Biol* **1**, 4.

Stamataki, D., Ulloa, F., Tsoni, S. V., Mynett, A. and Briscoe, J. (2005). A gradient of Gli activity mediates graded Sonic Hedgehog signaling in the neural tube. *Genes Dev* **19**, 626-41.

Stecca, B. and Ruiz i Altaba, A. (2005). Brain as a paradigm of organ growth: Hedgehog-Gli signaling in neural stem cells and brain tumors. *J Neurobiol* **64**, 476-90.

Storm, E. E., Garel, S., Borello, U., Hebert, J. M., Martinez, S., McConnell, S. K., Martin, G. R. and Rubenstein, J. L. (2006). Dose-dependent functions of Fgf8 in regulating telencephalic patterning centers. *Development* **133**, 1831-44.

Storm, E. E., Rubenstein, J. L. and Martin, G. R. (2003). Dosage of Fgf8 determines whether cell survival is positively or negatively regulated in the developing forebrain. *Proc Natl Acad Sci U S A* **100**, 1757-62.

Sturrock, R. R. (1979). A morphological study of the development of the mouse choroid plexus. *J Anat* **129**, 777-93.

Sur, M. and Rubenstein, J. L. (2005). Patterning and plasticity of the cerebral cortex. *Science* **310**, 805-10.

Takahashi, T., Kinsman, S., Makris, N., Grant, E., Haselgrove, C., McInerney, S., Kennedy, D. N., Takahashi, T., Fredrickson, K., Mori, S. et al. (2003). Semilobar holoprosencephaly with midline 'seam': a topologic and morphogenetic model based upon MRI analysis. *Cereb Cortex* **13**, 1299-312.

Tannahill, D., Harris, L. W. and Keynes, R. (2005). Role of morphogens in brain growth. *J Neurobiol* **64**, 367-75.

Thomas, T. and Dziadek, M. (1993). Capacity to form choroid plexus-like cells in vitro is restricted to specific regions of the mouse neural ectoderm. *Development* **117**, 253-62.

Thomas, W. D., Chen, J., Gao, Y. R., Cheung, B., Koach, J., Sekyere, E., Norris, M. D., Haber, M., Ellis, T., Wainwright, B. et al. (2009). Patched1 deletion increases N-Myc protein stability as a mechanism of medulloblastoma initiation and progression. *Oncogene* **28**, 1605-15.

Tian, H., Jeong, J., Harfe, B. D., Tabin, C. J. and McMahon, A. P. (2005). Mouse Disp1 is required in sonic hedgehog-expressing cells for paracrine activity of the cholesterol-modified ligand. *Development* **132**, 133-42.

Tomioka, N., Osumi, N., Sato, Y., Inoue, T., Nakamura, S., Fujisawa, H. and Hirata, T. (2000). Neocortical origin and tangential migration of guidepost neurons in the lateral olfactory tract. *J Neurosci* **20**, 5802-12.

Volpicelli, F., Consales, C., Caiazzo, M., Colucci-D'Amato, L., Perrone-Capano, C. and di Porzio, U. (2004). Enhancement of dopaminergic differentiation in proliferating midbrain neuroblasts by sonic hedgehog and ascorbic acid. *Neural Plast* **11**, 45-57.

Wall, D. S., Mears, A. J., McNeill, B., Mazerolle, C., Thurig, S., Wang, Y., Kageyama, R. and Wallace, V. A. (2009). Progenitor cell proliferation in the retina is dependent on Notch-independent Sonic hedgehog/Hes1 activity. *J Cell Biol* **184**, 101-12.

Wallace, V. A. (1999a). Purkinje-cell-derived Sonic hedgehog regulates granule neuron precursor cell proliferation in the developing mouse cerebellum. *Curr Biol*. **9**, 445-8.

Wallace, V. A. (1999b). Purkinje-cell-derived Sonic hedgehog regulates granule neuron precursor cell proliferation in the developing mouse cerebellum. *Curr Biol* **9**, 445-8.

Wang, B., Fallon, J. F. and Beachy, P. A. (2000). Hedgehog-regulated processing of Gli3 produces an anterior/posterior repressor gradient in the developing vertebrate limb. *Cell* **100**, 423-34.

Wang, V. Y., Rose, M. F. and Zoghbi, H. Y. (2005). Math1 expression redefines the rhombic lip derivatives and reveals novel lineages within the brainstem and cerebellum. *Neuron* **48**, 31-43.

Ward, R. J., Lee, L., Graham, K., Satkunendran, T., Yoshikawa, K., Ling, E., Harper, L., Austin, R., Nieuwenhuis, E., Clarke, I. D. et al. (2009). Multipotent CD15+ cancer stem cells in patched-1-deficient mouse medulloblastoma. *Cancer Res* **69**, 4682-90.

Weaver, M., Dunn, N. R. and Hogan, B. L. (2000). Bmp4 and Fgf10 play opposing roles during lung bud morphogenesis. *Development* **127**, 2695-704.

Wechsler-Reya, R. J. and Scott, M. P. (1999a). Control of neuronal precursor proliferation in the cerebellum by Sonic Hedgehog. *Neuron* **22**, 103-14.

Wechsler-Reya, R. J. and Scott, M. P. (1999b). Control of neuronal precursor proliferation in the cerebellum by Sonic Hedgehog. *Neuron*. **22**, 103-14.

Wicking, C., Shanley, S., Smyth, I., Gillies, S., Negus, K., Graham, S., Suthers, G., Haites, N., Edwards, M., Wainwright, B. et al. (1997). Most germ-line mutations in the nevoid basal cell carcinoma syndrome lead to a premature termination of the PATCHED protein, and no genotype-phenotype correlations are evident. *Am J Hum Genet* **60**, 21-6.

Willnow, T. E., Hilpert, J., Armstrong, S. A., Rohlmann, A., Hammer, R. E., Burns, D. K. and Herz, J. (1996). Defective forebrain development in mice lacking gp330/megalin. *Proc Natl Acad Sci U S A* **93**, 8460-4.

Wingate, R. J. and Hatten, M. E. (1999). The role of the rhombic lip in avian cerebellum development. *Development* **126**, 4395-404.

Woods, I. G. and Talbot, W. S. (2005). The you gene encodes an EGF-CUB protein essential for Hedgehog signaling in zebrafish. *PLoS Biol* **3**, e66.

Yamamoto, M., McCaffery, P. and Drager, U. C. (1996). Influence of the choroid plexus on cerebellar development: analysis of retinoic acid synthesis. *Brain Res Dev Brain Res* **93**, 182-90.

Yang, Z. J., Ellis, T., Markant, S. L., Read, T. A., Kessler, J. D., Bourboulas, M., Schuller, U., Machold, R., Fishell, G., Rowitch, D. H. et al. (2008). Medulloblastoma can be initiated by deletion of Patched in lineage-restricted progenitors or stem cells. *Cancer Cell* **14**, 135-45.

Yoon, J. W., Gilbertson, R., Iannaccone, S., Iannaccone, P. and Walterhouse, D. (2009). Defining a role for Sonic hedgehog pathway activation in desmoplastic medulloblastoma by identifying GLI1 target genes. *Int J Cancer* **124**, 109-19.

Yun, K., Potter, S. and Rubenstein, J. L. (2001). Gsh2 and Pax6 play complementary roles in dorsoventral patterning of the mammalian telencephalon. *Development* **128**, 193-205.

Yung, S. Y., Gokhan, S., Jurcsak, J., Molero, A. E., Abrajano, J. J. and Mehler, M. F. (2002). Differential modulation of BMP signaling promotes the elaboration of cerebral cortical GABAergic neurons or oligodendrocytes from a common sonic hedgehog-responsive ventral forebrain progenitor species. *Proc Natl Acad Sci U S A* **99**, 16273-8.

Zeng, X., Goetz, J. A., Suber, L. M., Scott, W. J., Jr., Schreiner, C. M. and Robbins, D. J. (2001). A freely diffusible form of Sonic hedgehog mediates long-range signalling. *Nature* **411**, 716-20.

Zhang, X. M. and Yang, X. J. (2001). Temporal and spatial effects of Sonic hedgehog signaling in chick eye morphogenesis. *Dev Biol* **233**, 271-90.

Zhao, Y., Sheng, H. Z., Amini, R., Grinberg, A., Lee, E., Huang, S., Taira, M. and Westphal, H. (1999). Control of hippocampal morphogenesis and neuronal differentiation by the LIM homeobox gene Lhx5. *Science* **284**, 1155-8.

Zhou, C. J., Zhao, C. and Pleasure, S. J. (2004). Wnt signaling mutants have decreased dentate granule cell production and radial glial scaffolding abnormalities. *J Neurosci* **24**, 121-6.

Zordan, P., Croci, L., Hawkes, R. and Consalez, G. G. (2008). Comparative analysis of proneural gene expression in the embryonic cerebellum. *Dev Dyn* **237**, 1726-35.